

THE PHYSICAL PROPERTIES AND PHASE EQUILIBRIA  
OF THE HYDROUS MG-Fe RICHTERITES

by

ROBERT WILSON CHARLES

B.S. Bucknell University

(1967)

SUBMITTED IN

PARTIAL FULFILLMENT

OF THE REQUIREMENTS FOR THE

DEGREE OF DOCTOR OF PHILOSOPHY

at the

MASSACHUSETTS INSTITUTE OF TECHNOLOGY

September, 1972

Signature of Author

\_\_\_\_\_  
Department of Earth and Planetary Sciences

Certified by

\_\_\_\_\_  
Thesis Supervisor

Accepted by

\_\_\_\_\_  
Chairman, Departmental Committee  
on Graduate Students

Lindgren  
MASS. INST. TECH.  
WITHDRAWN  
15 1972  
FROM  
LIBRARIES  
LIBRARIES

THE PHYSICAL PROPERTIES AND PHASE EQUILIBRIA OF THE  
HYDROUS MG-Fe RICHTERITES

by

Robert Wilson Charles

SUBMITTED TO THE DEPARTMENT OF EARTH AND PLANETARY SCIENCES

IN PARTIAL FULFILLMENT OF THE REQUIREMENTS FOR THE

DEGREE OF DOCTOR OF PHILOSOPHY

*ABSTRACT: Amphiboles along the join  $\text{Na}_2\text{CaMg}_5\text{Si}_8\text{O}_{22}(\text{OH})_2$ - $\text{Na}_2\text{-CaFe}_5\text{Si}_8\text{O}_{22}(\text{OH})_2$  have been synthesized. Six compositions along this join were studied with respect to  $P_{\text{Tot}}$ ,  $T$  and  $f_{\text{O}_2}$ .  $f_{\text{O}_2}$  was controlled by standard  $\text{O}_2$  buffering techniques. Iron bearing amphiboles were most easily synthesized along the Fe-FeO buffer. Refractive indices increase linearly from  $\alpha = 1.604(5)$  and  $\gamma = 1.622(3)$  at  $\text{Mg}_5$  to  $\alpha = 1.690(5)$  and  $\gamma = 1.710(4)$ . Experiments on more oxidizing buffers yielded large amounts of clinopyroxene in addition to amphibole.*

*Mössbauer studies indicate  $\text{Fe}^{+3}$  is present in all cases. This fact is explained by appealing to structural and local charge balance considerations. The conclusion is that Na in the M(4) site produces a local charge imbalance which is corrected by placing  $\text{Fe}^{+3}$  in the neighboring M(2) site. Na is lost from the A site to maintain charge balance.*

*The phase relations of the amphiboles along the join richterite-ferrorichterite have been defined using standard hydrothermal and oxygen buffer techniques. Richterite is found to be stable to  $1030 \pm 5^\circ\text{C}$  at 1 kb  $P_{\text{Tot}}$ . Above 150 bars richterite decomposes to forsterite + diopside + enstatite + melt + vapor. At conditions between  $930^\circ\text{C}$  at 50 bars and  $970^\circ\text{C}$  at 150 bars the decomposition assemblage is roedderite + forsterite + diopside + melt + vapor. Below  $930^\circ\text{C}$  and 50 bars richterite reacts to roedderite + 1:2:6 Na-Mg silicate + forsterite + diopside + vapor. Ferrorichterite on the Fe-FeO buffer is stable to  $715 \pm 5^\circ\text{C}$  at 1 kb  $P_{\text{Tot}}$ , decomposing to hedenbergitic pyroxene + fayalite + melt + vapor at higher  $T$ . Below 700 bars ferrorichterite decomposes to 1:2:6 Na-Fe silicate + hedenbergitic pyroxene + fayalite + melt + vapor. Ferrorichterite on the QFM buffer is stable to only  $535 \pm 10^\circ\text{C}$  at 1 kb, reacting to form acmite<sub>67</sub> hedenbergite<sub>33</sub> + fayalite + magnetite + quartz + vapor at higher  $T$ . Above  $820 \pm 10^\circ\text{C}$  at 1 kb this assemblage undergoes melting to form hedenbergitic pyroxene + fayalite + magnetite + melt + vapor. Above the Fe-FeO buffer the ferrorichterite bulk composition yields amphibole + acmitic pyroxene, indi-*

cating completely ferrous ferrorichterite is stable only at very low  $f_{O_2}$ .

The isobaric  $\log f_{O_2}$  vs.  $T$  phase diagrams for compositions along the richterite-ferrorichterite join show a lessening of amphibole stability with addition of iron with a great drop in stability between  $Mg_2Fe_3$  and  $MgFe_4$ . This reflects the greatly decreased linking of the double chains of silicon tetrahedra caused by the addition of iron to  $M(2)$ . All amphiboles at higher  $f_{O_2}$  trend in cell parameters toward riebeckite-riebeckite-arfvedsonite due to the local charge imbalance caused by Na in  $M(4)$ .

THESIS SUPERVISOR: Dr. David R. Wones

## TABLE OF CONTENTS

I. Title.....	1
II. Abstract.....	2
III. Table of Contents.....	4
IV. Introduction.....	7
A. Amphibole structure.....	7
B. Natural occurrence.....	7
C. Previous investigations.....	10
V. Part I Physical Properties.....	13
A. Experimental procedure.....	13
B. Description of phases.....	18
1. Percent yield of amphiboles and im-	
purities.....	18
2. Optical properties.....	19
C. X-ray determinations.....	26
1. Powder diffraction method.....	27
2. Uniformity of unit cell dimensions of Fe	
bearing amphiboles in P-T space and	
defined $f_{O_2}$ .....	27
3. Nonuniformity of $Mg_5$ with respect to P..	31
4. Variation of amphibole cell volume with	
$f_{O_2}$ at fixed $\chi_1$ , P, and T.....	31
D. Discussion.....	45
1. Presence of ferric iron.....	45
2. Local charge balance and structural	
constraints on site occupancy.....	46

3. Detailed examination of unit cell parameters for experiments on I-W.....	47
VI. Part II Phase Equilibria.....	50
A. Introduction.....	50
B. Mg-richterite ( $\text{Na}_2\text{CaMg}_5\text{Si}_8\text{O}_{22}(\text{OH})_2$ ).....	50
C. Ferrorichterite ( $\text{Na}_2\text{CaFe}_5\text{Si}_8\text{O}_{22}(\text{OH})_2$ ).....	56
1. P-T diagram $f_{\text{O}_2}$ defined by I-W.....	56
2. P-T diagram $f_{\text{O}_2}$ defined by QFM.....	61
3. Isobaric ( $P_{\text{Tot}} = 1 \text{ kb}$ ) $\text{Log } f_{\text{O}_2} - T$ diagram.....	66
D. Intermediate compositions.....	71
1. Introduction.....	71
2. $\text{Na}_2\text{CaMg}_4\text{FeSi}_8\text{O}_{22}(\text{OH})_2$ : Isobaric ( $P_{\text{Tot}} = 1 \text{ kb}$ ) $\text{Log } f_{\text{O}_2} - T$ diagram.....	73
3. $\text{Na}_2\text{CaMg}_3\text{Fe}_2\text{Si}_8\text{O}_{22}(\text{OH})_2$ : Isobaric ( $P_{\text{Tot}} = 1 \text{ kb}$ ) $\text{Log } f_{\text{O}_2} - T$ diagram.....	80
4. $\text{Na}_2\text{CaMg}_2\text{Fe}_3\text{Si}_8\text{O}_{22}(\text{OH})_2$ : Isobaric ( $P_{\text{Tot}} = 1 \text{ kb}$ ) $\text{Log } f_{\text{O}_2} - T$ diagram.....	86
5. $\text{Na}_2\text{CaMgFe}_4\text{Si}_8\text{O}_{22}(\text{OH})_2$ : Isobaric ( $P_{\text{Tot}} = 1 \text{ kb}$ ) $\text{Log } f_{\text{O}_2} - T$ diagram.....	92
E. Isobaric ( $P_{\text{Tot}} = 1 \text{ kb}$ ) T-X sections.....	98
1. $f_{\text{O}_2}$ defined by H-Mt.....	99
2. $f_{\text{O}_2}$ defined by QFM.....	101
3. $f_{\text{O}_2}$ defined by C- $\text{CH}_4$ .....	103
4. $f_{\text{O}_2}$ defined by W-Mt.....	105
5. $f_{\text{O}_2}$ defined by I-W.....	107
F. Thermodynamic discussion.....	109

G. Composite isobaric ( $P_{\text{Tot}} = 1 \text{ kb}$ ) Log $f_{\text{O}_2}$ - T diagram for amphiboles along the join $\text{Mg}_5$ - $\text{Fe}_5$ .....	113
H. Comparison of the thermal stabilities of richterite and ferrorichterite.....	116
I. Comparison of ferrorichterite with some other iron amphiboles.....	116
VII. Appendix I Roedderites.....	125
VIII. Appendix II Complete Experimental Tables for All Compositions.....	129
IX. Acknowledgements.....	150
X. Biographical Sketch.....	151
XI. References.....	152

TABLES

6a

Table I-1	Compositions and cell parameters of synthetic richterites.....	11
Table I-2	Reagents.....	14
Table I-3	Unit cell volumes of amphibole (QFM).....	22
Table I-4	Optical properties.....	25
Table I-5	Diffractometer patterns for Mg <sub>5</sub> and Fe <sub>5</sub> .....	28
Table I-7	Mg-richterite at increasing pressure.....	32
Table I-6	Cell parameters of amphibole across the Mg <sub>5</sub> - Fe <sub>5</sub> join.....	38
Table II-1	Bracketing experiments: Na <sub>2</sub> CaMg <sub>5</sub> Si <sub>8</sub> O <sub>22</sub> (OH) <sub>2</sub>	54
Table II-2	Bracketing experiments: Na <sub>2</sub> CaFe <sub>5</sub> Si <sub>8</sub> O <sub>22</sub> (OH) <sub>2</sub> (I-W).....	59
Table II-3	Bracketing experiments: Na <sub>2</sub> CaFe <sub>5</sub> Si <sub>8</sub> O <sub>22</sub> (OH) <sub>2</sub> (QFM).....	64
Table II-4	Unit cell parameters bulk composition: Na <sub>2</sub> CaFe <sub>5</sub> Si <sub>8</sub> O <sub>22</sub> (OH) <sub>2</sub> .....	65
Table II-5	Bracketing experiments: Na <sub>2</sub> CaFe <sub>5</sub> Si <sub>8</sub> O <sub>22</sub> (OH) <sub>2</sub> Log f <sub>O<sub>2</sub></sub> - T (P <sub>Tot</sub> = 1 kb).	69
Table II-6	Bracketing experiments: Na <sub>2</sub> CaMg <sub>4</sub> FeSi <sub>8</sub> O <sub>22</sub> (OH) <sub>2</sub> Log f <sub>O<sub>2</sub></sub> - T (P <sub>Tot</sub> = 1 kb).....	77
Table II-7	Unit cell parameters bulk composition: Na <sub>2</sub> CaMg <sub>4</sub> FeSi <sub>8</sub> O <sub>22</sub> (OH) <sub>2</sub> .....	78
Table II-8	Bracketing experiments: Na <sub>2</sub> CaMg <sub>3</sub> Fe <sub>2</sub> Si <sub>8</sub> O <sub>22</sub> (OH) <sub>2</sub> Log f <sub>O<sub>2</sub></sub> - T (P <sub>Tot</sub> = 1 kb).....	83

Table II-9	Unit cell parameters bulk composition:	
	$\text{Na}_2\text{CaMg}_3\text{Fe}_2\text{Si}_8\text{O}_{22}(\text{OH})_2$ .....	84
Table II-10	Bracketing experiments: $\text{Na}_2\text{CaMg}_2\text{Fe}_3\text{Si}_8\text{O}_{22}(\text{OH})_2$	
	Log $f_{\text{O}_2}$ - T ( $P_{\text{Tot}} = 1 \text{ kb}$ ).....	89
Table II-11	Unit cell parameters bulk composition:	
	$\text{Na}_2\text{CaMg}_2\text{Fe}_3\text{Si}_8\text{O}_{22}(\text{OH})_2$ .....	90
Table II-12	Bracketing experiments: $\text{Na}_2\text{CaMgFe}_4\text{Si}_8\text{O}_{22}(\text{OH})_2$	
	Log $f_{\text{O}_2}$ - T ( $P_{\text{Tot}} = 1 \text{ kb}$ ).....	95
Table II-13	Unit cell parameters bulk composition:	
	$\text{Na}_2\text{CaMgFe}_4\text{Si}_8\text{O}_{22}(\text{OH})_2$ .....	96
Table II-14	Unit cell parameters of riebeckitic amphibole..	117
Table II-15	Iron amphibole stabilities.....	122
Table A1-1	Roedderites: $\text{Na}_2(\text{Mg,Fe})_5\text{Si}_{12}\text{O}_{30}$ .....	126
Table A1-2	Roedderite unit cell dimensions.....	127
Table AII-1	Complete experimental table:	
	$\text{Na}_2\text{CaMg}_5\text{Si}_8\text{O}_{22}(\text{OH})_2$ .....	130
Table AII-2	Complete experimental table:	
	$\text{Na}_2\text{CaFe}_5\text{Si}_8\text{O}_{22}(\text{OH})_2$ (I-W).....	133
Table AII-3	Complete experimental table:	
	$\text{Na}_2\text{CaFe}_5\text{Si}_8\text{O}_{22}(\text{OH})_2$ (QFM).....	135
Table AII-4	Complete experimental table:	
	$\text{Na}_2\text{CaFe}_5\text{Si}_8\text{O}_{22}(\text{OH})_2$ Log $f_{\text{O}_2}$ - T ( $P_{\text{Tot}} = 1 \text{ kb}$ ).....	138
Table AII-5	Complete experimental table:	
	$\text{Na}_2\text{CaMg}_4\text{FeSi}_8\text{O}_{22}(\text{OH})_2$ Log $f_{\text{O}_2}$ - T ( $P_{\text{Tot}} = 1 \text{ kb}$ ).....	142
Table AII-6	Complete experimental table:	
	$\text{Na}_2\text{CaMg}_3\text{Fe}_2\text{Si}_8\text{O}_{22}(\text{OH})_2$ Log $f_{\text{O}_2}$ - T ( $P_{\text{Tot}} = 1 \text{ kb}$ )..	144



Table AII-7 Complete experimental table:

$\text{Na}_2\text{CaMg}_2\text{Fe}_3\text{Si}_8\text{O}_{22}(\text{OH})_2$  Log  $f_{\text{O}_2}$  - T ( $P_{\text{Tot}}=1\text{kb}$ )..146

Table AII-8 Complete experimental table:

$\text{Na}_2\text{CaMgFe}_4\text{Si}_8\text{O}_{22}(\text{OH})_2$  Log  $f_{\text{O}_2}$  - T ( $P_{\text{Tot}}=1\text{kb}$ )..148

## FIGURES

Figure I-1	Amphibole structure.....	8
Figure I-2	Buffering systems.....	16
Figure I-3	Cell volume vs. composition for amphibole on QFM buffer.....	20
Figure I-4	Refractive indices (I-W).....	23
Figure I-5	Uniformity of cell volume on I-W throughout P and T.....	29
Figure I-6	Uniformity of cell volume along a given buffer.	33
Figure I-7	Variation of cell volume with $f_{O_2}$ .....	36
Figure I-8	Unit cell parameter variation for amphibole a-f on I-W.....	41
Figure II-1	Experimentally determined stability relations for Mg-richterite bulk composition.....	52
Figure II-2	Experimentally determined stability relations for ferrorichterite bulk composition (I-W).....	57
Figure II-3	Experimentally determined stability relations for ferrorichterite bulk composition (QFM).....	62
Figure II-4	Isobaric ( $P_{Tot} = 1\text{kb}$ ) Log $f_{O_2}$ - T diagram for ferrorichterite bulk composition.....	67
Figure II-5	Isobaric ( $P_{Tot} = 1\text{kb}$ ) Log $f_{O_2}$ - T diagram for $Mg_4Fe$ bulk composition.....	75
Figure II-6	Isobaric ( $P_{Tot} = 1\text{kb}$ ) Log $f_{O_2}$ - T diagram for $Mg_3Fe_2$ bulk composition.....	81
Figure II-7	Isobaric ( $P_{Tot} = 1\text{kb}$ ) Log $f_{O_2}$ - T diagram for $Mg_2Fe_3$ bulk composition.....	87

	6e
Figure II-8	Isobaric ( $P_{Tot} = 1\text{kb}$ ) $\text{Log } f_{O_2} - T$ diagram for MgFe <sub>4</sub> bulk composition.....93
Figure II-9	Isobaric ( $P_{Tot} = 1\text{kb}$ ) T-X section with oxygen fugacities defined by the H-Mt buffer.....99
Figure II-10	Isobaric ( $P_{Tot} = 1\text{kb}$ ) T-X section with oxygen fugacities defined by the QFM buffer.....101
Figure II-11	Isobaric ( $P_{Tot} = 1\text{kb}$ ) T-X section with oxygen fugacities defined by the C-CH <sub>4</sub> buffer.....103
Figure II-12	Isobaric ( $P_{Tot} = 1\text{kb}$ ) T-X section with oxygen fugacities defined by the W-Mt buffer.....105
Figure II-13	Isobaric ( $P_{Tot} = 1\text{kb}$ ) T-X section with oxygen fugacities defined by the I-W buffer.....107
Figure II-14	Composite isobaric $\text{Log } f_{O_2} - T$ diagram showing the maximum amphibole stabilities.....114
Figure II-15	Comparison of the thermal stabilities of richterite and ferrichterite (I-W).....118
Figure II-16	Comparison of the thermal stabilities of the iron amphiboles.....120

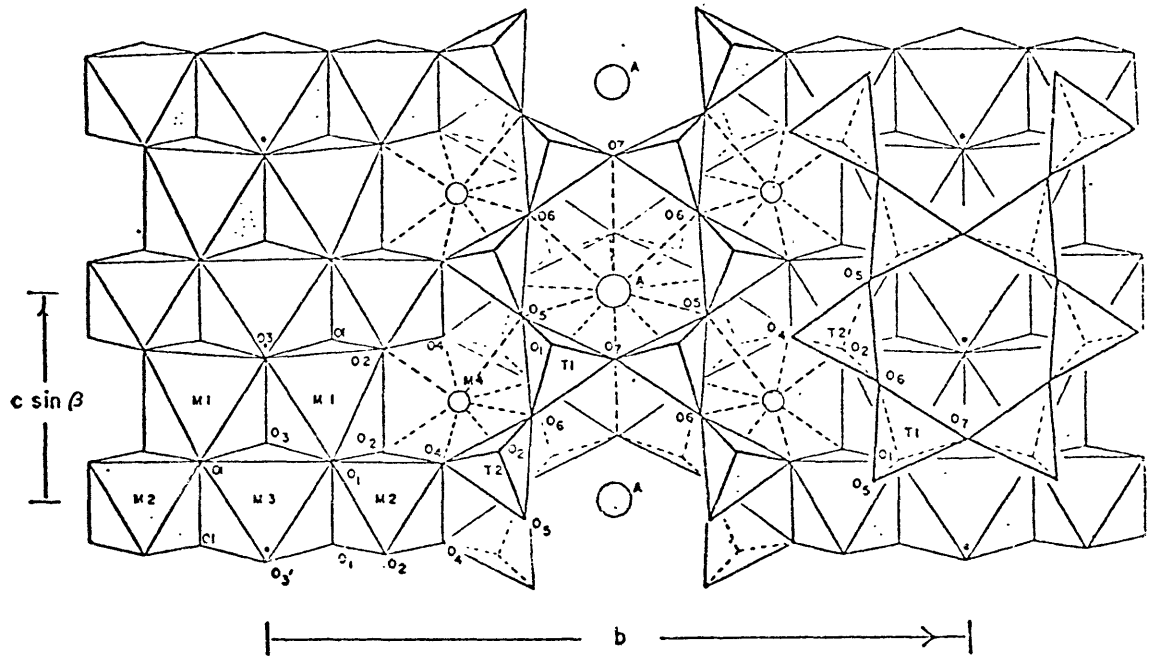
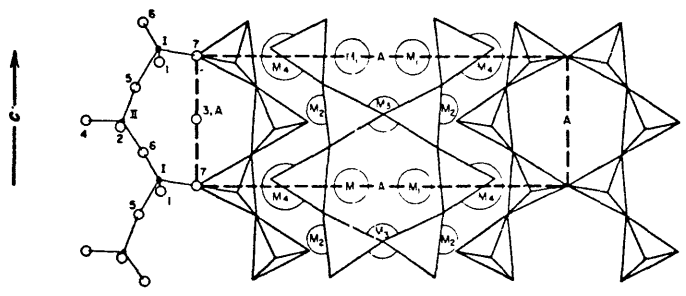
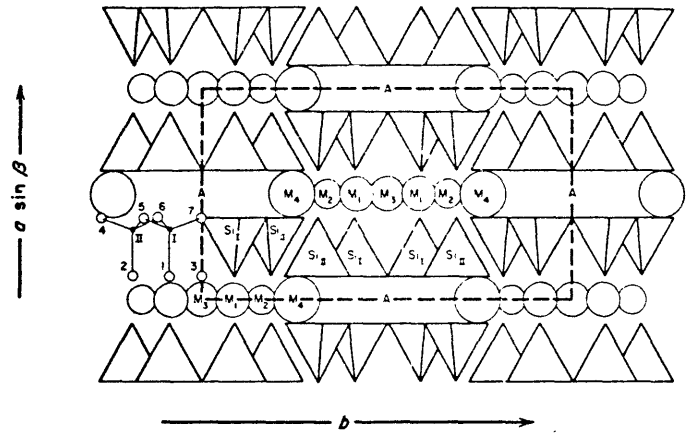
Richterites are monoclinic amphiboles containing high sodium, moderate calcium, and low alumina lying between the calcic and sodic amphiboles of Ernst (1968). Ideally, the formula is  $\text{Na}_2\text{Ca}(\text{Fe},\text{Mg})_5\text{Si}_8\text{O}_{22}(\text{OH})_2$ , but substitutions of  $\text{K}^+ \rightarrow \text{Na}^+$  and  $\text{Fe}^{2+} \rightarrow \text{OH}^-$  are common in nature. The amphibole structure (see fig. I-1) consists of double chains of silicon tetrahedra linked by 5 octahedra of six-fold coordination: 2 M(1), 2 M(2), and 1 M(3) and 2 larger 6-8 fold M(4) sites (Papike *et al.*, 1969). The still larger 8-12 fold A site completes this linking strip of cations. In richterite the A site is 8-fold and contains Na, while the M(4) site is also 8-fold and contains equal amounts of Na and Ca. Fe and Mg are distributed between the remaining M sites.  $\text{OH}^-$  occupies the O(3) sites.

Richterite is a rather uncommon alkali amphibole found in varied environments. Occurrences include alkaline and per-alkaline basalts, gneisses, impure metamorphosed limestones, and meteorites. Analyses compiled by Deer, Howie and Zussman (1963) indicate most natural samples are relatively Fe free, or, when containing iron, much of it is in the ferric state. Richteritic amphibole has also been reported in an iron meteorite (Olsen, 1967) and in an enstatite chondrite (Douglas *et al.*, 1968). Both of these examples contain significant amounts of  $\text{F}^-$  replacing  $\text{OH}^-$ .

Natural examples of ferrous richterites, though few in number, are known. The lunar basalts have yielded one rich-

Figure I-1. Amphibole structure. Top: Ernst (1968)

Bottom: Papike *et al.* (1969)



terite of composition  $(K_{0.28}Na_{2.47}Ca_{0.33})(Mg_{3.57}Fe_{1.50}Al_{0.12})(Si_{7.99}Al_{0.11}O_{22})(OH,F)_2$  (Gay *et al.*, 1970). All Fe was assumed to be ferrous. The fluorine content was uncertain and probably very high judging from the fluororichterites synthesized by Huebner and Papike (1970). Ferrorichterite has been reported by Nicholls and Carmichael (1969) from a Kenya pantellerite both in phenocrysts  $(K_{0.28}Na_{1.82}Ca_{0.77})(Fe_{4.68}Ti_{0.20}Mn_{0.13}Mg_{0.23})(Si_{7.78}Al_{0.11})O_{22}(OH_{1.39}F_{0.61})$  and as microclites in the glass  $(K_{0.31}Na_{2.02}Ca_{0.70})(Fe_{4.75}Ti_{0.19}Mn_{0.13}Mg_{0.17})(Si_{7.75}Al_{0.11})O_{22}(OH_{1.38}F_{0.62})$ .

#### Previous Investigations

Experimental work has been confined primarily to the magnesian end member. The fluorine analog was first synthesized by Eitel (1954) and Comeforo and Kohn (1955). Hydrous richterite was synthesized by Phillips and Rowbotham (1968). Huebner and Papike (1970) studied the effect of potassium substitution in richterite and the stability field of richterite was first defined by Forbes (1971).

Work on ferrous compositions has been limited to a study of the stability of the hydrous analog of a lunar richterite (Charles *et al.*, 1971) and to the synthesis of a potassic ferrorichterite by Huebner and Papike (1970). The cell parameters found by previous investigators and those reported in this paper are compared in table I-1.

The molecule  $Na_2Mg_6Si_8O_{22}(OH)_2$  "magnesiorichterite" was first prepared by Iiyama (1963). Gibbs (1962) determined

Table I-1. Compositions and Cell Parameters of Synthetic Richterites

Reference	a (Å)	b (Å)	c (Å)	$\beta$	V (Å <sup>3</sup> )
	$\text{Na}_2\text{CaMg}_5\text{Si}_8\text{O}_{22}(\text{OH})_2$				
Phillips and Rowbotham (1968) (refinement of Huebner and Papike 1970)	9.902(2)	17.980(4)	5.269(1)	104°12.7'(1.1')	909.4(3)
Huebner and Papike (1970)	9.907(2)	17.979(4)	5.269(1)	104°15.1'(0.9')	909.6(4)
Forbes (1971)	9.909(1)	17.978(5)	5.268(1)	104°13'(2')	909.9(2)
This paper	9.902(2)	17.980(3)	5.269(1)	104°13'(1')	909.3(3)
	$\text{KNaCaFe}_5\text{Si}_8\text{O}_{22}(\text{OH})_2$ (C-CH <sub>4</sub> Buffer)				
Huebner and Papike (1970)	10.172(3)	18.201(7)	5.290(2)	104°32'(2')	948.2(4)
	$\text{Na}_2\text{CaFe}_5\text{Si}_8\text{O}_{22}(\text{OH})_2$ (IW Buffer)				
This paper	9.982(7)	18.223(6)	5.298(5)	103°44'(7')	936.2(1.0)
Calculated from Huebner and Papike (1970)					936.6



the cell constants of its fluorine analog. In this paper magnesiorichterite will refer to the composition  $\text{Na}_2\text{CaMg}_5\text{Si}_8\text{O}_{22}(\text{OH})_2$  and should not be confused with the noncalcium bearing richterite.

## PART I: PHYSICAL PROPERTIES

## Experimental Procedure

Six compositions equally spaced along the join  $\text{Na}_2\text{CaMg}_5\text{Si}_8\text{O}_{22}(\text{OH})_2$ - $\text{Na}_2\text{CaFe}_5\text{Si}_8\text{O}_{22}(\text{OH})_2$  were prepared from constituent oxides. Chemicals and steps in their preparation are given in table I-2. The mixes were homogenized as follows:

- (1) 5 min. hand grinding in an agate mortar
- (2) 30 min. grinding in an auto-mortar
- (3) 10 min. hand grinding
- (4) 2 hrs. grinding in an auto-mortar.

Homogeneity was observed microscopically. Iron bearing mixes were reduced by heating them for 10 min. at approximately  $750^\circ\text{C}$  under hydrogen. If held longer at these conditions, the charge became welded and was difficult to work with. X-ray patterns were prepared to insure all iron was in the native state. Portions of each mix were reoxidized in air to convert the iron to a mixture of  $\text{Fe}_2\text{O}_3$  and  $\text{Fe}_3\text{O}_4$ . These mixes were used for experiments on HMT buffer and for checking experiments on QFM and NNO buffers. In effect the buffer curves were approached from both directions and uniform results were obtained in all cases.

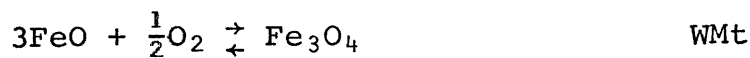
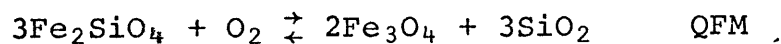
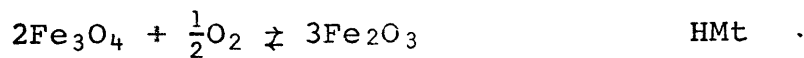
From 20 to 130 mgm of mix plus 3 to 15 mgm of water, depending upon the amount of iron in the mix and the additional 1.8-2.2%  $\text{H}_2\text{O}$  necessary for form amphibole, were encapsulated. Additional  $\text{H}_2\text{O}$  above these requirements was kept to a minimum to prevent leaching Na and Si from the products. Magnesio-

Table I-2. Reagents

<u>Oxide</u>	<u>Phase</u>	<u>Lot #</u>	<u>Preparation</u>
Na <sub>2</sub> O	Na <sub>2</sub> Si <sub>2</sub> O <sub>5</sub>	NaCO <sub>3</sub> -Baker 31373	as in Schairer and Bowen (1955)
		SiO <sub>2</sub> -Corning Lump cullet 7940	
CaO	CaO	CaCO <sub>3</sub> -Baker 11246	1. Decarbonate at 1000°C for 5 days to constant wt.
			2. Dried before each weighting to constant wt.
SiO <sub>2</sub>	SiO <sub>2</sub> (glass)	Corning Lump cullet 7940	1. Cleaned in Aqua Regia.
			2. Washed in distilled H <sub>2</sub> O.
			3. Dried at 1000°C to constant wt.
MgO	MgO(periclase)	Fisher 787699	Dried to constant wt. at 1000°C.
FeO	Fe <sub>2</sub> O <sub>3</sub>	Fisher 534290	Dried at 700°C to constant wt.

richterite mixes were sealed in Au or Pt capsules and welded shut with a carbon arc welder. Experimental mixtures containing iron were placed in  $\text{Ag}_{80}\text{Pd}_{20}$  capsules and buffered by one of three techniques:

- (1) The oxygen buffer technique of Eugster (1957).



- (2) The hydrogen diffusion membrane of Shaw (1967).

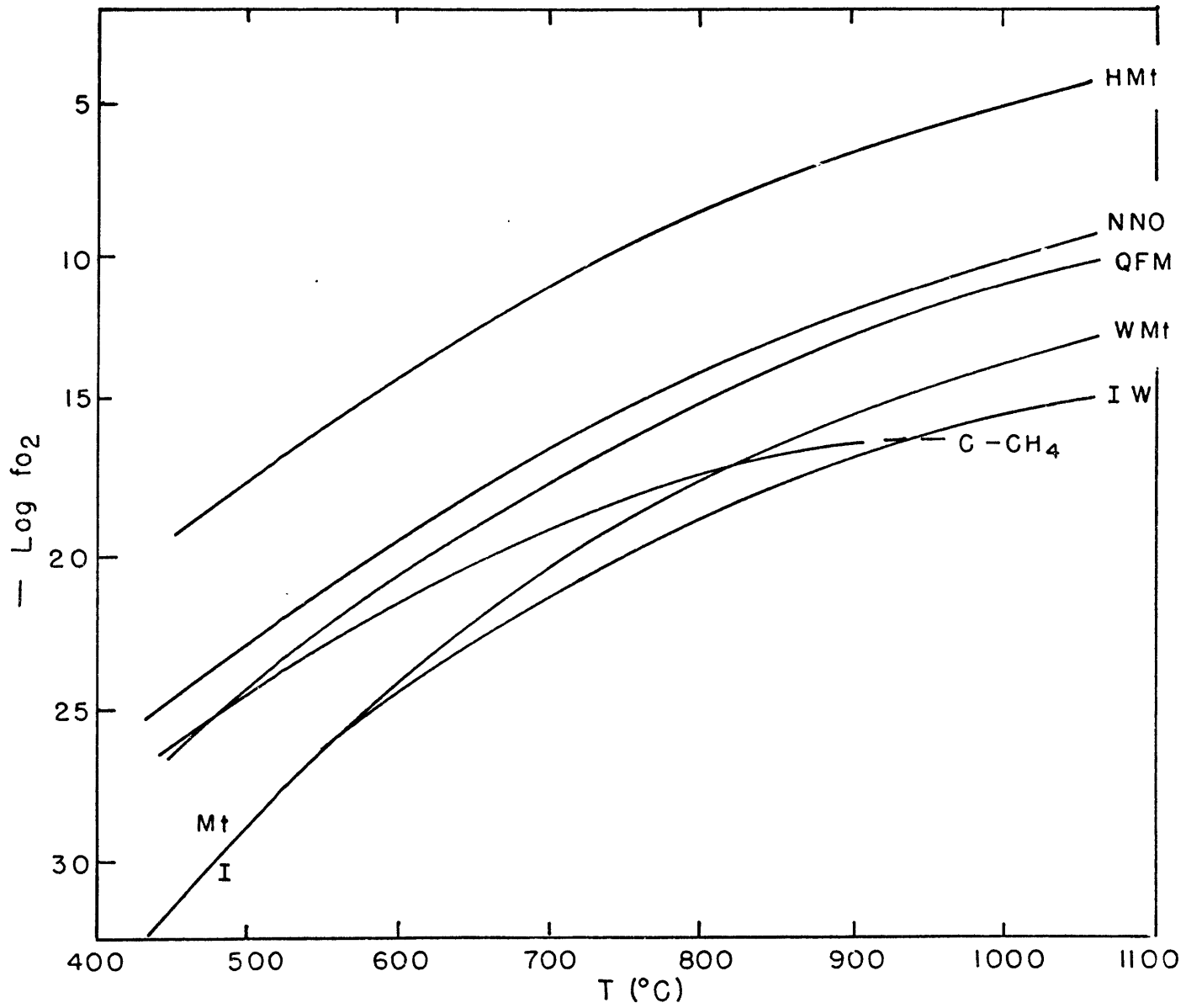
- (3) The graphite-methane buffer of Eugster and Skippen (1967):

These buffers are plotted in figure I-2. When making experiments on both NNO and QFM it was necessary to protect the  $\text{Ag}_{80}\text{Pd}_{20}$  tube with Au or Ag foil. This was necessary at all temperatures for NNO to prevent alloying of the Ni and  $\text{Ag}_{80}\text{Pd}_{20}$  and at temperatures above about  $800^\circ\text{C}$  for QFM to protect the  $\text{Ag}_{80}\text{Pd}_{20}$  from erosion by the buffer.

Capsules were placed in cold seal bombs of composition Haynes Alloy No. 25 (Stellite) or Rene' 41. The pressure medium was either water, methane, or argon, depending on the buffer, pressure, and temperature conditions required and was measured by a Heise bourdon gauge. Bombs were heated in ei-

Figure I-2. Isobaric ( $P_{\text{Tot}} = 1 \text{ kb}$ )  $\text{Log } f_{\text{O}_2}$  - T diagram illustrating the buffering systems used in this study.

HMt - Hematite - Magnetite  
NNO - Nickel - Bunsenite  
QFM - Quartz - Fayalite - Magnetite  
C-CH<sub>4</sub> - Graphite - Methane  
Wmt - Wustite - Magnetite  
IMt - Iron - Magnetite  
IW - Iron - Wustite



ther horizontal Lindberg Hevi-Duty furnaces or vertical furnaces produced by the Hevi-Duty Electric Company. Temperature was regulated by Harrel proportional, Barber Coleman on-off, or Honeywell on-off controllers. Temperature was recorded on a Honeywell recorder and monitored regularly with a Leeds and Northrup K-4 potentiometer. Temperature was measured by chromel-alumel thermocouples which were calibrated against the melting point of NaCl and CsCl. Errors in temperature are no more than 3 to 5°C and pressure no more than 15 bars.

#### Description of Phases

Microscopic examination reveals that magnesiorichterite crystallized at 800°C and 1 kb for 2 days produced 98-100% amphibole. The amphibole consisted of elongate euhedral grains sometimes occurring in a felty mass. Amphibole containing iron was produced most readily on the IW buffer. In fact, compositions containing more iron than  $Mg_2Fe_3$  invariably produced 20-30% clinopyroxene along with amphibole on more oxidizing buffers. Above C- $CH_4$  buffer only the  $Mg_4$ -Fe compositions could be produced at greater than 95% purity. Even  $Mg_4Fe$  would yield significant amounts of clinopyroxene (>10%) on the HMT buffer. High purity is important since the pyroxene produced on HMT is acmitic judging from the powder x-ray pattern. Any more than a few percent of this insures nonstoichiometric amphibole as the lattice parameters for  $MgFe_4$  on various buffers show. Small amounts (<5%) of

pyroxene, olivine, and glass were assumed to be roughly equal to the bulk composition of the mix. For such a small amount of pyroxene the partitioning of Fe and Mg between pyroxene and amphibole was ignored. The effect of the introduction of pyroxene to the products is shown in figure I-3 and table I-3. Between  $Mg_4Fe$  and  $Mg_3Fe_2$  pyroxene appears and on  $Mg_3Fe_2$  it is about 10-15% of the product. The cell volume for  $Mg_3Fe_2$  is approximately the same as that for  $Mg_4Fe$ . Pyroxene increases in abundance until 30-40% of the charge is pyroxene at  $Fe_5$ . Attempts to produce ferrorichterite on QFM yielded a very dark green amphibole plus pyroxene. Presumably, the color indicates the increased content of ferric iron in the amphibole.

The amphibole changed greatly in optical character along the magnesiorichterite-ferrorichterite join. Figure I-4 and table I-4 display the change in refractive indices on Fe-FeO. The extinction angle ( $\gamma \wedge Z$ ) increases slightly across the compositional field being roughly 5-10° on the magnesium end and 10-15° on the iron end. Color varies from white to a deep grass green across the compositional field. Pleochroism is green-yellow green-green and is most easily seen in the more ferrous amphiboles.

Experiments conducted on IW at low temperatures (500-550°C) produced a finely crystalline mass containing >95% amphibole with subordinate pyroxene, olivine, and clear glass for the compositions  $MgFe_4$  through  $Mg_2Fe_3$ . Most of the crystals, regardless of composition, were  $5\mu$  in greatest dimension.



Figure I-3. Cell volume vs. composition for amphibole grown on the QFM buffer at various pressures and temperatures.

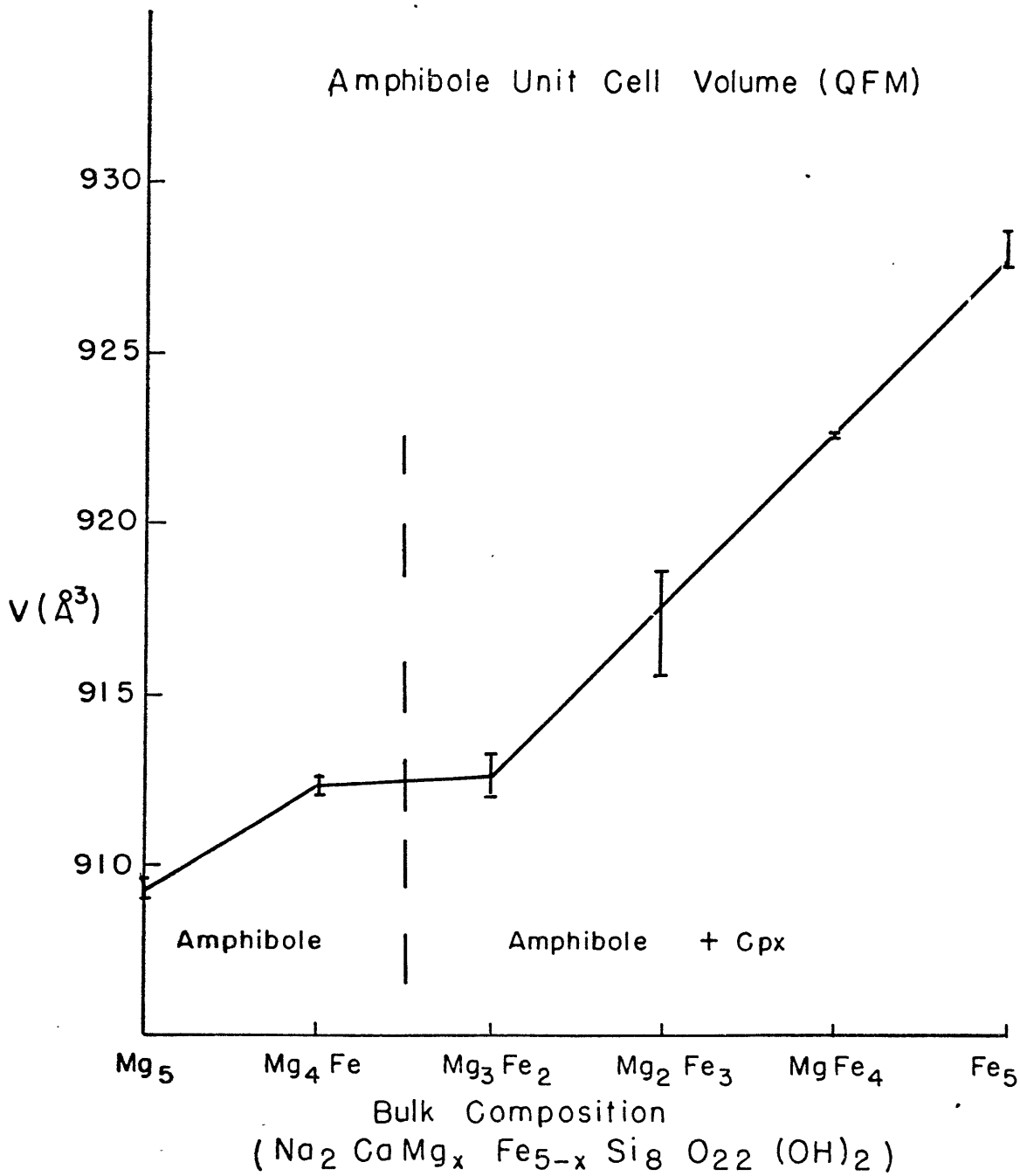


Table I-3. Unit Cell Volumes of Amphibole

Bulk Composition	Coexisting Phases	(QFM)			
		P (±15 bars)	T (±5°C)	V (Å <sup>3</sup> )	V <sub>Ave</sub> (Å <sup>3</sup> )
Na <sub>2</sub> CaMg <sub>5</sub> Si <sub>8</sub> O <sub>22</sub> (OH) <sub>2</sub>	A	-	-	-	909.3(0.3)
Mg <sub>4</sub> Fe	A	1000	800	912.2(0.3)	
"	"	"	"	912.3(0.3)	
"	"	"	650	912.4(0.4)	912.4(0.3)
"	"	"	600	912.9(0.8)	
Mg <sub>3</sub> Fe <sub>2</sub>	A + Cpx	"	900	911.7(1.8)	
"	"	"	850	911.0(0.2)	
"	"	"	700	914.5(2.8)	
"	"	"	650	912.9(0.3)	912.7(0.6)
"	"	"	550	913.1(1.2)	
"	"	7000	600	913.2(0.2)	
Mg <sub>2</sub> Fe <sub>3</sub>	"	1000	700	918.2(0.4)	
"	"	2000	500	916.1(0.6)	917.2(1.5)
MgFe <sub>4</sub>	"	1000	725	922.5(2.1)	
"	"	7000	500	922.7(0.6)	922.6(0.1)
Fe <sub>5</sub>	"	1000	475	929.0(0.9)	
"	"	4000	475	927.7(0.9)	
"	"	7000	500	927.7(0.7)	928.1(0.5)

Figure I-4.  $\alpha$  and  $\gamma$  refractive indices for the amphibole series grown on I-W buffer.  $\text{Mg}_3\text{Fe}_2$  and  $\text{Mg}_2\text{Fe}_3$  yielded only bulk indices.

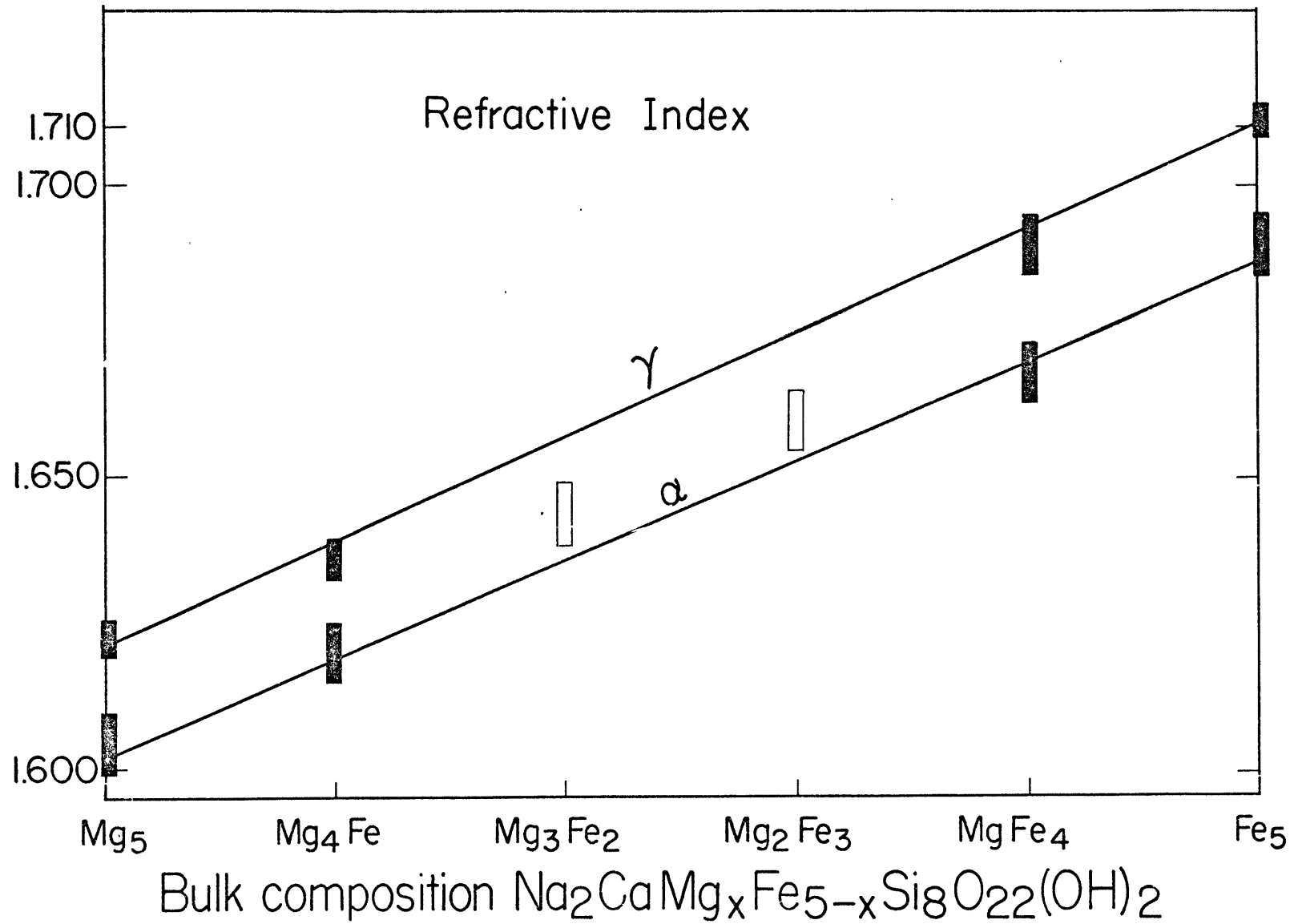


Table I-4. Optical Properties

Position $2\text{CaMg}_5\text{Fe}_{5-x}\text{Si}_8\text{O}_{22}(\text{OH})_2$	Buffer	$\alpha$	$\gamma$	Mean R.I.	Maximum Size ( $\mu$ )
	-----	1.604(5)	1.622(3)	-----	35 x 5
Fe	IW	1.620(5)	1.636(3)	-----	15 x 3
	C-CH <sub>4</sub>	-----	-----	1.632(5)	<5
	QFM	1.620(5)	1.636(3)	-----	25 x 5
	NNO	-----	-----	1.632(5)	7 x 1
	HMt	1.616(5)	1.630(3)	-----	10 x 2
Fe <sub>2</sub>	IW	-----	-----	1.644(5)	5 x 1
Fe <sub>3</sub>	"	-----	-----	1.660(5)	5 x 1
e <sub>4</sub>	"	1.668(5)	1.680(5)	-----	50 x 10
	"	1.690(5)	1.710(4)	-----	10 x 2

The  $MgFe_4$  richterite was difficult to produce at less than 5kb. Almost invariably charges of this composition contained >10% pyroxene at low pressures. This  $MgFe_4$  amphibole was always very hard and brittle while all other compositions with lower Fe were soft and fibrous.

Ferrorichterite can be characterized as a grass green stubby amphibole with  $n_\gamma = 1.710 \pm .003$  and  $n_\alpha = 1.690 \pm .005$ . Two varieties were synthesized. Shorter synthesis experiments (<10 days) at higher temperatures (600-700°C) resulted in a coarse amphibole with about 10% clinopyroxene, fayalite, and trace glass. Longer experiments (22-30days) at lower temperatures (500-530°C) yielded fine grained amphibole plus a few percent clinopyroxene, olivine, and clear glass. The pyroxene was a striking bright green with a refractive index around 1.730. Fayalite appeared as roughly equant grains with a light brown color. These longer experiments were of much greater purity being greater than 95% amphibole. It is important to point out that less ferrous compositions yielded only one amphibole regardless of the synthesis time.

For the series in general, clinopyroxene, olivine and glass were always less than 5% for compositions  $Mg_5$  through  $Mg_2Fe_3$  and long experiments on  $Fe_5$ . Short experiments on  $Fe_5$  and most experiments on  $MgFe_4$  had 10% or more clinopyroxene, olivine and glass. Long experiments on  $Fe_5$  contained more glass than those on any other composition, but still only about 2-3%.

#### X-ray Determinations

The unit cell parameters were determined using a Norelco x-ray powder diffraction goniometer. Scans of  $\frac{1}{2}^\circ/\text{min.}$  at a strip chart recorder rate of  $\frac{1}{2}"/\text{min.}$  were satisfactory to fix the peak positions of amphibole to  $\pm .01^\circ$  when standardized against  $\text{BaF}_2$  Baker Lot #308 ( $a=6.1971 \pm .002 \text{ \AA}$ ).  $\text{BaF}_2$  in turn was standardized against diamond ( $a=3.56703 \pm .0018 \text{ \AA}$ ).  $\text{BaF}_2$  has 4 usable reflections between  $24$  and  $49^\circ$ . The (220) reflection of  $\text{BaF}_2$  at  $41.164^\circ$  was not usable for compositions more ferrous than  $\text{Fe}_2\text{Mg}_3$  due to interference with the powerful (261) reflection of the richterites. The richterites were indexed and cell parameters calculated using a program developed by Evans, Appleman, and Handwerker (1963). Twenty-four reflections for magnesiorichterite were unambiguously indexed from Huebner and Papike (1970). As iron was added to the structure, the number of usable reflections decreased somewhat to sixteen for ferrorichterite. Some peaks, for example (020) decrease in intensity, others are less distinct due to poorer crystallization, and one, (261) interferes with a standard peak.

A continuous shift in peak position toward lower angles and changes in intensity of a given reflection occur with addition of iron. Sample results are reproduced in Table I-5 for magnesiorichterite and ferrorichterite. All cell dimension data with buffer and P-T conditions are listed in Table I-6.

The uniformity of cell parameters on IW in P-T space is shown in Figure I-5 for  $\text{Mg}_4\text{Fe}$ ,  $\text{Mg}_3\text{Fe}_2$ , and  $\text{Mg}_2\text{Fe}_3$ . Cell volume remains essentially constant in the pressure range 1 to 10kb and temperature range 500 to  $650^\circ\text{C}$ .



Table I-5.

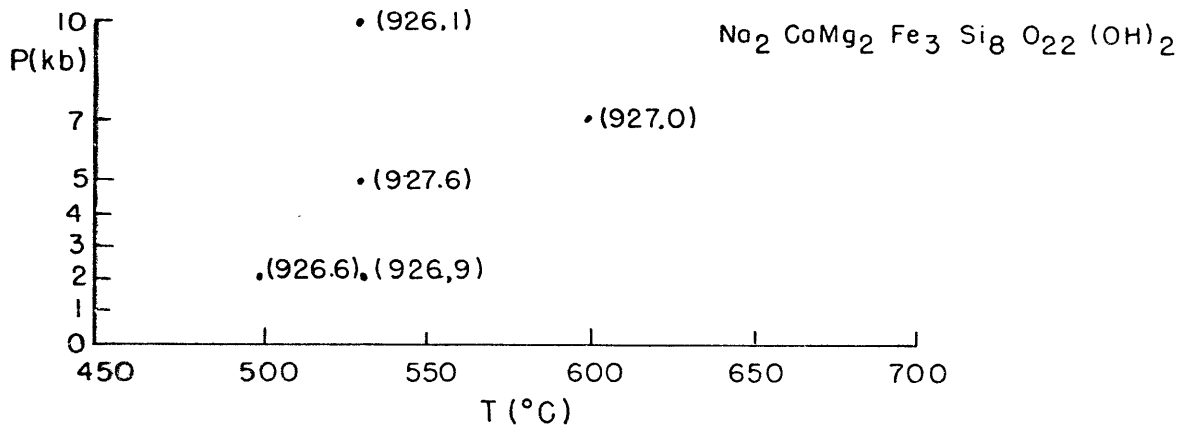
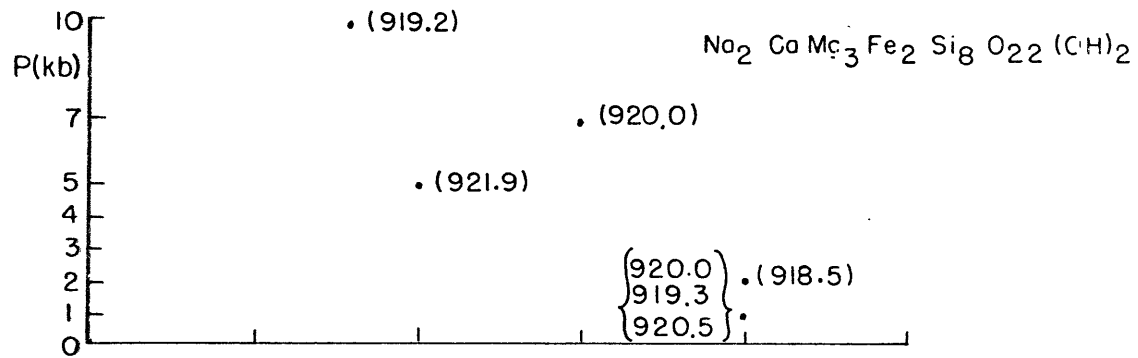
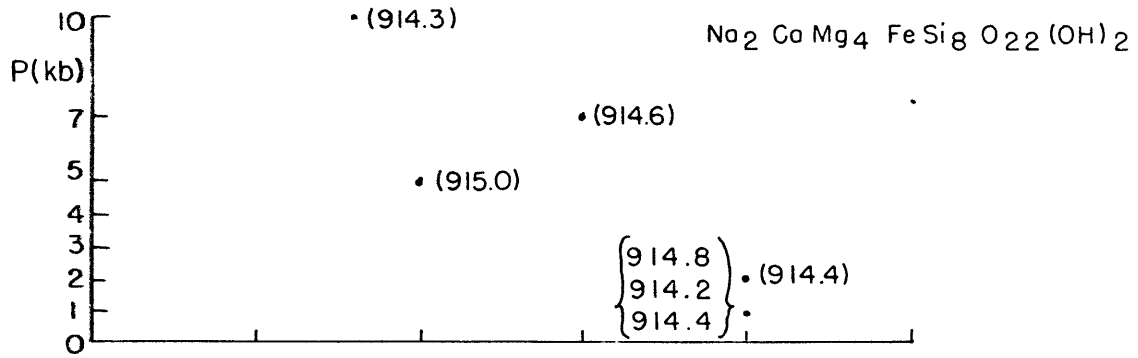
Na <sub>2</sub> CaMg <sub>5</sub> Si <sub>8</sub> O <sub>22</sub> (OH) <sub>2</sub>					Na <sub>2</sub> CaFe <sub>5</sub> Si <sub>8</sub> O <sub>22</sub> (OH) <sub>2</sub>					
hkl	d <sub>hkl</sub>		2θ		I/I <sub>0</sub>	d <sub>hkl</sub>		2θ		
	obs.	calc.	obs.	calc.		obs.	calc.	obs.	calc.	
020	8.9908	8.9928	9.829	9.827	10	-	9.1079	-	9.703	-
110	8.4682	8.4701	10.437	10.435	40	8.5767	8.5614	10.323	10.323	100
-111	4.8637	4.8603	18.224	18.237	20	-	4.8925	-	18.116	-
200	4.7997	4.7977	18.469	18.477	15	4.8522	4.8498	18.268	18.277	10
040	4.4954	4.4953	19.732	19.732	30	4.5582	4.5540	19.457	19.476	20
111	4.0053	4.0067	22.175	22.167	15	4.0542	4.0506	21.904	21.924	5
-131	3.8629	3.8615	23.003	23.012	30	3.8964	3.8958	22.796	22.806	10
131	3.3888	3.3899	26.275	26.267	65	3.4287	3.4288	25.964	25.964	35
240	3.2810	3.2801	27.155	27.163	45	3.3183	3.3198	26.844	26.832	25
310	3.1503	3.1514	28.305	28.295	90	3.1841	3.1834	27.998	28.004	65
221	2.9591	2.9588	30.175	30.179	60	2.9962	2.9953	29.793	29.803	25
-151	2.9298	2.9297	30.485	30.486	15	-	2.9604	-	30.162	-
330	2.8228	2.8217	31.670	31.683	25	2.8525	2.8538	31.332	31.317	15
-331	2.7341	2.7346	32.725	32.720	20	-	2.7550	-	32.470	-
151	2.7061	2.7056	33.075	33.068	100	2.7386	2.7392	32.670	32.663	70
061	2.5846	2.5859	34.677	34.673	45	2.6154	2.6152	34.256	34.258	35
-202	2.5260	2.5260	35.508	35.508	65	2.5396	2.5396	35.312	35.312	50
350	2.3905	2.3913	37.593	37.581	15	-	2.4182	-	37.147	-
-171	2.2898	2.2898	39.314	39.314	25	-	2.3160	-	38.851	-
-312	2.2703	2.2704	39.665	39.664	25	2.2823	2.2819	39.448	39.455	15
261	2.1659	2.1656	41.664	41.669	45	-	2.1932	-	41.122	-
202	2.0542	2.0546	44.043	44.034	25	2.0757	2.0773	43.565	43.579	10
351	2.0268	2.0265	44.627	44.679	15	2.0518	2.0520	44.099	44.093	20
510	1.9090	1.9091	47.593	47.596	15	-	1.9290	-	47.069	-

(800°C, 1kb, 2da.)

(IW, 530°C, 5kb, 30da.)

Figure I-5. Uniformity of unit cell volume throughout the P, T space investigated. Higher iron compositions were not plotted owing to fewer data points. Uniformity may not be true for Mg<sub>5</sub>.

CELL VOLUME vs P & T  
(Fe - FeO Buffer)



Mg-richterite has a rather low stability limit with respect to pressure as indicated by the experiments listed in table I-7. Changes in cell dimensions occurred between 2 and 7 kb while the charge was still >95% amphibole. Experiments of 6 days at 7 kb and 600°C using an oxide mix yielded quartz in addition to amphibole. This quartz is gradually resorbed and after 20 days is totally resorbed. At 10 kb and 510°C experiments of 25 days duration show persistent quartz. The amphibole at 10 kb has a powder pattern not unlike tremolite. The cell parameters with increasing P do show some trend toward tremolite. Most striking is the distinct trend of  $a \sin \beta$  and  $b$ .

Addition of Fe to richterite apparently stabilizes the structure at higher P since all experiments at high P containing iron show no variation in cell parameters. Higher iron concentrations were not plotted since only 3 or 4 high purity experiments were made on each. These did not show any trend in cell volume with P and T.

The uniformity of cell volume on a given buffer is shown in Figure I-6 for  $Mg_4Fe$  at a  $P_{Tot}$  of 1 kb. Two points should be noted here. One, the uniformity of amphibole cell volume even in the presence of large (>10%) amounts of pyroxene on HMT is evident. Actual characterization of the pyroxene will be presented when the entire phase equilibria of the richterites are examined. Preliminary examination of its cell constants indicate it is an acmitic diopside. Two, the apparent constancy of cell volume along C-CH<sub>4</sub> buffer is unexpected. Since the C-CH<sub>4</sub> buffer does not parallel the other buffer curves, the

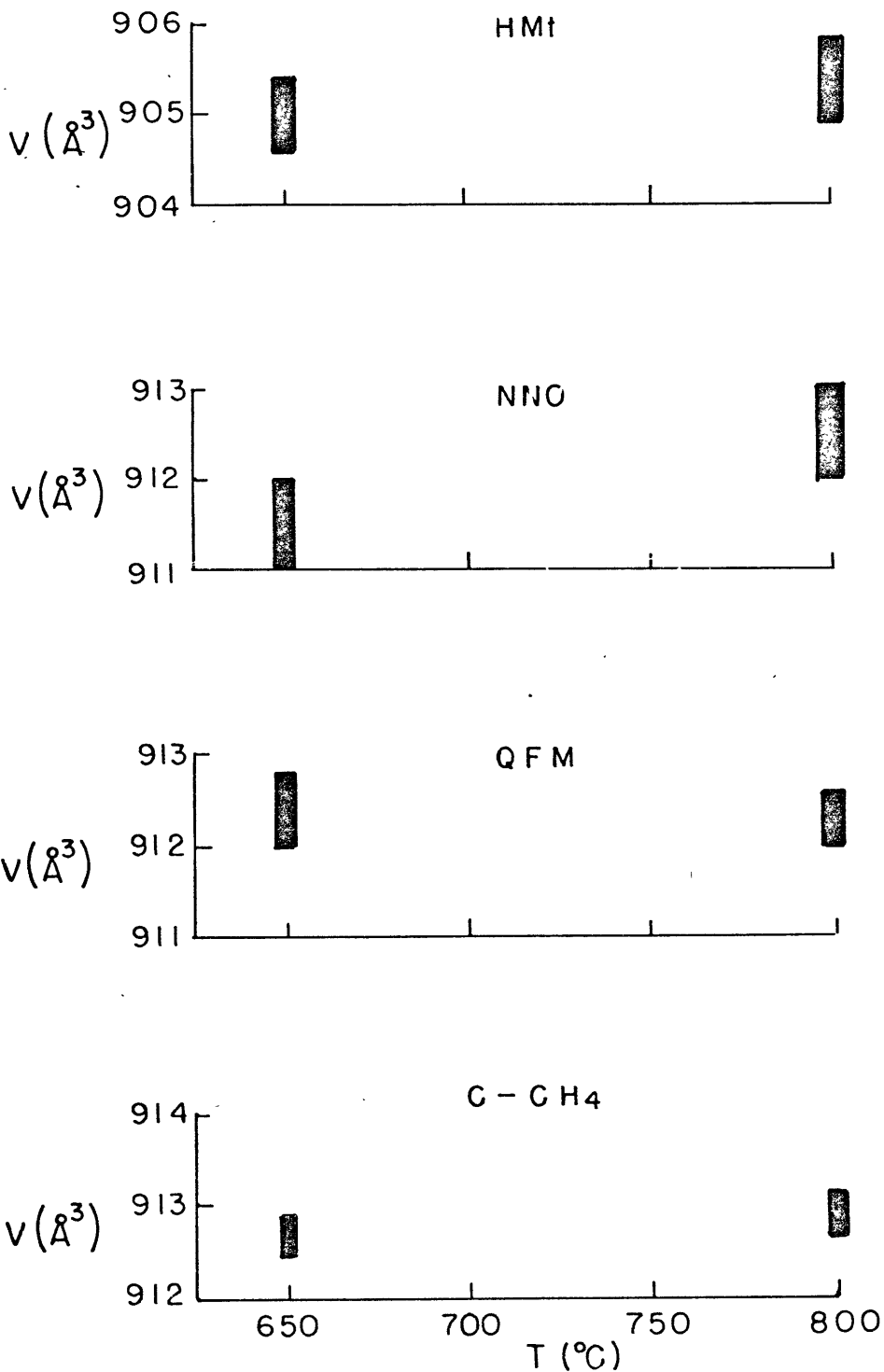
Table I-7. Mg-Richterite at Increasing Pressure

<u>P</u> (bars)	<u>T</u> (°C)	<u>Duration</u> (hrs)	<u>a<sub>o</sub></u> (Å)	<u>b<sub>o</sub></u> (Å)	<u>c<sub>o</sub></u> (Å)	<u>β</u> —	<u>V<sub>o</sub></u> (Å <sup>3</sup> )	<u>asinβ</u> (Å)
1000	700	72	9.901(2)	17.976(4)	5.270(1)	104°12'(1')	909.4(0.3)	9.599
2000	800	48	9.903(1)	17.982(2)	5.267(1)	104°14'(1')	909.2(0.1)	9.599
5000	700	119	9.884(7)	17.984(7)	5.268(3)	104°4'(5')	907.7(0.6)	9.587
7000	600	456	9.893(3)	18.003(8)	5.268(2)	104°14'(2')	909.5(0.4)	9.589
10,000	510	600	9.896(7)	18.001(9)	5.270(3)	104°20'(3')	909.6(0.6)	9.588
Tremolite (Papike et al. 1969)			9.818(5)	18.047(8)	5.275(3)	104°39'(3')	904.2(0.6)	9.499

---

Figure I-6. Uniformity of cell volume along a given buffer  
for  $\text{Mg}_4\text{Fe}$  at  $P_{\text{Tot}} = 1 \text{ kb}$ .

Cell Volume vs T For  
 $\text{Na}_2 \text{Ca Mg}_4 \text{Fe Si}_8 \text{O}_{22} (\text{OH})_2$



volume should increase with higher  $f_{\text{H}_2}$ . For so small a concentration of iron this is not recognized. Other compositions of amphibole on higher buffers will be examined closely in the phase equilibrium studies for uniformity with P and T.

Figure I-7 exhibits the variation in cell volume and  $a \sin \beta$  with oxygen fugacity at  $P_{\text{Tot}} = 1 \text{ kb}$ ,  $T = 650^\circ\text{C}$ , and constant composition ( $\text{Mg}_4\text{Fe}$ ). Cell volume and  $a \sin \beta$  are seen to decrease and then level off. Somewhere above an  $f_{\text{O}_2}$  defined by the NNO buffer, pyroxene appears in increasing amounts causing the unit cell volume of the amphibole to drop off rapidly. The trend in lattice parameters is generally toward magnesioriebeckite.

Since amphibole of higher purity was synthesized along the IW buffer, the cell parameters calculated from these compositions will be examined very closely. Variations in these parameters lend insight into the richterite structure. The data plotted in Figure I-8 a-f are taken from Table I-6. Both ferrorichteritic amphiboles are plotted with the one of less total amphibole in parens. Certain facts should be noted. a, c, and  $a \sin \beta$  increase almost linearly proceeding from  $\text{Mg}_5$  to  $\text{MgFe}_4$ . Above this bulk composition, the curve is seen to branch. This branching feature is observed for all parameters. b exhibits a slight dip below linearity on the compositions  $\text{Mg}_4\text{Fe}$ ,  $\text{Mg}_3\text{Fe}_2$ , and  $\text{Mg}_2\text{Fe}_3$ .  $\beta$  decreases almost monotonically. The volume shows a slightly negative volume of mixing for the compositions  $\text{Mg}_4\text{Fe}$  and  $\text{Mg}_3\text{Fe}_2$ . Ideal mixing of course would be a linear curve.



Figure I-7. Variation of cell volume with  $\text{Log } f_{\text{O}_2}$  for  $\text{Mg}_4\text{Fe}$   
at  $T=650^\circ\text{C}$ ,  $P_{\text{Tot}}=1 \text{ kb}$ .

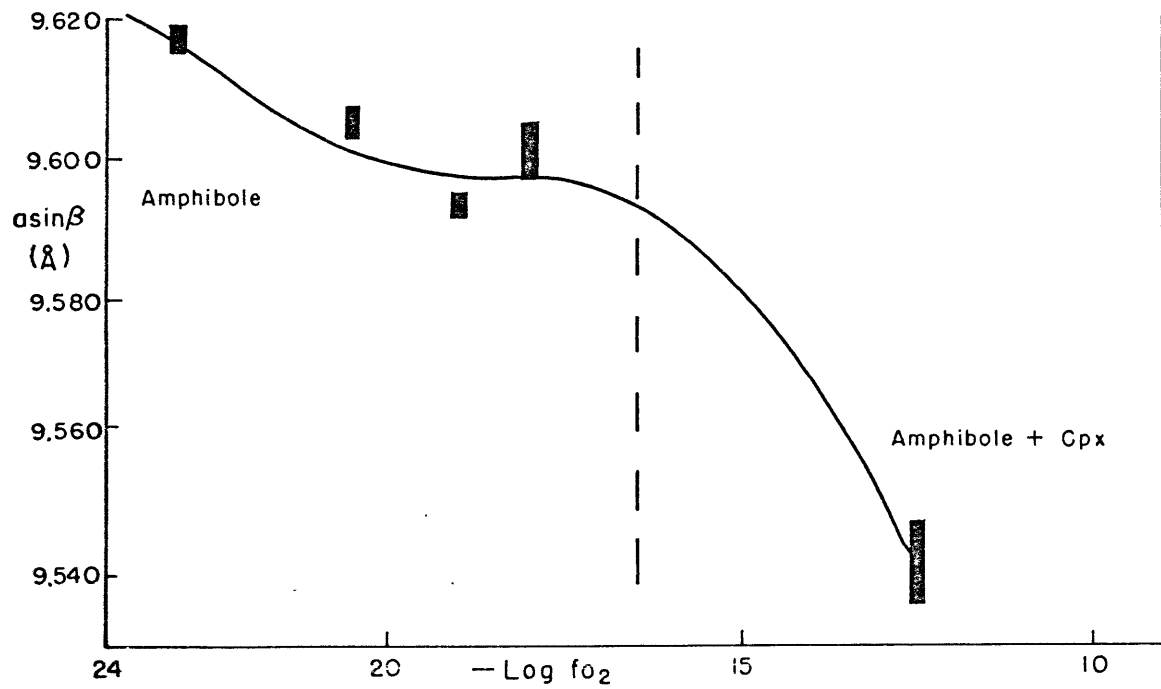
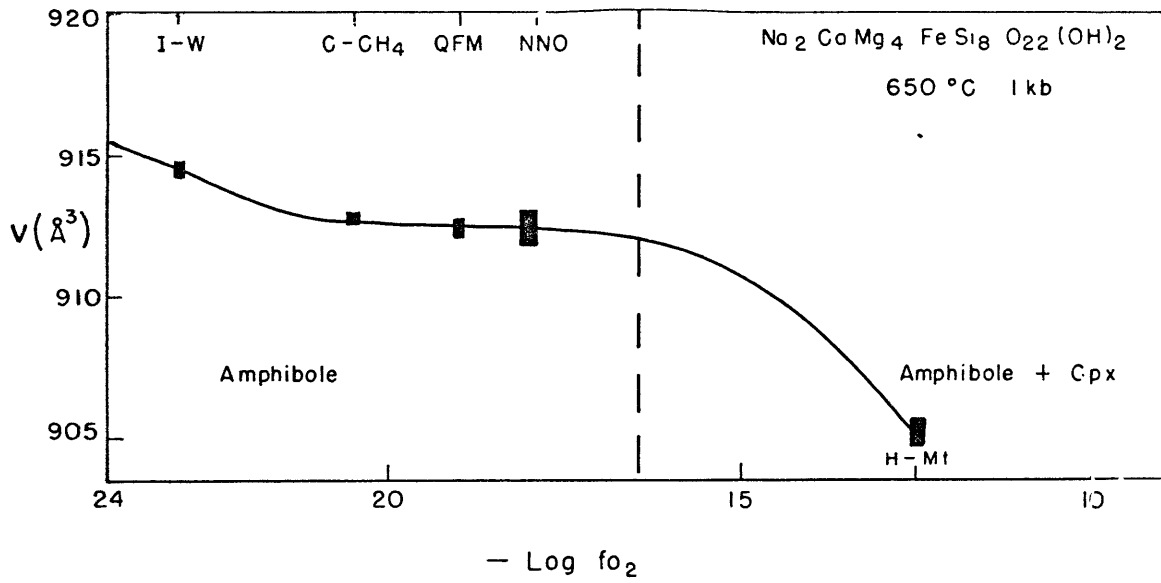


Table I-6. Cell parameters for amphibole grown across the richterite-ferrorichterite join.

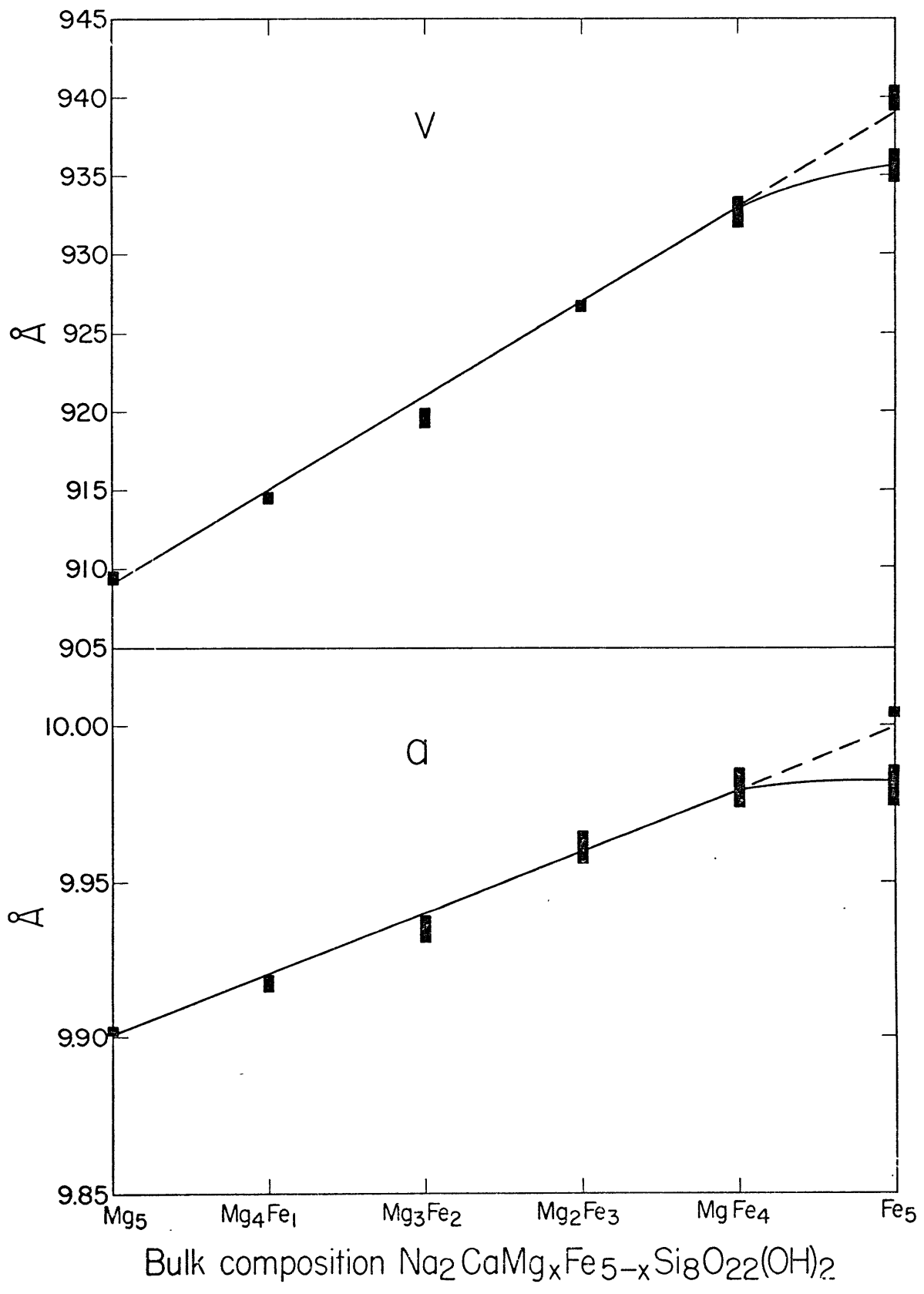
Cell Parameters

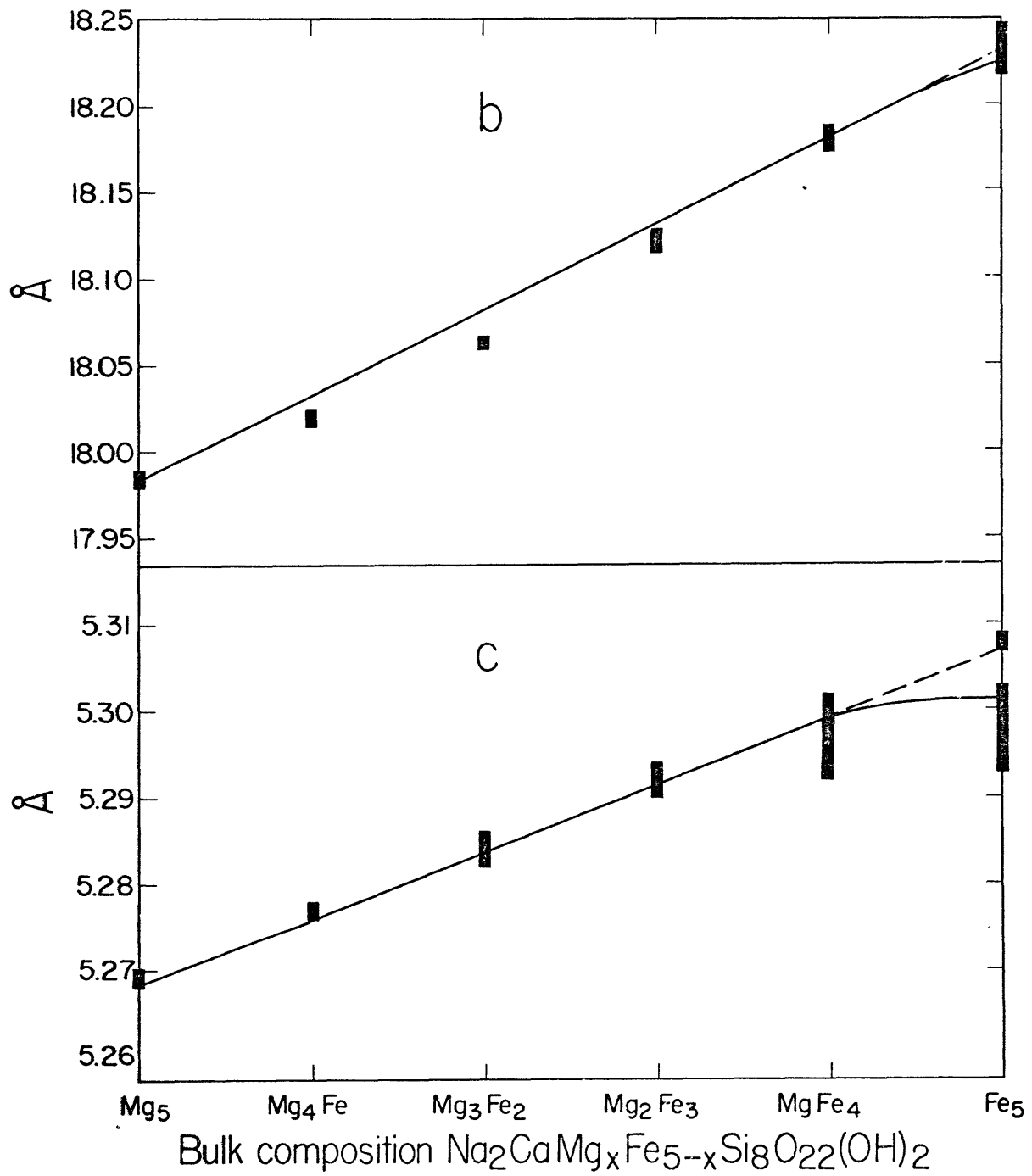
Composition	T(°C)	P(kb)	Duration (hrs)	a(Å)	b(Å)	c(Å)	$\beta$	V(Å <sup>3</sup> )	asin $\beta$ (Å)
Na <sub>2</sub> CaMg <sub>5</sub> Si <sub>8</sub> O <sub>22</sub> (OH) <sub>2</sub>	850	1	48	9.903(1)	17.982(2)	5.267(1)	104°14' (1')	909.2(1)	
"	850	1	96	9.903(3)	17.976(4)	5.270(2)	104°13' (1')	909.4(3)	
"	800	1	48	9.901(2)	17.976(4)	5.270(1)	104°12' (1')	909.3(3)	
"	800	1	96	9.901(2)	17.987(2)	5.270(1)	104°12' (1')	909.9(4)	
Ave				9.902(1)	17.980(4)	5.269(1)	104°13' (1')	909.4(3)	9.599(1)
Fe <sub>3</sub> O <sub>4</sub> -Fe <sub>2</sub> O <sub>3</sub> Buffer									
"Na <sub>2</sub> CaFeMg <sub>4</sub> Si <sub>8</sub> O <sub>22</sub> (OH) <sub>2</sub> " + Px	800	1	72	9.839(4)	17.963(7)	5.276(2)	104°2' (2')	904.6(4)	
"	800	1	96	9.835(5)	17.978(6)	5.282(2)	104°4' (2')	906.0(4)	
"	650	1	288	9.823(5)	17.964(6)	5.285(3)	103°59' (2')	905.0(4)	
"	650	1	240	9.838(3)	17.944(6)	5.281(2)	103°56' (2')	904.9(4)	
Ave				9.834(6)	17.962(10)	5.281(3)	104°0' (3)	905.1(5)	9.542(6)
Ni-NiO Buffer									
Na <sub>2</sub> CaFeMg <sub>4</sub> Si <sub>8</sub> O <sub>22</sub> (OH) <sub>2</sub>	800	1	96	9.898(3)	18.019(7)	5.279(3)	104°7' (3')	913.1(5)	
"	800	1	96	9.894(2)	18.004(3)	5.279(2)	104°3' (1')	912.0(4)	
"	800	1	72	9.901(1)	18.003(4)	5.278(1)	104°5' (1')	912.5(2)	
"	650	1	240	9.894(3)	18.005(8)	5.275(2)	104°5' (3')	911.5(5)	
Ave				9.898(4)	18.009(7)	5.277(2)	104°5' (2')	912.4(6)	9.601(4)
Fe <sub>2</sub> SiO <sub>4</sub> -SiO <sub>2</sub> -Fe <sub>3</sub> O <sub>4</sub> Buffer									
Na <sub>2</sub> CaFeMg <sub>4</sub> Si <sub>8</sub> O <sub>22</sub> (OH) <sub>2</sub>	800	1	72	9.896(2)	18.003(4)	5.279(2)	104°5' (1')	912.3(3)	
"	800	1	144	9.890(2)	18.003(6)	5.282(1)	104°4' (1')	912.2(3)	
"	650	1	240	9.891(4)	18.000(13)	5.283(2)	104°3' (2')	912.4(4)	
"	600	7	96	9.891(8)	18.013(5)	5.285(4)	104°10' (4')	912.9(8)	
Ave				9.892(2)	18.005(5)	5.282(2)	104°6' (3')	912.4(3)	9.593(2)
C-CH <sub>4</sub> Buffer									
Na <sub>2</sub> CaFeMg <sub>4</sub> Si <sub>8</sub> O <sub>22</sub> (OH) <sub>2</sub>	650	1	240	9.904(4)	18.017(3)	5.276(1)	104°10' (3')	912.8(4)	
"	650	1	144	9.906(4)	17.995(6)	5.278(2)	104°9' (3')	912.3(5)	
"	650	1	288	9.904(3)	18.000(4)	5.279(1)	104°6' (1)	912.7(3)	
Ave				9.905(2)	18.004(9)	5.278(1)	104°8' (2')	912.7(2)	9.605(2)
	800	1	72	9.902(3)	18.017(4)	5.276(1)	104°6' (1')	912.9(2)	

Fe-FeO Buffer

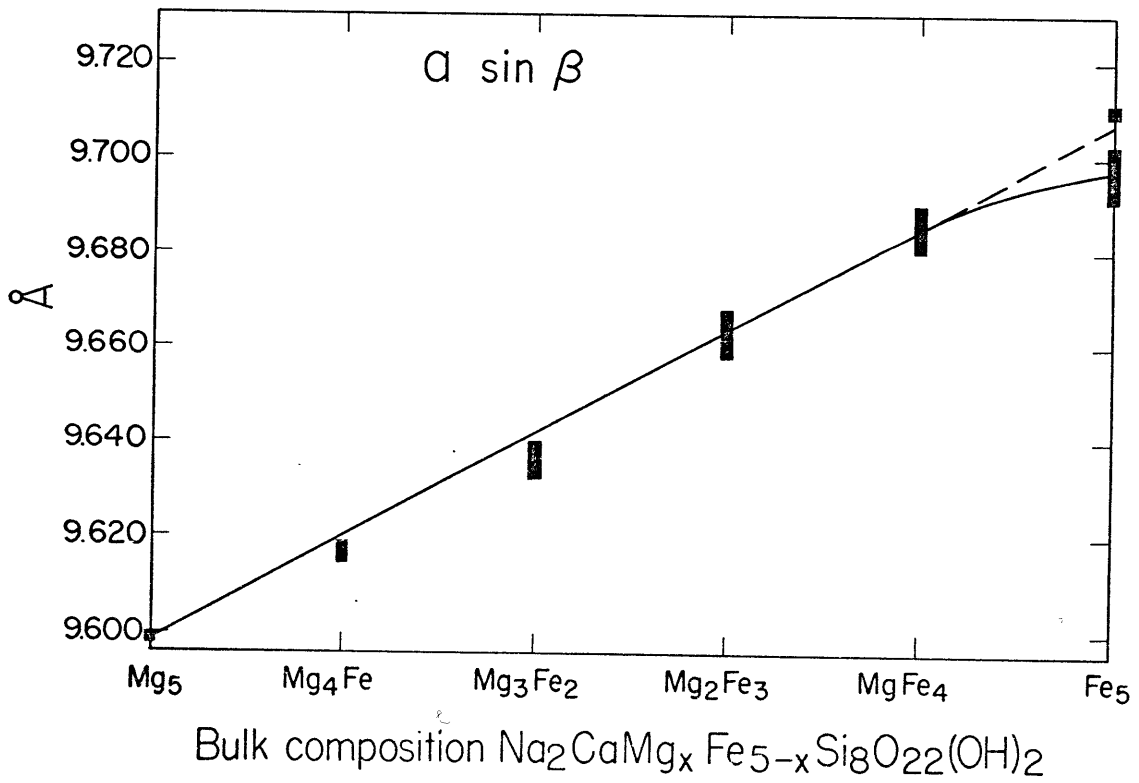
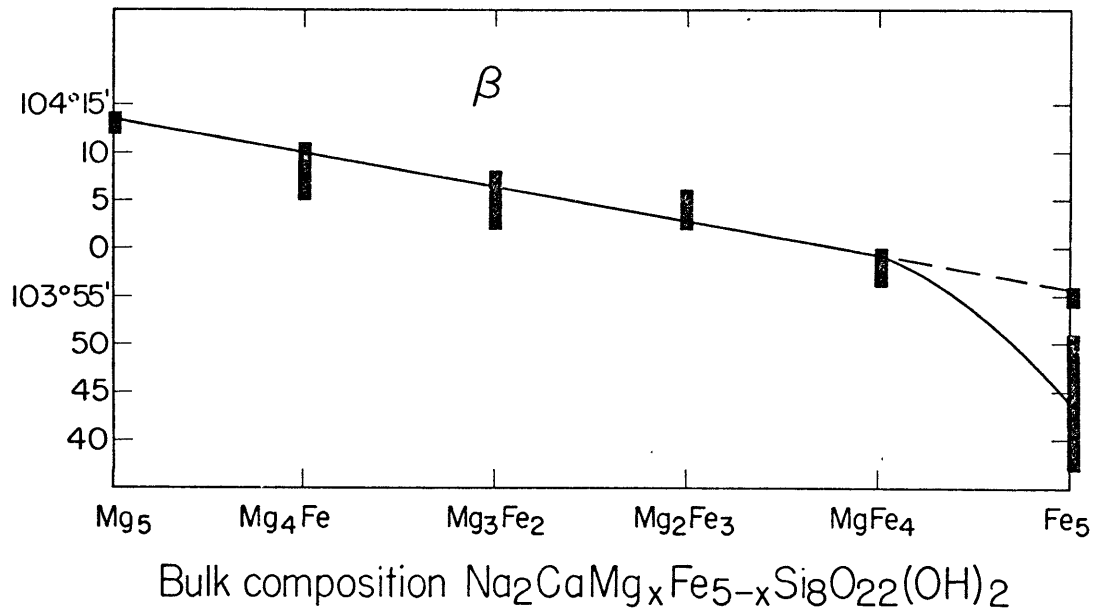
Na <sub>2</sub> CaFeMg <sub>4</sub> Si <sub>8</sub> O <sub>22</sub> (OH) <sub>2</sub>	650	1	144	9.916(2)	18.017(4)	5.276(1)	104°4′(1′)	914.8(2)	
"	650	1	144	9.913(4)	18.017(7)	5.277(2)	104°4′(3′)	914.2(4)	
"	650	1	168	9.918(3)	18.019(5)	5.277(2)	104°10′(2′)	914.4(4)	
"	650	2	96	9.919(4)	18.022(6)	5.276(2)	104°10′(2′)	914.4(4)	
"	600	7	120	9.917(2)	18.027(4)	5.276(1)	104°10′(1′)	914.6(2)	
"	550	5	96	9.916(4)	18.024(4)	5.280(1)	104°8′(2′)	915.0(3)	
"	530	10	312	9.918(6)	18.015(9)	5.277(3)	104°9′(4′)	914.3(5)	
Ave				9.917(2)	18.020(5)	5.277(1)	104°8′(3′)	914.5(3)	9.617(2)
Na <sub>2</sub> CaFe <sub>2</sub> Mg <sub>3</sub> Si <sub>8</sub> O <sub>22</sub> (OH) <sub>2</sub>	650	1	144	9.936(4)	18.062(7)	5.285(2)	104°4′(3′)	920.0(4)	
"	650	1	144	9.930(4)	18.054(6)	5.283(3)	104°3′(2′)	919.3(4)	
"	650	1	168	9.936(4)	18.065(6)	5.287(2)	104°4′(2′)	920.5(4)	
"	650	2	144	9.935(4)	18.057(6)	5.279(2)	104°6′(2′)	918.5(4)	
"	600	7	120	9.938(2)	18.067(3)	5.284(1)	104°10′(3′)	920.0(2)	
"	550	5	198	9.942(5)	18.089(11)	5.287(3)	104°9′(3′)	921.9(7)	
"	530	10	333	9.927(5)	18.064(8)	5.285(2)	104°5′(2′)	919.2(5)	
Ave				9.935(4)	18.063(3)	5.284(2)	104°5′(3′)	919.6(6)	9.636(4)
Na <sub>2</sub> CaFe <sub>3</sub> Mg <sub>2</sub> Si <sub>8</sub> O <sub>22</sub> (OH) <sub>2</sub>	600	7	120	9.970(4)	18.126(5)	5.289(1)	104°6′(2′)	927.0(4)	
"	530	2	599	9.955(3)	18.130(5)	5.293(1)	104°0′(1′)	926.9(3)	
"	530	5	547	9.962(4)	18.122(6)	5.294(2)	104°4′(3′)	927.6(4)	
"	530	10	595	9.958(9)	18.113(11)	5.293(3)	104°4′(5′)	926.1(7)	
"	500	2	480	9.964(3)	18.121(4)	5.291(1)	104°5′(1′)	926.6(3)	
Ave				9.962(5)	18.122(6)	5.292(2)	104°4′(2′)	926.7(3)	9.663(5)
Na <sub>2</sub> CaFe <sub>4</sub> MgSi <sub>8</sub> O <sub>22</sub> (OH) <sub>2</sub>	700	5	240	9.980(4)	18.185(6)	5.300(1)	103°56′(1′)	933.6(4)	
"	600	7	120	9.988(2)	18.184(4)	5.292(1)	103°57′(2′)	932.8(2)	
"	530	10	962	9.973(3)	18.172(5)	5.301(1)	104°0′(2′)	931.8(3)	
Ave				9.980(7)	18.180(7)	5.297(5)	103°58′(2′)	932.7(9)	9.685(5)
I. Na <sub>2</sub> CaFe <sub>5</sub> Si <sub>8</sub> O <sub>22</sub> (OH) <sub>2</sub> +Px	600	7	120	10.002(4)	18.232(7)	5.307(2)	103°56′(2′)	939.4(5)	
"	700	5	216	10.003(5)	18.245(7)	5.309(2)	103°56′(2′)	940.4(5)	
Ave				10.003(1)	18.238(8)	5.308(1)	103°55′(1′)	940.0(7)	9.710(1)
II. Na <sub>2</sub> CaFe <sub>5</sub> Si <sub>8</sub> O <sub>22</sub> (OH) <sub>2</sub>	530	10	535	9.975(2)	18.226(6)	5.292(2)	103°37′(8′)	935.0(5)	
"	530	5	721	9.990(3)	18.216(6)	5.303(2)	103°51′(2′)	937.0(4)	
"	500	2	672	9.980(8)	18.227(6)	5.300(6)	103°44′(5′)	936.5(6)	
Ave				9.982(7)	18.223(6)	5.298(5)	103°44′(7′)	936.2(1.0)	9.697(6)

Figure I-8 a-f. Variation of unit cell parameters for the amphibole series grown on I-W. Both  $Fe_5$  varieties are plotted.







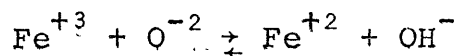


Statistically speaking, two points must differ by at least  $2\sigma$  to be considered as distinct values at the 95% confidence level. Some of the above observations are not statistically real but there is structural evidence which can be presented to support them.

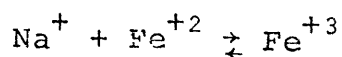
The straight line and its dotted extension were drawn not as a least squares fit but with these considerations in mind: (1) The  $Mg_5$  composition yields correct parameters. (2) It is assumed that  $\underline{A}$  and  $M(4)$  are uniformly occupied by the same cations throughout and all other  $M$  sites are the same size with no preferred ordering of cations. Obviously, (2) is not true and deviations from linearity will be discussed on such a basis.

#### Discussion

Preliminary results from Mossbauer work by D. Virgo (personal communication) indicate roughly 5% ferric iron is present in the ferrichterite which is on the linear trend shown in the cell parameter diagrams. The purist ferrichterite, however, contains noticeably more (~10%) ferric iron and deviates from this trend. At least four reasons can be cited for ferric iron. First, ferric iron commonly can be explained by producing an oxyamphibole.



Effectively, hydrogen is removed from the structure and iron is oxidized to  $Fe^{+3}$ . Second,  $H_2O$  may leach  $Na$  from the amphibole according to:



Third, either of these substitutions could be accomplished if there is a structural limitation which prevents the five M(1), M(2), and M(3) sites from being filled with ferrous iron. Bancroft and Burns (1969), Wilkins (1970), and Mitchell (1970) indicate the M(2) sites are smaller in hydrous amphiboles and generally accept magnesium or ferric iron instead of the larger ferrous iron. This may not be true for fluoroamphiboles (Cameron, 1971) since iron does not coordinate well with fluorine. The only M sites not coordinated with fluorine are the two M(2) sites. Fourth, Ghose (1965) and Whittaker (1949, 1960) postulated that if Na occupies the M(4) site a local charge imbalance will result since the Na is coordinated with 6 oxygens. Such an imbalance would be corrected by addition of a ferric iron into the M(2) site because M(2) lies closest to M(4) (Papike et al., 1969).\* To complete charge balance in richterites either  $\text{Na}^+$  or  $\text{H}^+$  must be removed elsewhere. Burns and Prentice (1968) support the charge balance theory by reporting the preferential positioning of  $\text{Fe}^{+3}$  in M(2) in riebeckites ( $\text{Na}_2\text{Fe}_3^{+2}\text{Fe}_2^{+3}\text{Si}_8\text{O}_{22}(\text{OH})_2$ ) which necessarily have  $\text{Fe}^{+3}$  in their composition.

The key to the interpretation appears to be that (1) all experiments on IW contain a trace amount of glass and (2) the long syntheses of ferrichterite (22-30 days) contain a larger amount of glass. A strictly hydrogen loss would produce no

---

\*for potassic richterite:  $\text{M}(2) - \text{M}(4) = 3.182 \text{ \AA}$ ;  
 $\text{M}(1) - \text{M}(4) = 3.410 \text{ \AA}$ .

glass.  $H_2O$  leaching of Na and Si should have caused more scatter in the data points due to time dependence. Anyway, leaching would not have preferentially occurred only in long synthesis of ferrorichterite. Syntheses of equal or longer duration were performed on  $Mg_2Fe_3$  and  $MgFe_4$  with no such branching of the cell parameters. Any explanation such as alloying of iron in the  $Ag_{80}Pd_{20}$  fails for the same reason. One is left with the conclusion that five ferrous irons may just be too large to fit comfortably in the amphibole structure, especially in close proximity to an M(4) Na. Since experiments on IW always started with a reduced mix containing native iron, short experiments on IW may have produced a relatively "stable" metastable ferrous amphibole on ferrorichterite composition which conforms more readily to the trends indicated by the cell parameter curves. The point is that this amphibole while presumably not the stable form is more nearly a completely ferrous amphibole. Preliminary Mossbauer results indicate the  $Fe^{+3}/Fe^{+2}$  ratio is less for this phase than that for  $Mg_2Fe_3$ .

Using these interpretations the observed lattice constants can be explained completely.  $a$  depends upon the mean size of the cations in the linking cation strip (Ernst, 1968; Huebner and Papike, 1970). It should be a linear function if the incremental change in cation size remains constant. Beyond  $MgFe_4$  the mean size of the cations increases at a smaller rate due to sodium loss and the introduction of more ferric iron.

$b$  is influenced most by the occupancy of the M(4) and M(2) sites which actually link the double chains of silicon tetra-

hedra (Colville et al., 1969; Ernst, 1968). M(4) in these amphiboles is occupied by Na and Ca in all cases. Of secondary importance are the other M sites. While not actually linking the double chains, they may cause some increase in the b dimension when occupied by larger cations. The diagram presented here clearly shows that while the 2 M(1) and M(3) sites are filling preferentially with ferrous iron ( $Mg_4Fe$  to  $Mg_2Fe_3$ ) the observed points drop below the line representing uniform totally disordered filling of the M sites. Complete ordering is not observed from the Mossbauer spectra. More will be stated on this point when all of the Mossbauer data is analyzed. The deviation at  $Fe_5$  is almost nonexistent. Only 10% ferric iron apparently has little effect on the b dimension.

c, or chain length, is controlled by: (1), the size of cations in the M(1) and M(3) sites (Colville et al., 1966) or, (2), by the size of the tetrahedral cations (Ernst, 1968). In spite of the great difference in size between  $Fe^{+3}$  and Si in 4 fold coordination, .40 Å vs. .63 Å, (Shannon and Prewitt, 1969) local charge imbalance may require some  $Fe^{+3}$  to enter and lengthen the chain to balance the Na in the A site. Judging from the structure, large cations in M(2) should also affect the chain length. Once again an essentially uniform linear trend is observed until more ferric iron is present causing a much smaller stretching of the chain. If the increased  $Fe^{+3}$  goes into M(2) vs. a tetrahedral site less expansion would occur along c which is observed.

Huebner and Papike (1970) show clearly that the A site con-

trols  $\beta$  as well as influencing  $\underline{a}$ . Addition of larger cations to  $\underline{A}$  causes  $\beta$  to increase. In sodic richterite the  $\underline{A}$  is uniformly filled with Na, but as one proceeds from  $\text{Mg}_5$  to  $\text{Fe}_5$  the structure expands around the Na yielding the effect of placing a relatively smaller cation in the  $\underline{A}$  site. Consequently,  $\beta$  decreases. Near  $\text{Fe}_5$   $\beta$  decreases more sharply due to not only  $\text{Fe}^{+3}$  but actual Na loss.

$\underline{a \sin \beta}$  reflects the mean size of the cations in the linking cation layer more clearly than does  $\underline{a}$  since this dimension is perpendicular to the layer of M sites. The M(1) sites project more into the rings formed by the double chains and have less influence than the other M sites. Also a larger portion of the iron is  $\text{Fe}^{+3}$  in lower iron compositions due to Na in M(4). The effect is small, but it can be seen in the compositions  $\text{Mg}_4\text{Fe}$  and  $\text{Mg}_3\text{Fe}_2$  which fall below the linear curve. Loss of Na and oxidation of  $\text{Fe}^{+2}$  cause a small dip at  $\text{Fe}_5$ .

Combining the effects of all other cell parameters, the cell volume shows a slightly negative volume of mixing on the low iron compositions and slightly positive volume of mixing on the high iron compositions.

## PART II: PHASE EQUILIBRIA:

## Introduction

The phase relations of the Mg-Fe richterites were determined for compositions along the Mg-richterite-ferrorichterite join. Oxide mixes of the appropriate bulk compositions were prepared and sealed in precious metal capsules with excess H<sub>2</sub>O. These were subjected to temperature and pressure in standard cold seal apparatus (Tuttle, 1949), in an internally heated gas apparatus, or in 1 atm. quench furnaces depending upon the conditions desired. Oxygen buffers were used for the iron bearing compositions.

Mg-richterite ( $\text{Na}_2\text{CaMg}_5\text{Si}_8\text{O}_{22}(\text{OH})_2$ )

Figure II-1 presents the stability relations of Mg-richterite for the P-T region 800°C - 1150°C and 0 to 1000 bars P<sub>H<sub>2</sub>O</sub>.

The univariant equilibria represented are:

AB: richterite  $\rightleftharpoons$  1:2:6 Na-Mg silicate + roedderite + forsterite  
diopside + vapor.

BC: 1:2:6 Na-Mg silicate  $\rightleftharpoons$  roedderite + melt.

BD: richterite  $\rightleftharpoons$  roedderite + forsterite + diopside + melt +  
vapor

DE: roedderite  $\rightleftharpoons$  enstatite + melt

DF: richterite  $\rightleftharpoons$  forsterite + diopside + enstatite + melt +  
vapor.

Richterite consists of 5 components and, necessarily, seven univariant curves must emanate from each invariant point. Only those shown were found using a mix of richterite bulk composition.

## Key to Figure Abbreviations

A	-	amphibole
En	-	enstatite
Di	-	diopside
Ac <sub>67</sub> Hd <sub>33</sub>	-	acmite <sub>67</sub> hedenbergite <sub>33</sub>
Cpx	-	clinopyroxene
1:2:6	-	1:2:6 Na-(Mg,Fe) silicate
Ro	-	roedderite
Fo	-	forsterite
Fa	-	fayalite
Ol	-	olivine
Mt	-	magnetite
H	-	hematite
Q	-	quartz
M	-	melt
V	-	vapor
Mix	-	reduced mix (Fe <sup>o</sup> )
(X)	-	~5% content



Figure II-1. Experimentally determined stability relations for Mg-richterite bulk composition. Symbol size approximates the errors in measuring P and T. Superimposed is Forbes' (1971) stability limit for Mg-richterite.

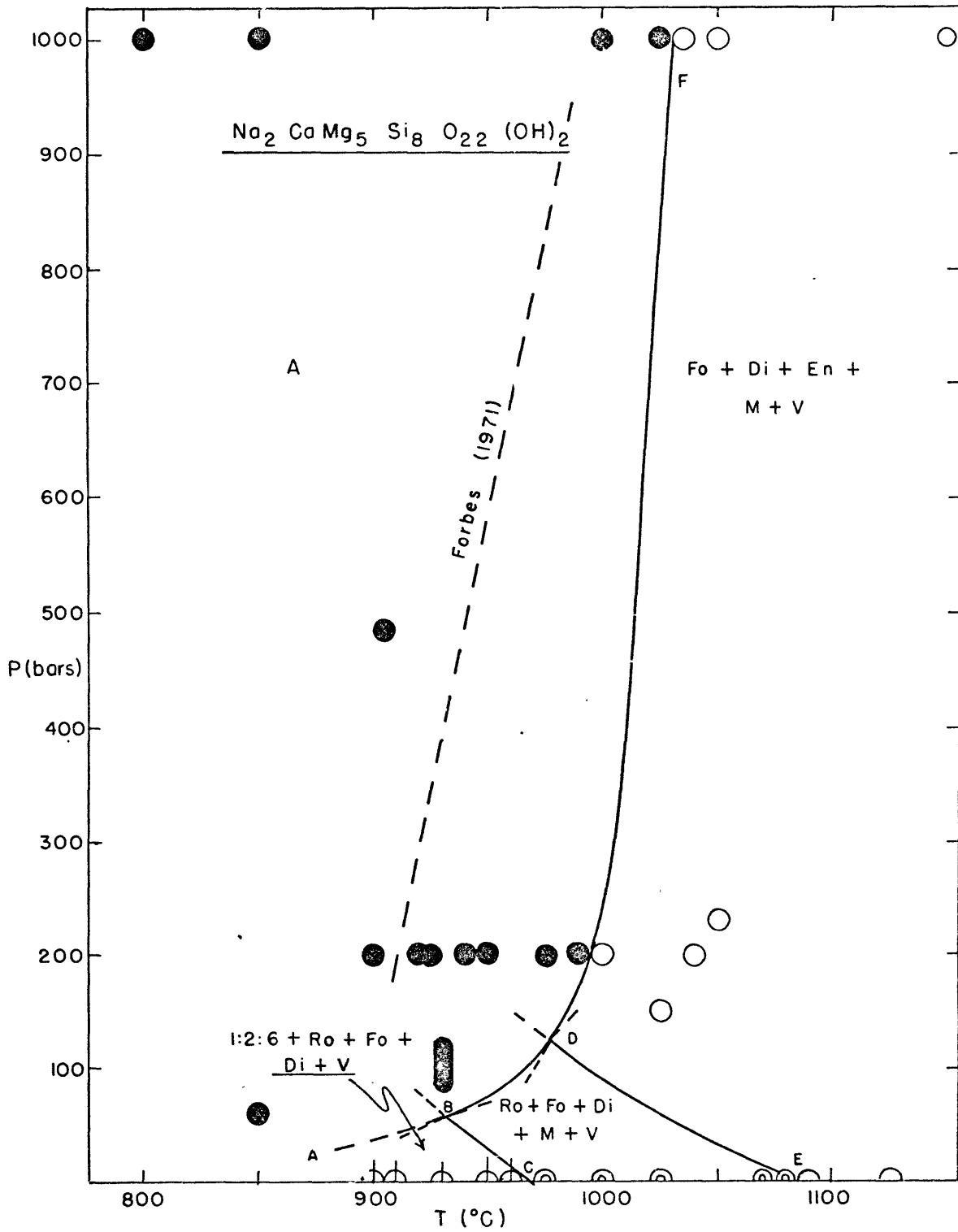


Table II-1. Bracketing Experiments:  $\text{Na}_2\text{CaMg}_5\text{Si}_8\text{O}_{22}(\text{OH})_2$

<u>P</u> (±15 bars)	<u>T</u> (±5°C)	<u>Duration</u> (hrs)	<u>Reactants</u>	<u>Products</u>
1000	1050	18	A	Fo+Di+M+(En)+(A)
"	1035	23	"	"
"	"	"	1:2:6+Fo+Ro+Di	"
"	1025	"	A	A
"	"	7	Ro+Fo+Di+M	"
"	1000	18	"	"
200	1040	71	Ro+Fo+Di+M	Fo+Di+En+M
"	1000	23 $\frac{1}{2}$	A	Fo+Di+M+(En)
"	"	"	Fo+Di+M+(En)	"
"	990	27	1:2:6+Fo+Ro+Di	A
"	"	"	A	"
"	975	24	1:2:6+Fo+Ro+Di	"
"	1090	5	Fo+Fi+M+(En)	"
"	1080	4	Mix	Ro+Fo+Di+M
"	975	17 $\frac{1}{2}$	"	"
"	960	23	Ro+Fo+Di+M	1:2:6+Fo+Ro+Di
"	950	16	Mix	"
"				

Within its stability field Mg-richterite crystallized essentially 100% pure. Experiments at 800°C and 2 kb of 2-3 days duration yielded 98-100% amphibole. This amphibole had the following properties:

<u>a</u> (Å)	<u>b</u> (Å)	<u>c</u> (Å)	<u>V</u> (Å <sup>3</sup> )	<u>β</u>
9.902(1)	17.980(4)	5.269(1)	909.4(3)	104°13(1)
	<u>α</u>	<u>γ</u>		
	1.604(5)	1.622(3)		

Experiments in the field forsterite + diopside + enstatite + melt + vapor at 1 kb always contained 10-20% quench amphibole. This amphibole consisted of fine isotropic needles compared to the large (20 x 40 $\mu$ ) pyroxenes and irregularly shaped forsterites. Experiments at 200 bars and beyond the amphibole field produced almost no quench amphibole. Clinoenstatite appeared in the powder x-ray patterns in experiments of greater than 2 days duration. It was identified on the basis of the presence of the (221) and (310) reflections. Shorter experiments yielded forsterite + diopside + melt + vapor with possible small amounts of clinoenstatite which are difficult to distinguish from diopside optically.

Based on calculations of the H<sub>2</sub>O solubility in Na<sub>2</sub>O-SiO<sub>2</sub> melts (Morey and Hesselgesser, 1951 and 1952) the melt may dissolve more H<sub>2</sub>O than released by the amphibole structure. Glasses quenched from 1 kb P<sub>Tot</sub> and 1050°C were vesiculate and this may indicate exsolution of a vapor phase upon release of pressure. Roedderite (a = 10.147(1), c = 14.240(3)) and 1:2:6 Na-Mg silicate were identified using the diffractometer patterns of Schairer

and Yoder (1970). Mg-Fe roedderites were studied as a companion project. The preliminary results are in appendix I.

Forbes (1971) indicates richterite is about 80°C less stable at 200 bars and approximately 20°C less stable at 1 kb than the results presented here. Experiments using forsterite + diopside + enstatite + melt + vapor as starting materials and held for 68 hours at 940°C and 200 bars produced >95% amphibole even though this well beyond Forbes' stability limit. Experiments near the stability curve were duplicated 2 or 3 times using mix, decomposition products, or amphibole (see Table II-1).\* In addition, the new work has yielded the low pressure field of 1:2:6 Na-Mg silicate + roedderite + forsterite + diopside + vapor.

#### Ferrorichterite ( $\text{Na}_2\text{CaFe}_5\text{Si}_8\text{O}_{22}(\text{OH})_2$ )

The phase relations of the ferrous end member ferrorichterite are presented in Figures II-2, II-3 and II-4 and Tables II-2, II-3 and II-5.

Figure II-2 displays the relations of ferrorichterite in P, T space at oxygen fugacities defined by the Fe-FeO buffer. At pressures greater than 700 bars ferrorichterite decomposes to hedenbergitic pyroxene + fayalite + melt + vapor. Reversals were obtained at 1, 2, and 5 kb. Some metastable amphibole was observed in the decomposition region at 5 kb but not at lower pressures. Reversal experiments used amphibole crystallized for

\*Only bracketing experiments are included in the text. See Appendix II for complete experiment tables.

Figure II-2. Experimentally determined stability relations for ferrorichterite bulk composition with oxygen fugacities defined by the I-W buffer.

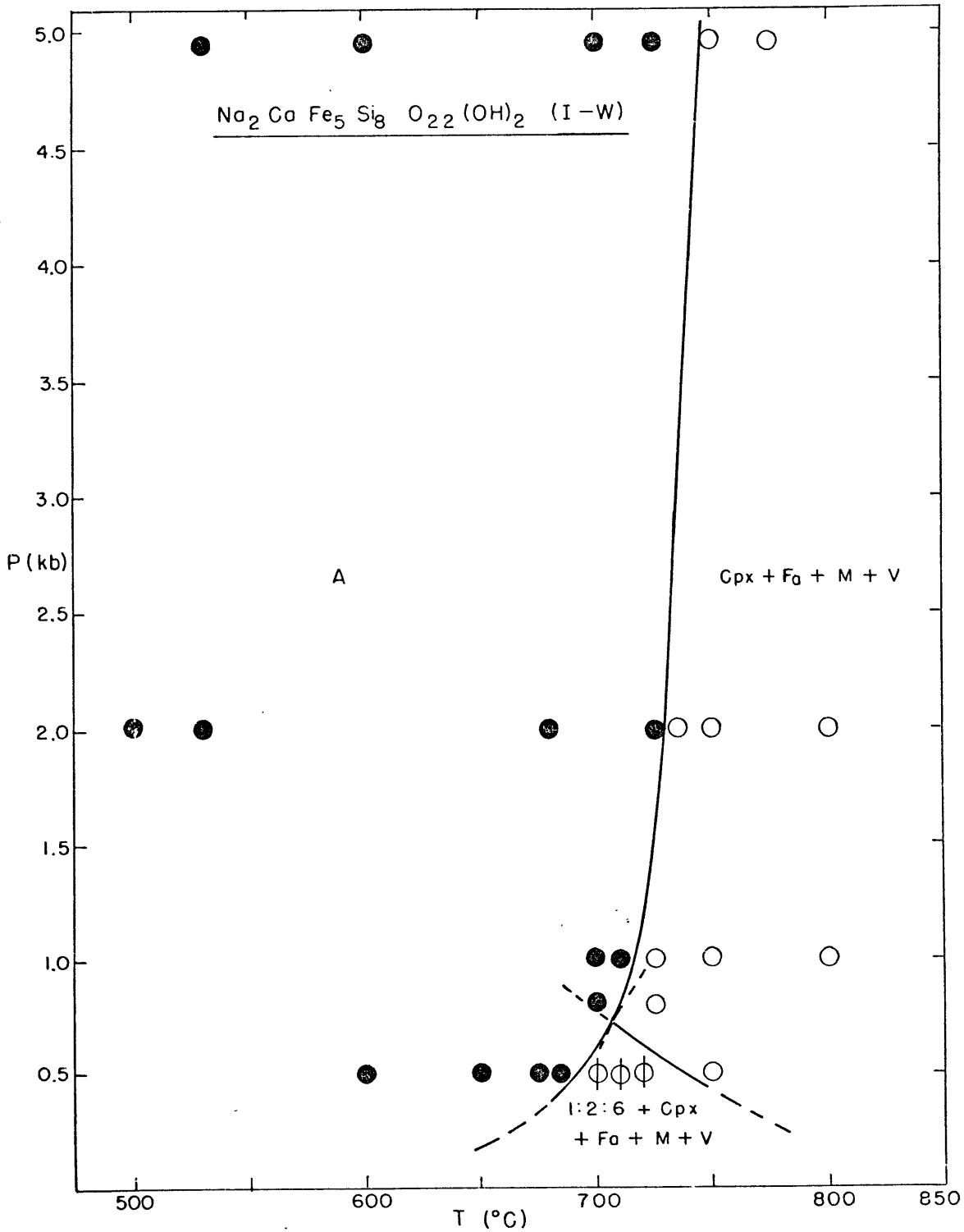


Table II-2. Bracketing Experiments:  $\text{Na}_2\text{CaFe}_5\text{Si}_8\text{O}_{22}(\text{OH})_2(\text{IW})$

<u>P</u> ( $\pm 15$ bars)	<u>T</u> ( $\pm 5^\circ\text{C}$ )	<u>Duration</u> (hrs)	<u>Reactants</u>	<u>Products</u>
5000	750	48	Cpx+Fa+M	Cpx+Fa+M+ (A)
"	725	83	"	"
"	700	72	A	A
2000	750	47	A	Cpx+Fa+M
"	735	54	Cpx+Fa+M	"
"	725	63	"	A
1000	725	137	A	Cpx+Fa+M+ (A)
"	"	48	Cpx+Fa+M	Cpx+Fa+M+ (A)
"	710	52	A	A
"	700	46	Cpx+Fa+M	A
750	725	41	"	Cpx+Fa+M
"	700	72	"	A
500	750	51	Cpx+Fa+M	Cpx+Fa+M
"	720	52	"	1:2:6+Cpx+Fa+M
500	700	69	"	"
"	685	51	A	A
"	675	67	Cpx+Fa+M	A+ (Cpx+Fa+M)



20 - 30 days at 7 - 10 kb and decomposition products grown at 800°C and 2 kb for 2 days. Complete transformation of one assemblage to the other was accomplished in experiments of only three days or less at >700°C.

Below 700 bars ferrorichterite reacts to form hedenbergitic pyroxene + 1:2:6 Na-Fe silicate + fayalite + melt + vapor. The 1:2:6 Na-Fe silicate decomposes to fayalite + melt at higher temperatures. The fayalite has a  $d_{130}$  of  $2.83 \pm .003 \text{ \AA}$  and is believed to be pure  $\text{Fe}_2\text{SiO}_4$  judging from the determinative curves of Fisher and Medaris (1969).

The hedenbergitic pyroxene has cell parameters of:

<u>a(Å)</u>	<u>b(Å)</u>	<u>c(Å)</u>	<u>β</u>	<u>v(Å<sup>3</sup>)</u>
9.809(4)	8.999(7)	5.288 (18)	105°15(7)	465.7 (1.3)

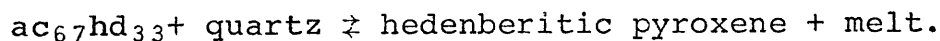
Because of poor resolution of pyroxene peaks and interference with fayalite, only six reflections were used for refinement: (110), (220), ( $\bar{2}21$ ), (310), (311), and ( $\bar{1}31$ ). Refinements using these peaks generally yielded values of c and hence volume with large errors. Using the determinative curves of Nolan (1969), the pyroxene is found to be about  $\text{Hd}_{80}\text{Ac}_{20}$ . Aoki (1964) and Nolan (1969) have pointed out the limitations of the determinative curves when the pyroxene coexists with a melt. The pyroxene stoichiometry apparently is not reflected when pyroxene coexists with a melt. Consequently, this value may be somewhat inaccurate. Compositions determined by electron microprobe were poor because of small crystal size and Na volatilization. Microprobe results do indicate  $\text{Ca} + \text{Na} < \text{Fe}$  and obviously there must be some ferrosilite component in the pyroxene which moves the composition

from the Ac-Hd join.

The presence of 1:2:6 Na-Fe silicate is determined on the basis of the study of Mg-Fe roedderites (see Appendix I).

The stability of amphibole on the ferrichterite bulk composition is greatly reduced at  $f_{O_2}$  above the FeO-Fe<sub>3</sub>O<sub>4</sub> buffer. Figure II-3 shows the phase equilibria defined by the QFM buffer at variable P and T. A larger amount of Fe<sup>+3</sup> is present here as indicated by the Mössbauer fit. Accordingly, 30-40% of the charge in the amphibole field was an acmitic pyroxene. Experiments at higher pressure (7 kb) yielded somewhat greater amounts of Fe<sup>+3</sup> amphibole with a distinctly smaller unit cell volume than amphibole on Fe-FeO (929.7 Å vs. 936.0 Å). Larger amounts of Fe<sup>+3</sup> and loss of Na and Fe to the pyroxene presumably brings about the volume decrease. In order to prove the non-metastability of the pyroxene, amphibole prepared on Fe-FeO was recrystallized on QFM and yielded amphibole plus pyroxene.

Amphibole plus pyroxene decomposes between 1 and 7 kb and 535 ± 10°C to acmite<sub>67</sub>hedenbergite<sub>33</sub> + fayalite + magnetite + quartz + vapor. At higher temperatures this assemblage undergoes partial melting:



Ac<sub>67</sub>Hd<sub>33</sub> was determined directly by microprobe analysis and from Nolan (1969) since no melt is present. Its unit cell parameters as well as those of other pyroxenes grown in the bulk composition Fe<sub>5</sub> are given in Table II-4. Based on estimates from Nolan (1969) with the reservations expressed previously, the pyroxene above the solidus is somewhat more ferrous (hd<sub>75</sub>ac<sub>25</sub>).

Figure II-3. Experimentally determined stability relations for ferrorichterite bulk composition with oxygen fugacities defined by the QFM buffer.

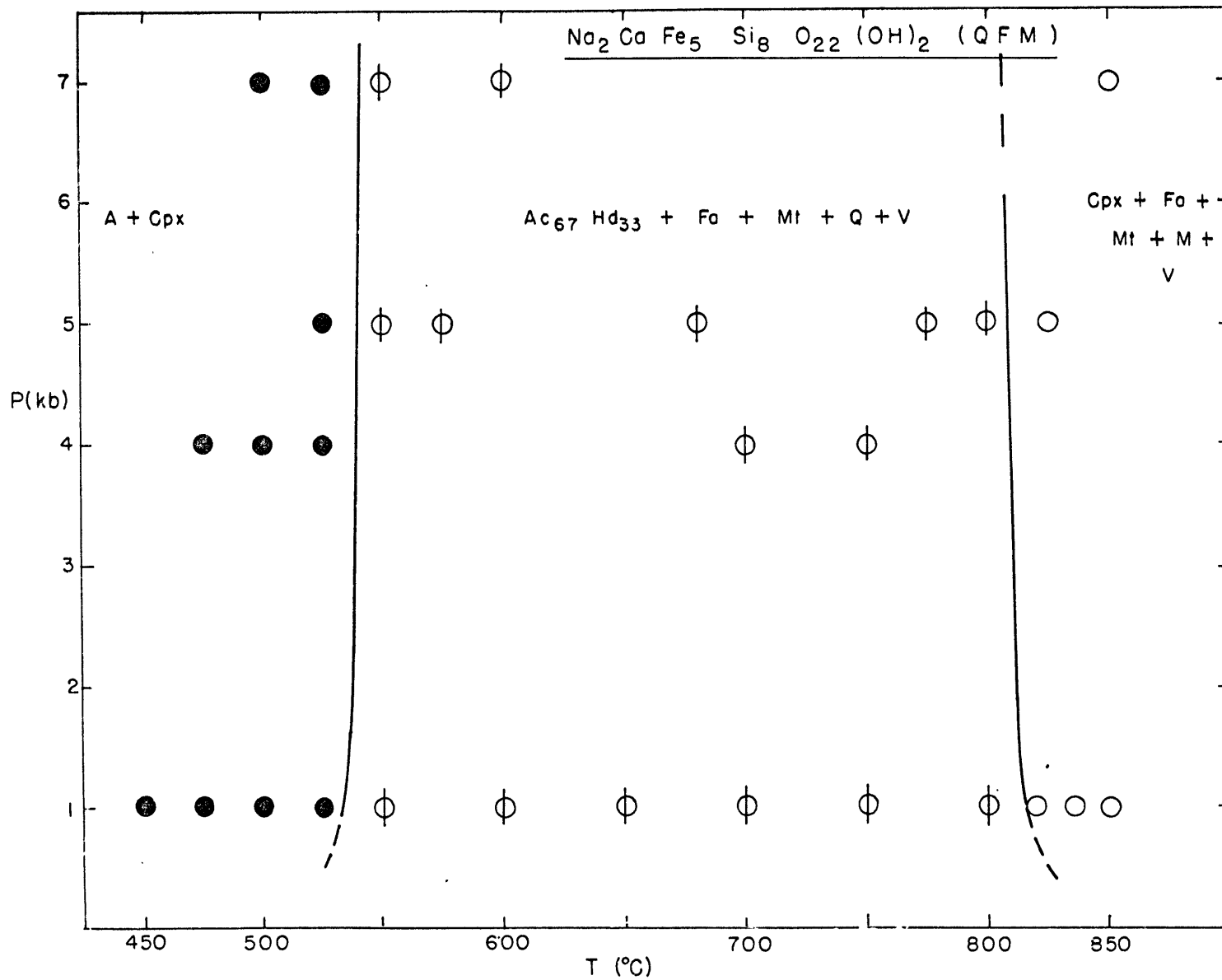


Table II-3. Bracketing Experiments:  $\text{Na}_2\text{CaFe}_5\text{Si}_8\text{O}_{22}(\text{OH})_2$  (QFM)

<u>P</u> ( $\pm 15$ bars)	<u>T</u> ( $\pm 5^\circ\text{C}$ )	<u>Duration</u> (hrs)	<u>Reactants</u>	<u>Products</u>
7000	850	28	Mix	Cpx+Fa+mt+M
"	600	350	"	$\text{Ac}_{67}\text{Hd}_{33}+\text{Fa}+\text{Q}+\text{Mt}$
"	550	336	$\text{Ac}_{67}\text{Hd}_{33}+\text{Fa}+\text{Q}+\text{Mt}$	"
"	525	493	Mix	A + Cpx
5000	825	48	$\text{Ac}_{67}\text{Hd}_{33}+\text{Fa}+\text{Q}+\text{Mt}$	Cpx+Fa+ t+M
"	800	$72\frac{1}{2}$	"	$\text{Ac}_{67}\text{Hd}_{33}+\text{Fa}+\text{Q}+\text{Mt}$
"	550	310	"	"
"	525	336	"	A + Cpx
4000	700	162	"	$\text{Ac}_{67}\text{Hd}_{33}+\text{Fa}+\text{Q}+\text{Mt}$
"	525	356	"	A + Cpx
1000	835	52	$\text{Ac}_{67}\text{Hd}_{33}+\text{Fa}+\text{Q}+\text{Mt}$	Cpx+Fa+Mt+M
"	820	72	Cpx+Fa+Mt+M	"
"	800	117	$\text{Ac}_{67}\text{Hd}_{33}+\text{Fa}+\text{Q}+\text{Mt}$	$\text{Ac}_{67}\text{Hd}_{33}+\text{Fa}+\text{Q}+\text{Mt}$
"	800	$65\frac{1}{2}$	Mix	"
"	550	504	$\text{Ac}_{67}\text{Hd}_{33}+\text{Fa}+\text{Q}+\text{Mt}$	"
"	525	504	"	A + Cpx
"	500	675	A + Cpx	"
"	450	2154	$\text{Ac}_{67}\text{Hd}_{33}+\text{Fa}+\text{Q}+\text{Mt}$	"

Table II-4. Unit Cell Parameters

Bulk Composition:  $\text{Na}_2\text{CaFe}_5\text{Si}_8\text{O}_{22}(\text{OH})_2$ 

Phase	Coexisting Phase(s)	P (bars)	T (°C)	a (Å)	b (Å)	c (Å)	$\beta$	V (Å <sup>3</sup> )
Fe <sub>3</sub> O <sub>4</sub> - Fe <sub>2</sub> O <sub>3</sub> Buffer								
Cpx	H+Mt+Q	1000	700	9.696(5)	8.844(5)	5.289(3)	106°47'(3')	434.2(0.3)
Fe <sub>2</sub> SiO <sub>4</sub> - SiO <sub>2</sub> - Fe <sub>3</sub> O <sub>4</sub> Buffer								
A	Cpx	7000	500	9.937(5)	18.180(9)	5.280(4)	103°27'(5')	927.7(0.7)
A	Cpx	4000	475	9.881(11)	18.136(8)	5.330(4)	103°46'(4')	927.7(0.9)
A	Cpx	4000	475	9.898(9)	18.146(9)	5.328(11)	103°57'(4')	929.0(0.9)
Cpx	Fa+Mt+Q	1000	700	9.698(10)	8.869(11)	5.282(5)	106°42'(7')	435.5(0.5)
Cpx	Fa+Mt+M	1000	820	9.744(4)	8.838(4)	5.471(18)	105°19'(6')	454.5(0.5)
Cpx	A	1000	475	9.746	8.855	5.280	106°28'	437.0
Fe - FeO Buffer								
Cpx	Fa+M	1000	800	9.809(4)	8.999(7)	5.288(18)	105°15'(7')	465.7(1.3)
A	-	10000	530	9.975(2)	18.226(6)	5.292(2)	103°37'(8')	935.0(0.5)
A	-	5000	530	9.990(3)	18.216(6)	5.303(2)	103°51'(2')	937.0(0.4)
A	-	2000	500	9.980(8)	18.227(6)	5.300(6)	103°44'(5')	936.5(0.6)

Problems with metastable 1:2:6 Na-Fe silicate were encountered due to the lesser buffering capacity of QFM. Starting materials containing  $\text{Fe}^{\circ}$  reacted on QFM for a few days invariably recrystallized to charges containing 1:2:6 Na-Fe silicate if grown within the field of stable 1:2:6 Na-Fe silicate which occurs on Fe-FeO. This region is approximately 600°C to 750°C at pressures up to 4 kb. Such charges when resubmitted converted to  $\text{ac}_{67}\text{hd}_{33}$  + fayalite + magnetite + quartz on QFM. Similar problems were found with amphibole. A ferrous amphibole may crystallize within a few days using a reduced mix if it were held just beyond the stability limit of amphibole plus clinopyroxene. In order to avoid these problems only materials equilibrated for several weeks on QFM were used for reversal experiments.

Figure II-4 displays the phase equilibria for the ferrosichterite bulk composition at a  $P_{\text{Tot}}$  of 1 kb with variable  $f_{\text{O}_2}$  and T. Within its field of stability the amphibole is on the ferrosichterite bulk composition only at low  $f_{\text{O}_2}$  (Fe-FeO). On buffers of progressively higher  $f_{\text{O}_2}$  increasing amounts of pyroxene appear with amphibole and approaches 30-40% of the charge on QFM buffer.

Maximum stabilities of amphibole in  $\text{Fe}_5$  bulk composition at  $P_{\text{Tot}} = 1$  kb are:

(QFM)	535±10°C
(C-CH <sub>4</sub> )	580±10°C
(W-Mt)	760±10°C
(I-W)	715± 5°C

Figure II-4. Isobaric ( $P_{\text{Tot}} = 1 \text{ kb}$ )  $\text{Log } f_{\text{O}_2} - T$  diagram for ferrorichterite bulk composition. Field boundaries are dashed where inferred. In this and succeeding diagrams of this type, amphibole gradationally changes to amphibole + clinopyroxene as  $f_{\text{O}_2}$  increases until the stability limit of the remaining amphibole is reached.





Table II-5. Bracketing Experiments:  $\text{Na}_2\text{CaFe}_5\text{Si}_8\text{O}_{22}(\text{OH})_2$  ( $P_{\text{Tot}} = 1 \text{ Kb}$ )

Buffer	T ( $\pm 5^\circ\text{C}$ )	Duration (hrs)	Reactants	Products
HMt	700	120	Oxidized Mix	$\text{Ac}_{67}\text{Hd}_{33}+\text{Fa}+\text{Mt}+\text{Q}$
"	"	"	Mix	"
"	"	"	$\text{Ac}_{67}\text{Hd}_{33}+\text{Fa}+\text{Mt}+\text{Q}$	"
NNO	850	96	Mix	Cpx+Mt+M
"	600	336	"	$\text{Ac}_{67}\text{Hd}_{33}+\text{Fa}+\text{Mt}+\text{Q}$
QFM	835	52	$\text{Ac}_{67}\text{Hd}_{33}+\text{Fa}+\text{Mt}+\text{Q}$	Cpx+Fa+Mt+M
"	820	72	Cpx+Fa+Mt+M	"
"	800	117	$\text{Ac}_{67}\text{Hd}_{33}+\text{Fa}+\text{Mt}+\text{Q}$	$\text{Ac}_{67}\text{Hd}_{33}+\text{Fa}+\text{Mt}+\text{Q}$
"	550	504	"	"
"	525	"	"	A+Cpx
"	500	675	A+Cpx	"
C-CH <sub>4</sub>	775	92	Cpx+Fa+M	Cpx+Fa+M
"	750	552	"	$\text{Ac}_{67}\text{Hd}_{33}+\text{Fa}+\text{Mt}+\text{Q}$
"	625	192	"	"
"	600	240	A+Cpx	A+Cpx
Wmt	775	48	Cpx+Fa+M	Cpx+Fa+Mt+ (A)
"	750	"	"	A+ (Cpx+Fa+M)
IW	725	"	"	Cpx+Fa+M
"	"	137	A	"
"	710	52	"	A
"	700	46	Cpx+Fa+M	"

Amphibole + clinopyroxene decomposes to:

(QFM) Amphibole + clinopyroxene  $\rightleftharpoons$   $ac_{67}hd_{33}$  + fayalite + magnetite + quartz + vapor.

(C-CH<sub>4</sub>) Amphibole + clinopyroxene  $\rightleftharpoons$   $ac_{67}hd_{33}$  + fayalite + quartz + vapor.

(W-Mt) Amphibole + (clinopyroxene)  $\rightleftharpoons$  clinopyroxene + fayalite + melt + vapor.

(I-W) Amphibole  $\rightleftharpoons$  clinopyroxene + fayalite + melt + vapor.

The subsolidus assemblage melts at high  $f_{O_2}$ :

(Ni-NiO)  $ac_{67}hd_{33}$  + magnetite + quartz + vapor  $\rightleftharpoons$  clinopyroxene + magnetite + melt + vapor.

(QFM)  $ac_{67}hd_{33}$  + fayalite + magnetite + quartz + vapor  $\rightleftharpoons$  clinopyroxene + fayalite + magnetite + melt + vapor.

(C-CH<sub>4</sub>)  $ac_{67}hd_{33}$  + fayalite + quartz + vapor  $\rightleftharpoons$  clinopyroxene + fayalite + melt + vapor.

Table II-4 yields the cell parameters of coexisting phases in the bulk composition Fe<sub>5</sub>. At higher  $f_{O_2}$  the amphibole becomes a ferririchterite coexisting with an acmitic pyroxene. The pyroxene coexisting with melt greatly increases in a, b, and V with a large decrease in  $\beta$  from QFM to I-W. This indicates an increase in acmite component as  $f_{O_2}$  is increased if the data of Nolan (1969) is loosely applied. Judging from the gradual disappearance of (020) and (310) reflections as  $f_{O_2}$  decreases and the limited unit cell data, the conclusion is that the pyroxene reacts continuously with the melt and possibly the other solid phases as  $f_{O_2}$  is varied. Na and silica from the melt and Fe

react to yield a more acmitic pyroxene at higher  $f_{O_2}$ . Such variations are not present in the subsolidus region. The pyroxene,  $ac_{67}hd_{33}$ , remains at constant composition on QFM and HMT as verified by the unit cell dimensions, the determinative curves of Nolan (1969), and the electron microprobe. The result of these observations is that there is a singular invariant point occurring just above the WMt buffer at approximately 770°C at 1 kb  $P_{Tot}$ .

The dashed extension of the melting curve to higher  $f_{O_2}$  is estimated using the data of Bailey (1969) for the melting of acmite.

Clinopyroxene Stability

P (kb)	Buffer	T (±10°C)	
		Acmite (Bailey, 1969)	$Ac_{67}Hd_{33}$ (+Fa+Mt+Q)
1	HMT	890	---
1	NNO	850	845
1	QFM	810	815

The partial melting of  $ac_{67}hd_{33}$  occurs almost at the same conditions as does acmite. Another similarity is that  $ac_{67}hd_{33}$  (+fayalite + magnetite + quartz + vapor) reacts to form amphibole (ferrorichterite) at lower  $f_{O_2}$ , while acmite also forms amphibole under similar conditions (riebeckite-arfvedsonite).

Intermediate Compositions:  $(Na_2Ca(Mg,Fe)_5Si_8O_{22}(OH)_2)$

The phase equilibria of compositions along the join  $Na_2CaMg_5-Si_8O_{22}(OH)_2 - Na_2CaFe_5Si_8O_{22}(OH)_2$  are defined on 2 buffers for

the compositions  $Mg_4Fe$  through  $Mg_2Fe_3$  and on all 6 buffers for  $MgFe_4$  and  $Fe_5$ . W-Mt and I-W buffers were impracticable for experiments above 850 °C. Even with heavy gauge gold capsules with methane as a pressure medium,  $H_2$  readily leaked from these systems. Experiments of 18-24 hrs. at 850°C and 1 kb were the maximum duration possible. Equilibrium in such short duration experiments is difficult to prove. The Ni-NiO buffer could not be used above about 900°C. At 1000°C reaction of the buffer with the outer gold capsule was great enough to erode away over 1/2 of the gold making the buffer useless.

Actual compositions of the individual decomposition phases has only been partially successful. Olivine compositions could be easily obtained by measuring the  $d_{130}$  interplanar spacing and applying the determinative formula empirically derived by Fisher and Madaris (1969):

$$X_{FeO} = 15.8113 \sqrt{3.0358 - d_{130}} - 7.2250$$

Here  $X$  is the mole fraction of  $Mg_2SiO_4$ . Errors are about  $\pm 0.02$  mole fraction  $Mg_2SiO_4$ . The addition of Ca to olivine was considered negligible. Experiments on  $Fe_5$  contained olivine with a  $d_{130}$  of 2.828 Å ( $Fa_{100 \pm 3}$ ) while those on  $Mg_5$  yielded a  $d_{130}$  of 2.765 Å ( $Fa_{0 \pm 3}$ ). Glasses were usually clear and contain only Na and Si judging from the microprobe results. Addition of small amounts of Fe produces a bluish glass on I-W buffer.

Pyroxene compositions were not determined exactly. Lattice parameters on various buffers and different P, T conditions are tabulated but can be interpreted only in a vague manner.

Microprobe data has been of little value due to the small crystal size and the volatilization of Na. Such data at least did show the pyroxenes do drift off the di-ac-hd triangle of Nolan (1969). As for the unit cell refinements themselves, in many cases only 5 or 6 reflections could be unambiguously identified. Poor crystallization and interference with coexisting phases were always a problem. The peaks chosen (even in refinements with small standard errors) usually did not yield good control on  $c$  and hence volume. The  $a$  and  $b$  dimensions were resolved well in most cases. All of these limitations make compositional interpretations difficult. In special cases as on H-Mt and I-W buffers where one may assume larger and smaller amounts of ferric iron, respectively, some interpretations will be made. Compositional interpretations are based primarily upon comparing the  $a$  and  $b$  dimensions with those observed in the system ac-di-hd (Nolan, 1969). Large errors in  $c$  and  $\beta$ , the presence of a melt phase, and the possibility of small amounts of hedenbergite (on H-Mt) make the (221)-(002) and (002)-(131) determinative curves of Nolan and Edgar (1963) for the system acmite-diopside of little value. Data for pyroxenes grown on intermediate buffers have been tabulated, but any conclusions drawn from them will be with great reservations.

Each composition will be treated in order from  $Mg_4Fe$  to  $MgFe_4$ .  $Na_2CaMg_4FeSi_8O_{22}(OH)_2$ : On H-Mt the bulk composition  $Mg_4Fe$  yields amphibole + clinopyroxene. Results on QFM are >95% amphibole. The phase relations of amphibole in the bulk composition  $Mg_4Fe$  are shown in the isobaric  $\log f_{O_2}$  vs.  $T$  plot in

figure II-5. Experimental data for this diagram are in table II-6. Numerically the stability limits of amphibole at  $P_{\text{Tot}} = 1 \text{ kb}$  are:

(H-Mt)  $980 \pm 10^\circ\text{C}$

(QFM)  $985 \pm 10^\circ\text{C}$

All lattice parameters of amphibole on QFM and H-Mt are in table II-7. Pyroxene unit cell parameters encountered in this bulk composition are listed in the same table.

The decomposition relations are:

(H-Mt) Amphibole + clinopyroxene  $\rightleftharpoons$  clinopyroxene + forsterite + magnetite + hematite + melt + vapor.

(QFM) Amphibole  $\rightleftharpoons$  clinopyroxene + olivine + magnetite + melt + vapor.

Amphibole was always present in the high temperature assemblage. The experiments at  $1000^\circ\text{C}$  were in the transition loop between amphibole + clinopyroxene and clinopyroxene + forsterite + hematite + magnetite + melt. Amphibole at  $1025^\circ\text{C}$  is probably quench since it consists of fine isotropic needles. Olivine changes composition from  $\text{Fa}_{16 \pm 5}$  on QFM to  $\text{Fa}_{0 \pm 5}$  on H-Mt. Only this bulk composition (other than  $\text{Mg}_5$  of course) has olivine present on H-Mt. Under these highly oxidizing conditions no fayalite component exists in the olivine. The glass varies in R. I. from  $1.529 \pm .001$  on QFM to  $1.537 \pm .001$  on H-Mt. This order of difference is persistent across the iron bearing members of the series indicating at higher  $f_{\text{O}_2}$  Na is removed from the glass

Figure II-5. Isobaric ( $P_{\text{Tot}} = 1 \text{ kb}$ )  $\text{Log } f_{\text{O}_2} - T$  diagram for  $\text{Mg}_4\text{Fe}$  bulk composition. See T-X sections for interpretation of the transition loop.



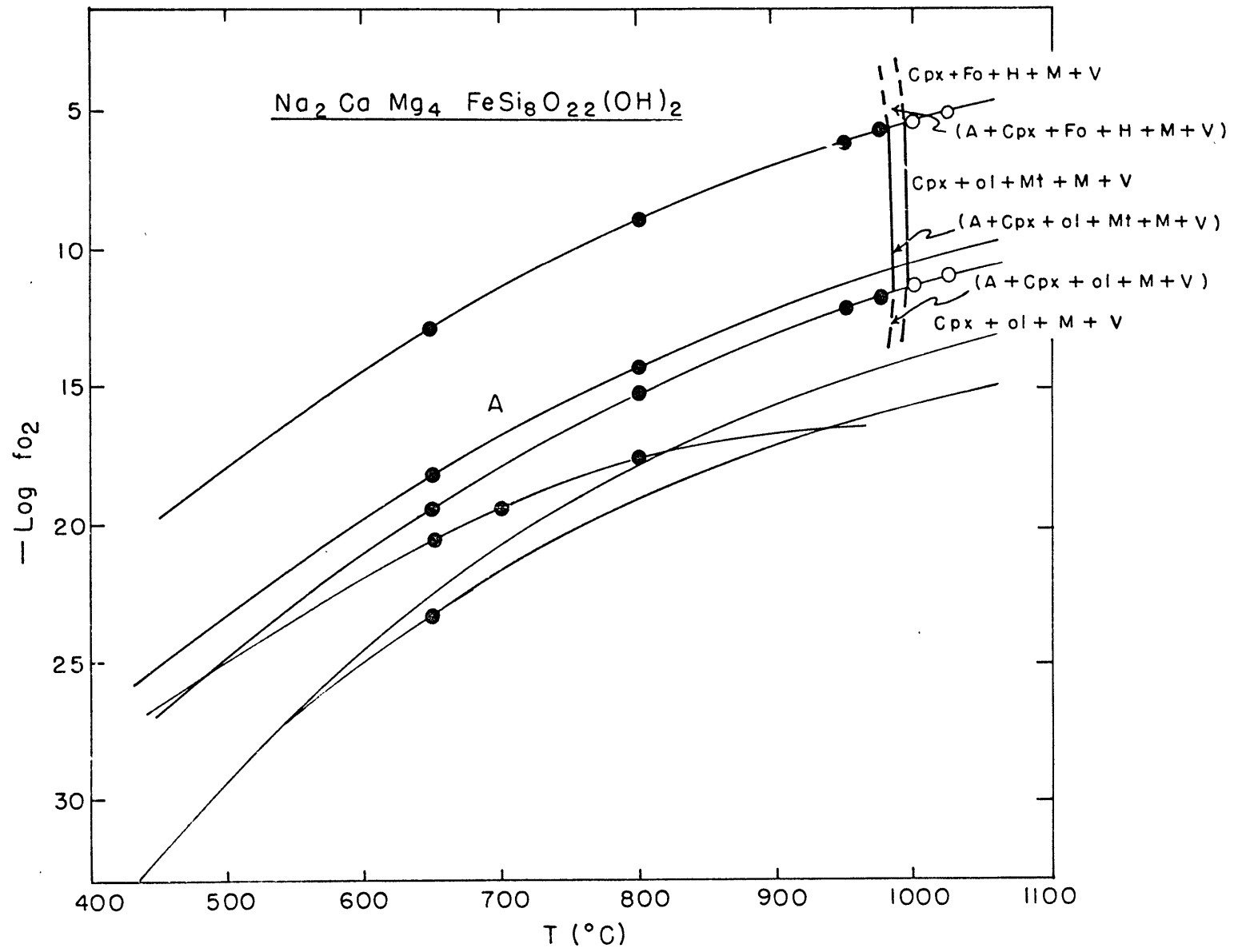


Table II-6. Bracketing Experiments:  $\text{Na}_2\text{CaMg}_4\text{FeSi}_8\text{O}_{22}(\text{OH})_2$  ( $P_{\text{Tot}} = 1 \text{ Kb}$ )

<u>Buffer</u>	<u>T</u> <u>(<math>\pm 5^\circ\text{C}</math>)</u>	<u>Duration</u> <u>(hrs.)</u>	<u>Reactants</u>	<u>Products</u>
HMt	1000	33	Oxidized Mix	Cpx+Fo+Mt+H+M
"	"	29	A+Cpx	"
"	975	24	Cpx+Fo+Mt+H+M	A+Cpx
"	950	24	Mix	"
NNO	800	96	"	A+ (Cpx)
QFM	1000	28	A	Cpx+Ol+Mt+M
"	975	23	"	A
"	950	24	Mix	"
C-CH <sub>4</sub>	800	100	"	"
IW	650	140	"	"

Table II-7. Unit Cell Parameters

Bulk Composition:  $\text{Na}_2\text{CaMg}_4\text{FeSi}_8\text{O}_{22}(\text{OH})_2$ 

Phase	Coexisting Phase (s)	P (bars)	T (°C)	a (Å)	b (Å)	c (Å)	$\beta$	V (Å <sup>3</sup> )
$\text{Fe}_3\text{O}_4 - \text{Fe}_2\text{O}_3$ Buffer								
Cpx	A	1000	800	9.702(7)	8.854(13)	5.276(11)	106°26' (4')	434.7(7)
Cpx	A	1000	800	9.704	8.880	5.255	106°25'	434.4
Cpx	A	1000	650	9.709(8)	8.866(15)	5.258(13)	106°22' (4')	434.2(7)
Cpx	Fo+H+Mt+gl	1000	1000	9.719(2)	8.920(16)	5.220(15)	106°37' (7')	434.1(9)
A	Cpx	1000	800	9.839(4)	17.963(7)	5.276(2)	104°2' (2')	904.6(4)
A	Cpx	1000	800	9.835(5)	17.978(6)	5.282(2)	104°4' (2')	906.0(4)
A	Cpx	1000	650	9.823(5)	17.964(6)	5.285(3)	103°59' (2')	905.0(4)
A	Cpx	1000	650	9.838(3)	17.944(6)	5.281(2)	103°56' (2')	904.9(4)
$\text{Ni} - \text{NiO}$ Buffer								
A	Cpx	1000	800	9.898(3)	18.019(7)	5.279(3)	104°7' (3')	913.1(5)
A	Cpx	1000	800	9.894(2)	18.004(3)	5.279(2)	104°3' (1')	912.0(4)
A	Cpx	1000	800	9.901(1)	18.003(4)	5.278(1)	104°5' (1')	912.5(2)
A	Cpx	1000	650	9.894(3)	18.005(8)	5.275(2)	104°5' (3')	911.5(5)
$\text{Fe}_2\text{SiO}_4 - \text{SiO}_2 - \text{Fe}_3\text{O}_4$ Buffer								
Cpx	Ol+Mt+gl	1000	1000	9.752(4)	8.907(7)	5.201(10)	106°52' (10')	432.3(1.1)
A	-	1000	800	9.896(2)	18.003(4)	5.279(2)	104°5' (1')	912.3(3)
A	-	1000	800	9.890(2)	18.003(6)	5.282(1)	104°4' (1')	912.2(3)

Table II-7 (Cont.)

Phase	Coexisting Phase(s)	P (bars)	T (°C)	a (Å)	b (Å)	c (Å)	$\beta$	V (Å <sup>3</sup> )
Fe <sub>2</sub> SiO <sub>4</sub> - SiO <sub>2</sub> - Fe <sub>3</sub> O <sub>4</sub> Buffer (Cont'd.)								
A	-	1000	650	9.891(4)	18.000(13)	5.283(2)	104°3'(2')	912.4(4)
A	-	7000	600	9.891(8)	18.013(5)	5.285(4)	104°10'(4')	912.9(8)
C - CH <sub>4</sub> Buffer								
A	-	1000	650	9.904(4)	18.017(3)	5.276(1)	104°10'(3')	912.8(4)
A	-	1000	650	9.906(4)	17.995(6)	5.278(2)	104°9'(3')	912.3(5)
A	-	1000	650	9.904(3)	18.000(4)	5.279(1)	104°6'(1')	912.7(3)
Fe - FeO Buffer								
A	-	1000	650	9.916(2)	18.017(4)	5.276(1)	104°4'(1')	914.8(2)
A	-	1000	650	9.913(4)	18.017(7)	5.277(2)	104°4'(3')	914.2(4)
A	-	1000	650	9.918(3)	18.019(5)	5.277(2)	104°10'(2')	914.4(4)
A	-	2000	650	9.919(4)	18.022(6)	5.276(2)	104°10'(2')	914.4(4)
A	-	7000	600	9.917(2)	18.027(4)	5.276(1)	104°10'(1')	914.6(2)
A	-	5000	550	9.916(4)	18.024(4)	5.280(1)	104°8'(2')	915.0(3)
A	-	10000	530	9.918(6)	18.015(9)	5.277(3)	104°9'(4')	914.3(5)

making it more silica rich. Na and Fe increase the acmite component of the pyroxene. Variations in pyroxene composition are subtle. The cell data indicate a somewhat larger a and b for pyroxenes existing with glass on H-Mt compared with those existing with amphibole. A small enhancement of the di or hd component upon partial melting is one of the mechanisms for producing such a change. On H-Mt if most of the iron is assumed to be ferric, the variation of pyroxene is from  $ac_{40}hd_{60}$  coexisting with amphibole to  $ac_{30}di_{70}$  coexisting with melt using a and b for the system ac-di-hd of Nolan (1969). The decrease in a from QFM to H-Mt may indicate a similar change although this is admittedly vague. Variations in c and V are not interpreted due to the insensitivity of the data.

$Na_2CaMg_3Fe_2Si_8O_{22}(OH)_2$ : All experiments on this bulk composition above C-CH<sub>4</sub> within the area of amphibole stability contained stable clinopyroxene in the product. The phase relations of amphibole in this composition are shown in figure II-6 and table II-8. The maximum stability of the amphibole is:

(H-Mt) 945± 5°C

(QFM) 955±10°C

The decomposition relations are:

(H-Mt) Amphibole + clinopyroxene ⇌ clinopyroxene + hematite + magnetite + melt + vapor.

(QFM) Amphibole + clinopyroxene ⇌ clinopyroxene + olivine + magnetite + melt + vapor.

The decomposition assemblage could be quenched without the

Figure II-6. Isobaric ( $P_{\text{Tot}} = 1 \text{ kb}$ )  $\text{Log } f_{\text{O}_2} - T$  diagram for  
 $\text{Mg}_3\text{Fe}_2$  bulk composition.

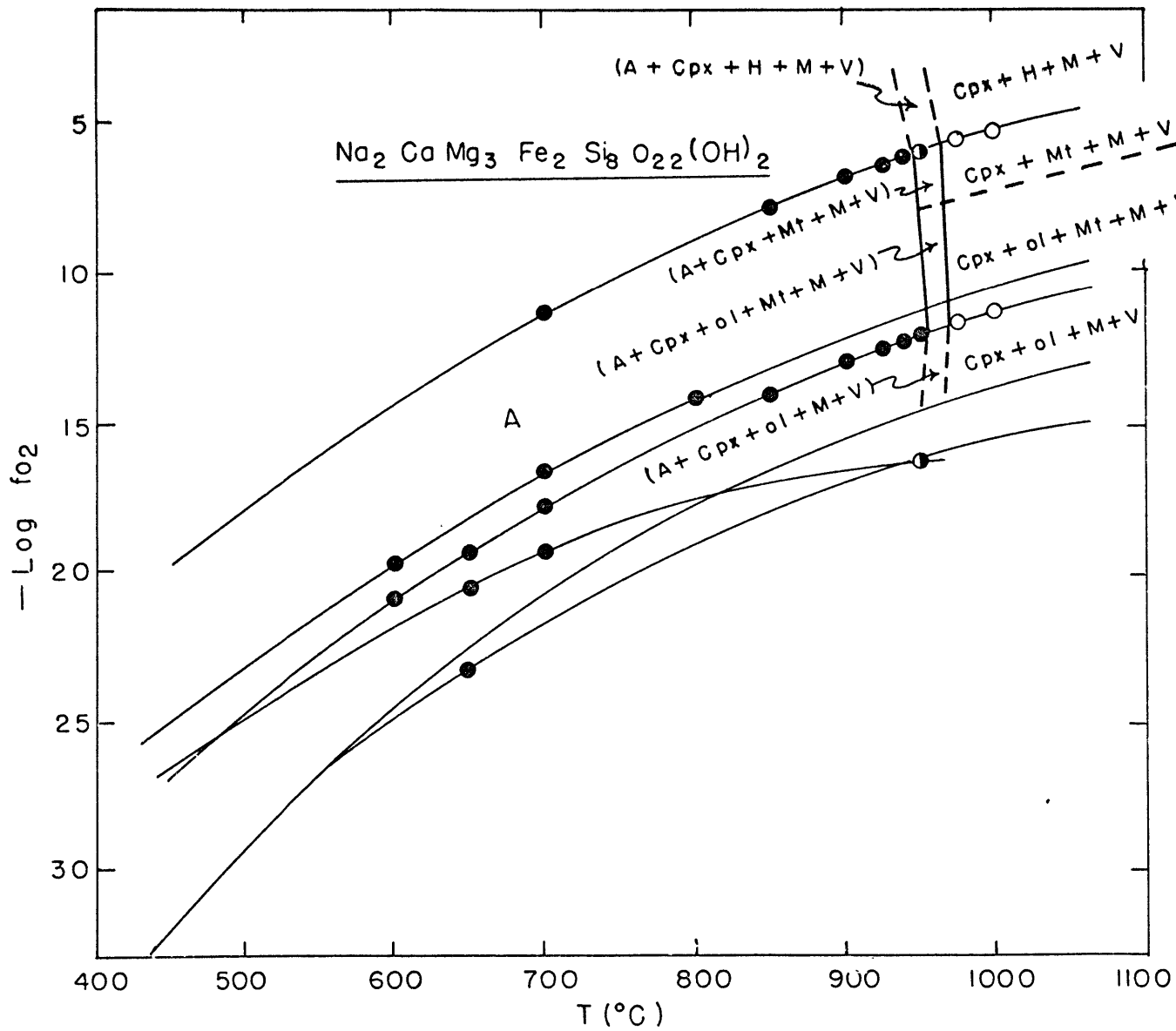


Table II-8. Bracketing Experiments:  $\text{Na}_2\text{CaMg}_3\text{Fe}_2\text{Si}_8\text{O}_{22}(\text{OH})_2$  ( $P_{\text{Tot}} = 1 \text{ Kb}$ )

<u>Buffer</u>	<u>T</u> ( $\pm 5^\circ\text{C}$ )	<u>Duration</u> (hrs.)	<u>Reactants</u>	<u>Products</u>
HMt	975	19	Cpx+Mt+H+M	Cpx+Mt+H+M
"	950	24	Mix	"
"	940	24	A+Cpx	A+Cpx+Mt+H+M
"	925	45	Cpx+Mt+H+M	A+Cpx
NNO	800	48	Mix	"
QFM	975	26	A+Cpx	Cpx+Ol+Mt+M
"	950	24	Mix	A+Cpx
"	940	24	A+Cpx	"
C-CH <sub>4</sub>	700	144	Mix	A
IW	950	10	A	A+Cpx+Fa+M



Table II-9. Unit Cell Parameters

Bulk Composition:  $\text{Na}_2\text{CaMg}_3\text{Fe}_2\text{Si}_8\text{O}_{22}(\text{OH})_2$ 

Phase	Coexisting Phase(s)	P (bars)	T (°C)	a (Å)	b (Å)	c (Å)	$\beta$	V (Å <sup>3</sup> )
Fe <sub>3</sub> O <sub>4</sub> - Fe <sub>2</sub> O <sub>3</sub> Buffer								
A	Cpx	1000	900	9.822(6)	17.982(11)	5.281(5)	103°36'(6')	906.6(0.9)
A	Cpx	1000	850	9.823(2)	17.999(3)	5.287(1)	103°49'(1')	907.8(0.2)
Cpx	A	1000	850	9.702(8)	8.848(11)	5.281(14)	106°45'(5')	434.1(0.8)
Cpx	H+Mt+gl	1000	1000	9.717(13)	8.865(18)	5.246(45)	107°3'(16')	432.1(3.1)
Cpx	H+Mt+gl	1000	1000	9.730(6)	8.864(5)	5.252(20)	106°50'(8')	433.6(1.7)
Ni - NiO Buffer								
A	Cpx	1000	700	9.870(14)	18.032(12)	5.266(20)	103°35'(18')	911.0(3.2)
A	Cpx	1000	550	9.848(4)	18.003(4)	5.279(2)	104°5'(1')	912.3(0.3)
Fe <sub>2</sub> SiO <sub>4</sub> - SiO <sub>2</sub> - Fe <sub>3</sub> O <sub>4</sub> Buffer								
A	Cpx	1000	900	9.864(8)	18.052(7)	5.265(11)	103°27'(10')	911.7(1.8)
A	Cpx	1000	850	9.845(2)	18.016(4)	5.291(1)	103°53'(1')	911.0(0.2)
A	Cpx	1000	700	9.859(12)	18.010(10)	5.303(18)	103°45'(16')	914.5(2.8)
A	Cpx	1000	650	9.863(3)	18.010(4)	5.294(1)	103°53'(2')	912.9(0.8)
A	Cpx	1000	550	9.864(10)	18.029(15)	5.291(6)	103°57'(9')	913.1(1.2)
A	Cpx	7000	600	9.861(5)	18.030(9)	5.292(3)	103°58'(4')	913.2(0.5)
Cpx	A	1000	700	9.723(11)	8.856(15)	5.291(20)	106°36'(6')	436.6(1.1)

Table II-9. (Cont.)

Phase	Coexisting Phase (s)	P (bars)	T (°C)	a (Å)	b (Å)	c (Å)	$\beta$	V (Å <sup>3</sup> )
Cpx	A	1000	650	9.729 (5)	8.889 (10)	5.236 (16)	106°32' (4')	434.1 (0.9)
Cpx	Ol+Mt+gl	1000	1000	9.752 (5)	8.907 (8)	5.201 (10)	106°52' (5')	432.3 (0.8)
Cpx	Ol+Mt+gl	1000	1000	9.765 (5)	8.916 (7)	5.200 (15)	106°47' (6')	433.3 (0.9)
Fe - FeO Buffer								
A	-	1000	650	9.936 (4)	18.062 (7)	5.285 (2)	104°4' (3')	920.0 (0.4)
A	-	1000	650	9.930 (4)	18.064 (6)	5.283 (3)	104°3' (2')	919.3 (0.4)
A	-	1000	650	9.936 (4)	18.065 (6)	5.287 (2)	104°4' (2')	920.5 (0.4)
A	-	2000	650	9.935 (4)	18.057 (6)	5.279 (2)	104°6' (2')	918.5 (0.4)
A	-	7000	600	9.938 (2)	18.067 (3)	5.284 (1)	104°10' (3')	920.0 (0.2)
A	-	5000	550	9.942 (5)	18.089 (11)	5.287 (3)	104°9' (3')	921.9 (0.7)
A	-	10000	530	9.927 (5)	18.064 (8)	5.285 (2)	104°5' (2')	919.2 (0.5)

the growth of amphibole. Olivine is no longer present on the H-Mt buffer. The olivine present on QFM is  $\text{Fe}_{25\pm 5}$ . The quench glass varies from R.I.  $1.527\pm.001$  on QFM to  $1.542\pm.001$  on H-Mt. Lattice parameters of coexisting amphibole and pyroxene and pyroxene and glass are reported in table II-9.

With the onset of partial melting the pyroxenes show a move away from acmite on both buffers enhancing di and possibly hd components (larger a, b, and smaller c). If most of the iron on H-Mt is ferric, the change is from  $\text{ac}_{50}\text{di}_{50}$  to  $\text{ac}_{40}\text{di}_{60}$ . Probably a continuous reaction exists between the pyroxene and melt as one proceeds to higher T. Pyroxenes grown on QFM in the solidus region have larger a, b, and smaller c than corresponding ones on H-Mt. With lower  $f_{\text{O}_2}$  addition of the more reduced component hedenbergite would produce such a change.

$\text{Na}_2\text{CaMg}_2\text{Fe}_3\text{Si}_8\text{O}_{22}(\text{OH})_2$ :  $\text{Mg}_2\text{Fe}_3$  could not be grown on composition above the I-W buffer. Clinopyroxene exists with amphibole on all higher buffers. Phase relations are presented in figure II-7 and experimental data in table II-10. Maximum stability limits of amphibole were investigated only on QFM and H-Mt. These are:

(H-Mt)  $905\pm 10^\circ\text{C}$

(QFM)  $910\pm 10^\circ\text{C}$

The decomposition relations are:

(H-Mt) Amphibole + clinopyroxene  $\rightleftharpoons$  clinopyroxene + hematite + magnetite + melt + vapor.

(QFM) Amphibole + clinopyroxene  $\rightleftharpoons$  clinopyroxene + olivine + magnetite + melt + vapor.

Figure II-7. Isobaric ( $P_{\text{Tot}} = 1 \text{ kb}$ )  $\text{Log } f_{\text{O}_2} - T$  diagram for  $\text{Mg}_2\text{Fe}_3$  bulk composition.

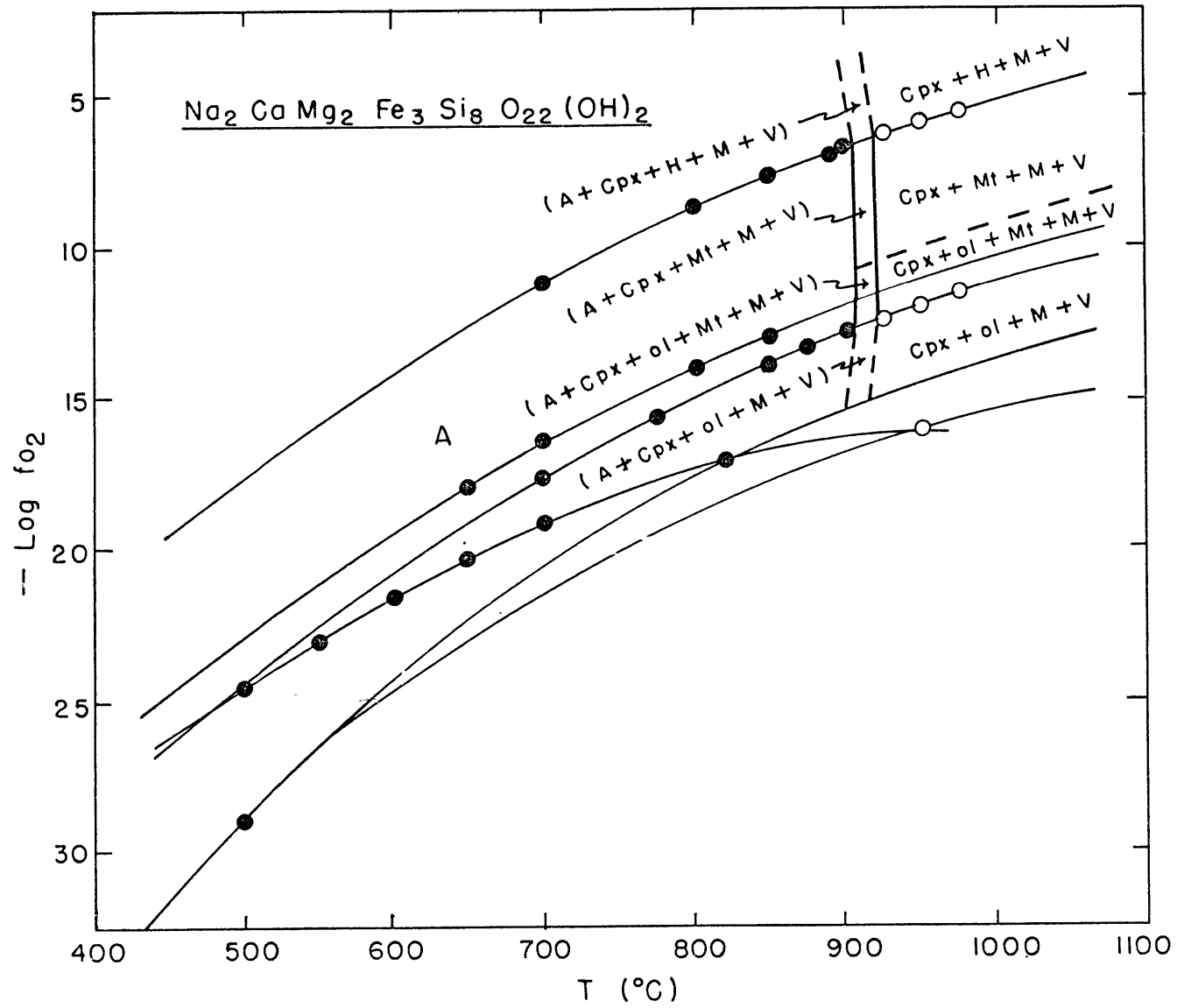


Table II-10. Bracketing Experiments:  $\text{Na}_2\text{CaMg}_2\text{Fe}_3\text{Si}_8\text{O}_{22}(\text{OH})_2$  ( $P_{\text{Tot}} = 1 \text{ Kb}$ )

<u>Buffer</u>	<u>T</u> ( $\pm 5^\circ\text{C}$ )	<u>Duration</u> (hrs.)	<u>Reactants</u>	<u>Products</u>
HMt	925	26	Cpx+Ol+Mt+M	Cpx+Mt+H+M
"	900	27	A+Cpx	A+Cpx
"	890	36	Cpx+Ol+Mt+M	"
NNO	850	48	Mix	"
QFM	925	26	Cpx+Ol+Mt+M	Cpx+Ol+Mt+M
"	900	27	A+Cpx	A+Cpx
C-CH <sub>4</sub>	820	48	Mix	A+(Cpx)
IW	950	10	A	Cpx+Ol+M
"	500	960	Mix	A

Table II-11. Unit Cell Parameters

Bulk Composition:  $\text{Na}_2\text{CaMg}_2\text{Fe}_3\text{Si}_8\text{O}_{22}(\text{OH})_2$ 

Phase	Coexisting Phase (s)	P (bars)	T (°C)	a (Å)	b (Å)	c (Å)	$\beta$	V (Å <sup>3</sup> )
Fe <sub>3</sub> O <sub>4</sub> - Fe <sub>2</sub> O <sub>3</sub> Buffer								
A	Cpx	1000	900	9.795(5)	17.981(8)	5.298(3)	103°54' (4')	905.7(0.6)
A	Cpx	1000	700	9.790(1)	18.015(2)	5.298(1)	103°42' (1)	907.8(0.2)
Cpx	A	1000	900	9.703(5)	8.854(4)	5.270(6)	106°50' (3')	433.5(0.4)
Cpx	H+Mt+gl	1000	950	9.703(5)	8.844(5)	5.276(7)	106°46' (3')	433.5(0.5)
Ni - NiO Buffer								
A	Cpx	1000	764	9.844(2)	18.052(4)	5.296(2)	103°41' (2')	915.3(0.3)
A	Cpx	1000	700	9.851(3)	18.059(7)	5.297(3)	103°38' (3')	915.7(0.4)
Cpx	A	1000	700	9.724(7)	8.846(10)	5.295(32)	106°37' (11')	439.7(0.5)
Fe <sub>2</sub> SiO <sub>4</sub> - SiO <sub>2</sub> - Fe <sub>3</sub> O <sub>4</sub> Buffer								
A	Cpx	1000	700	9.867(3)	18.075(6)	5.300(3)	103°44' (3')	918.2(0.4)
A	Cpx	2000	500	9.857(4)	18.061(7)	5.301(4)	103°52' (4')	916.1(0.6)
Cpx	A	1000	700	9.730(4)	8.891(6)	5.256(7)	106°32' (2')	435.9(0.4)
Cpx	Ol+Mt+gl	1000	975	9.729	8.899	5.319	106°12'	442.2
C - CH <sub>4</sub> Buffer								
A	Cpx	1000	820	9.919(4)	18.103(5)	5.291(3)	103°52' (2')	922.4(0.4)
A	Cpx	1000	600	9.872(4)	18.073(5)	5.296(3)	103°49' (3')	917.5(0.5)
A	Cpx	1000	550	9.870(5)	18.070(7)	5.301(4)	103°44' (5')	918.4(0.7)

Table II-11. (Cont.)

Phase	Coexisting Phase(s)	P (bars)	T (°C)	a (Å)	b (Å)	c (Å)	$\beta$	V (Å <sup>3</sup> )
C - CH <sub>4</sub> Buffer (cont'd.)								
A	Cpx	1000	500	9.881(14)	18.072(21)	5.299(11)	104°14'(12')	917.2(1.7)
Fe - FeO Buffer								
A	-	7000	600	9.970(4)	18.126(5)	5.289(1)	104°6'(2')	927.0(4)
A	-	2000	530	9.955(3)	18.130(5)	5.293(1)	104°0'(1')	926.9(3)
A	-	5000	530	9.962(4)	18.122(6)	5.294(2)	104°4'(3')	927.6(4)
A	-	10000	530	9.958(9)	18.113(11)	5.293(3)	104°4'(5')	926.1(7)
A	-	2000	500	9.964(3)	18.121(4)	5.291(1)	104°5'(1')	926.6(3)



The olivine has a composition of  $Fa_{39\pm 5}$ . The glasses are still clear and have a R.I. of  $1.529\pm .001$  (QFM) and  $1.536\pm .001$  (H-Mt). Data concerning amphiboles and pyroxenes encountered on this bulk composition are presented in table II-11. Once again the pyroxenes show a definite change to larger a and b with decreasing  $f_{O_2}$ . Upon melting (H-Mt) the pyroxene becomes less acmitic ( $ac_{60}di_{40}$  to  $ac_{50}di_{50}$ ). Addition of data on C-CH<sub>4</sub> shows a nonuniformity of amphibole cell parameters which was not observed for a similar series of experiments on Mg<sub>4</sub>Fe due to the low total iron content. Since the C-CH<sub>4</sub> becomes more reducing with higher T compared to the other oxygen buffers, the amphibole becomes more ferrous. This is reflected by a larger a, b, and V at 820°C. 820°C on C-CH<sub>4</sub> is equivalent to W-Mt and 500°C on C-CH<sub>4</sub> approximately QFM. Variations in amphibole cell parameters on buffers of succeedingly higher  $f_{O_2}$  show smaller volume, a, b, and  $\beta$ . Absorbtion of Na and  $Fe^{+3}$  into the clinopyroxene is responsible for the change.

$Na_2CaMgFe_4Si_8O_{22}(OH)_2$ : All buffers above I-W caused significant amounts of clinopyroxene to grow with amphibole. On H-Mt only about 30% of the charge was amphibole by volume at 550°C. Even on I-W experiments at 1 kb yielded 10-20% clinopyroxene.

Experiments of long duration at high pressure ( $\geq 5$  kb) on I-W were necessary to grow a relatively pure charge of amphibole. The phase relations are represented in figure II-8 and table II-12. Maximum stabilities of amphibole in the bulk composition MgFe<sub>4</sub> are:

Figure II-8. Isobaric ( $P_{\text{Tot}} = 1 \text{ kb}$ )  $\text{Log } f_{\text{C}_2} - T$  diagram for  $\text{MgFe}_4$  bulk composition.

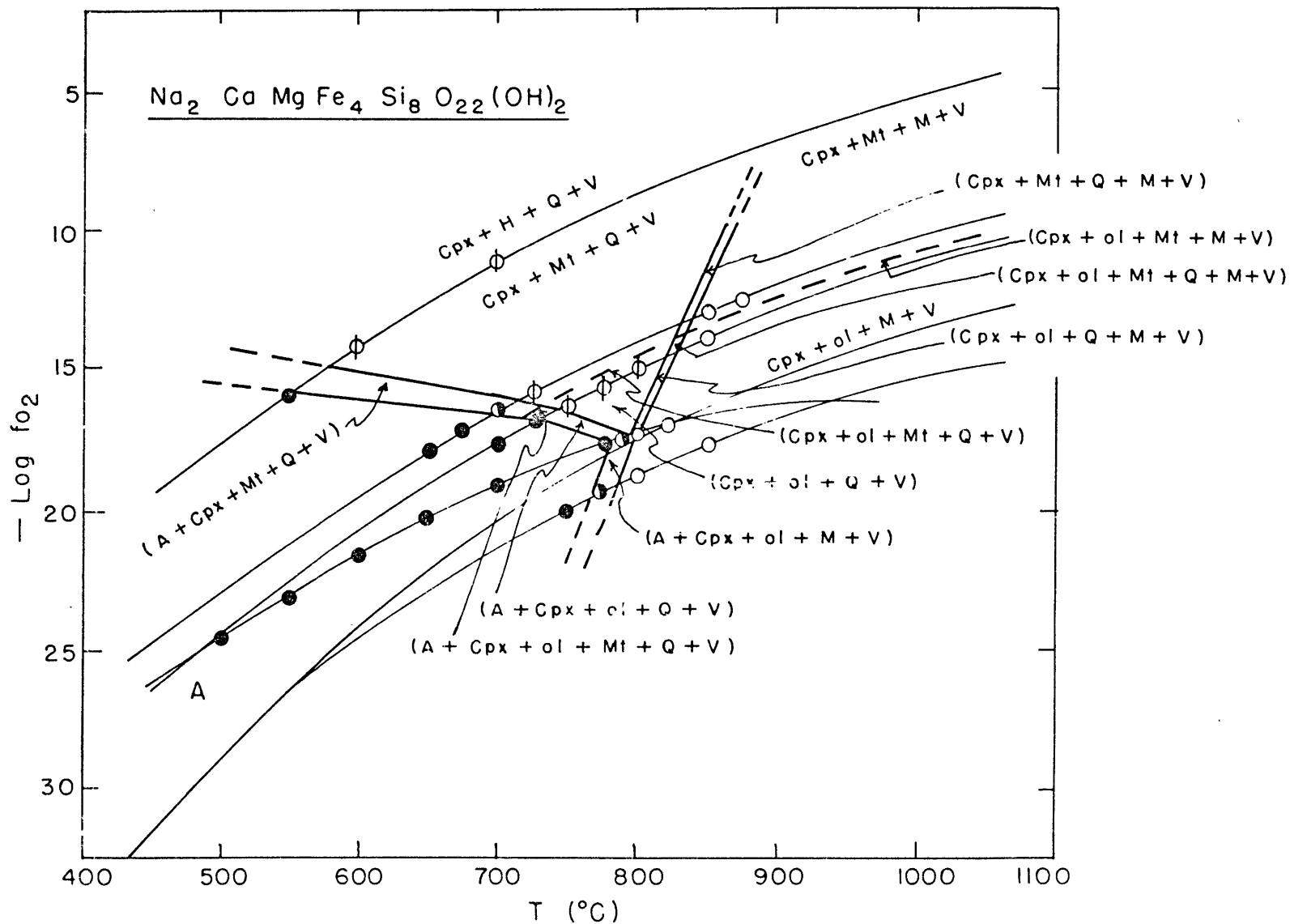


Table II-12. Bracketing Experiments:  $\text{Na}_2\text{CaMgFe}_4\text{Si}_8\text{O}_{22}(\text{OH})_2$  ( $P_{\text{Tot}} = 1 \text{ Kb}$ )

Buffer	T ( $\pm 5^\circ\text{C}$ )	Duration (hrs.)	Reactants	Products
HMt	600	326	Mix	Cpx+Mt+H+Q
"	550	360	Cpx+Ol+M	A+Cpx
NNO	875	47	Cpx+Mt+ (Q) + (A)	Cpx+Mt+M
"	850	48	Mix	Cpx+Mt+M+ (A)
"	725	164	Cpx+Mt+ (Q)	Cpx+Mt+ (Q)
"	700	138	A+Cpx	A+Cpx+ (Mt) + (Q)
"	675	182	Cpx+Ol+M	A+Cpx
QFM	850	48	Mix	Cpx+Ol+Mt+M+ (1:2:6)
"	800	121	"	Cpx+Ol+Mt+ (1:2:6)
"	750	67	Cpx+Ol+Mt+ (Q) + (1:2:6)	Cpx+Ol+Mt+ (Q)
"	725	138	A+Cpx	A+Cpx
C-CH <sub>4</sub>	800	48	Mix	Cpx+Ol+M
"	790	60	Cpx+Ol+M	A+Cpx+Ol+M
"	775	144	"	A+Cpx
IW	800	36	Cpx+Ol+Mt+ (1:2:6)	Cpx+Ol+M
"	775	49	Cpx+Ol+M	A+Cpx+Ol+M
"	750	58	Mix	A+Cpx

Table II-13. Unit Cell Parameters

Bulk Composition:  $\text{Na}_2\text{CaMgFe}_4\text{Si}_8\text{O}_{22}(\text{OH})_2$ 

Phase	Coexisting Phase(s)	P (bars)	T (°C)	a (Å)	b (Å)	c (Å)	$\beta$	V (Å <sup>3</sup> )
$\text{Fe}_3\text{O}_4 - \text{Fe}_2\text{O}_3$ Buffer								
Cpx	H+Mt+(Q)	1000	600	9.654(4)	8.936(6)	5.276(5)	106°49'(2')	435.7(0.3)
Ni - NiO Buffer								
A	Cpx	1000	700	9.827(1)	18.127(1)	5.275(2)	103°22'(1')	914.2(0.3)
Cpx	A	1000	700	9.685(2)	8.845(2)	5.299(3)	106°49'(1')	434.3(0.2)
$\text{Fe}_2\text{SiO}_4 + \text{SiO}_2 + \text{Fe}_3\text{O}_4$ Buffer								
A	Cpx+(Ol)	1000	725	9.849(10)	18.178(10)	5.297(14)	103°23'(13')	922.5(2.1)
A	Cpx	7000	500	9.879(5)	18.104(7)	5.315(3)	103°54'(4')	922.7(0.6)
Cpx	A+(Ol)	1000	700	9.703(5)	8.864(5)	5.280(8)	106°47'(3')	434.8(0.5)
Cpx	A	1000	725	9.715(6)	8.862(11)	5.340(29)	106°22'(9')	441.2(3.6)
C - CH <sub>4</sub> Buffer								
A	Cpx	1000	650	9.886(4)	18.127(5)	5.304(3)	103°38'(2')	923.7(0.4)
A	Cpx	1000	550	9.870(4)	18.119(3)	5.308(3)	103°35'(3')	922.8(0.5)
A	Cpx	1000	500	9.897(9)	18.159(14)	5.311(6)	103°42'(7')	927.3(1.1)
Fe - FeO Buffer								
A	-	5000	700	9.980(4)	18.185(6)	5.300(1)	103°56'(1')	933.6(4)
A	-	7000	600	9.988(2)	18.184(4)	5.292(1)	103°57'(2')	932.8(2)
A	-	10000	530	9.973(3)	18.172(5)	5.301(1)	104°0'(2')	931.8(3)

(H-Mt) 550±20°C

(Ni-NiO) 700±10°C

(QFM) 730±10°C

(C-CH<sub>4</sub>) 780±10°C

(I-W) 740±10°C

Decomposition relations are:

(H-Mt) Amphibole + clinopyroxene  $\rightleftharpoons$  clinopyroxene + hematite + magnetite + (quartz) + vapor.

(Ni-NiO) Amphibole + clinopyroxene  $\rightleftharpoons$  clinopyroxene + magnetite + (quartz) + vapor.

(QFM) Amphibole + clinopyroxene  $\rightleftharpoons$  clinopyroxene + olivine + magnetite + (quartz) + vapor.

(C-CH<sub>4</sub>) Amphibole + clinopyroxene  $\rightleftharpoons$  clinopyroxene + olivine + melt + vapor.

(I-W) Amphibole  $\rightleftharpoons$  clinopyroxene + olivine + melt + vapor.

The subsolidus decomposition assemblage partially melts according to:

(H-Mt) Clinopyroxene + hematite + magnetite + (quartz) + vapor  $\rightleftharpoons$  clinopyroxene + hematite + magnetite + melt + vapor.

(Ni-NiO) Clinopyroxene + magnetite + (quartz) + vapor  $\rightleftharpoons$  clinopyroxene + magnetite + melt + vapor.

(QFM) Clinopyroxene + olivine + magnetite + (quartz) + vapor  $\rightleftharpoons$  clinopyroxene + olivine + magnetite + melt + vapor.

The actual point of decomposition of amphibole was difficult to determine accurately. Amphibole undergoes a gradual

decomposition by continuous reaction with the decomposition assemblage as T is increased. The range of decomposition is spread over possibly 50°C. A further complication is the large quantity of clinopyroxene coexisting with amphibole. Also, metastable 1:2:6 Na-(Mg,Fe) silicate appears in the transition loop on QFM with clinopyroxene + olivine + magnetite + (quartz) + melt.

The olivine coexisting with melt on C-CH<sub>4</sub> and QFM is the same composition - pure fayalite (Fa<sub>95±5</sub>).

Small fields of clinopyroxene + olivine + magnetite + (quartz) + vapor and clinopyroxene + olivine + magnetite + melt + vapor are inferred just above the QFM buffer because small amounts of Mg<sub>2</sub>SiO<sub>4</sub> are probably present in the olivine. Olivine is not present on Ni-NiO.

Judging from the results on MgFe<sub>4</sub> the amphibole on intermediate compositions <sup>goes</sup> ^ through a zone of decomposition. Looking at the unit cell parameters for other intermediate compositions, this zone of decomposition is probably smaller than 20°C at one kb. Data points within 30°C of the decomposition curve show no significant change in lattice parameters from points further from the curve.

Figures II-9 through II-13 are isobaric (1 kb) T-X sections for the pseudo-binary: Na<sub>2</sub>CaMg<sub>5</sub>Si<sub>8</sub>O<sub>22</sub>(OH)<sub>2</sub> - Na<sub>2</sub>CaFe<sub>5</sub>Si<sub>8</sub>O<sub>22</sub>(OH)<sub>2</sub>. Experiments were performed only on the six labeled compositions. These diagrams show clearly why a transition loop between MgFe<sub>4</sub> + clinopyroxene and the subsolidus decomposition assemblage appears experimentally and why other transition loops do not. The configuration of transition loops around the "invariant

Figure II-9. Isobaric ( $P_{\text{Tot}} = 1\text{kb}$ ) T-X section for the pseudo-binary join richterite - ferrichterite with oxygen fugacities defined by the H-Mt buffer.



# Fe<sub>2</sub>O<sub>3</sub> - Fe<sub>3</sub>O<sub>4</sub> Buffer

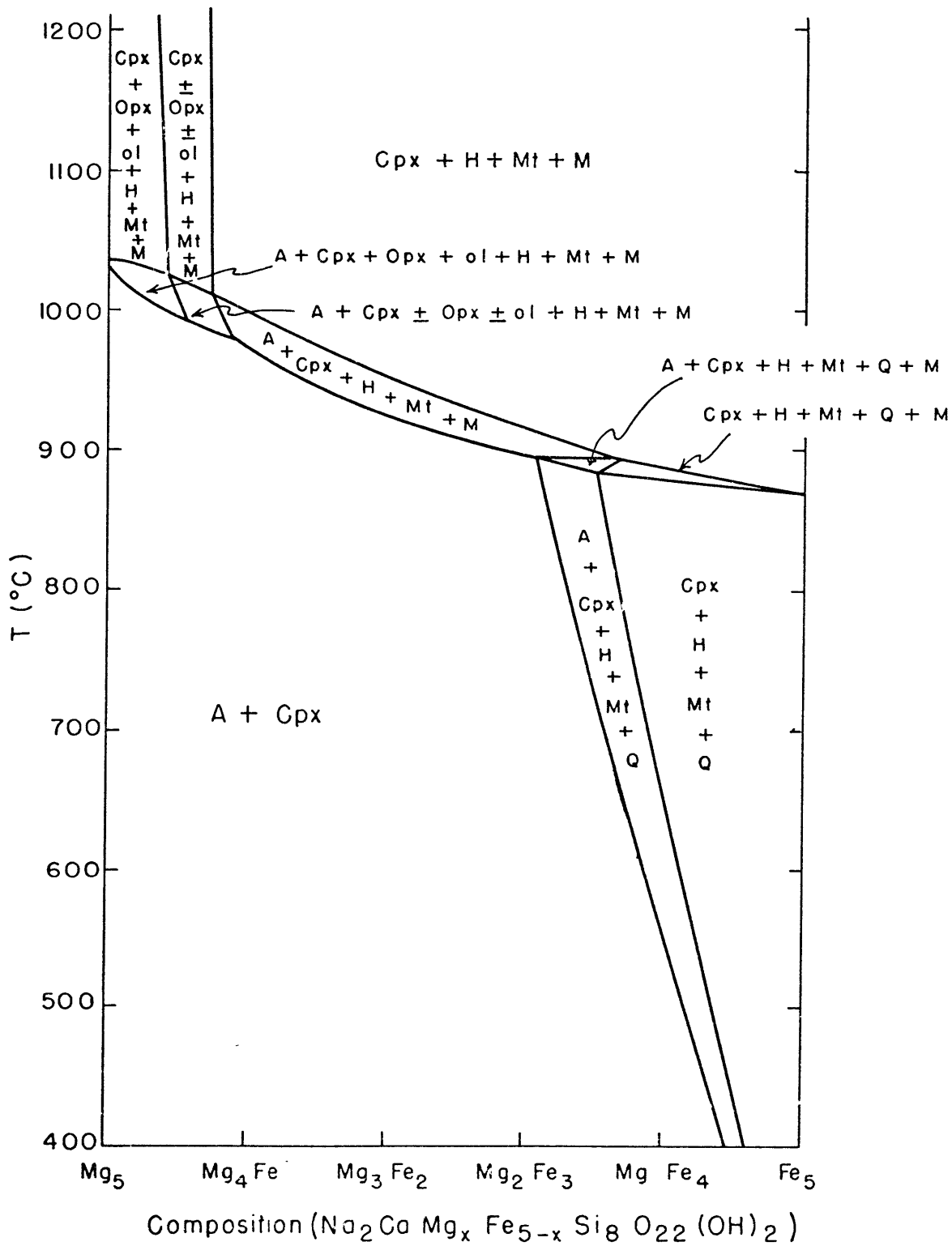


Figure II-10. Isobaric ( $P_{\text{Tot}} = 1 \text{ kb}$ ) T-X section for the pseudo-binary join richterite - ferrorichterite with oxygen fugacities defined by the QFM buffer.

Fe<sub>2</sub>SiO<sub>4</sub> - Fe<sub>3</sub>O<sub>4</sub>-SiO<sub>2</sub> Buffer

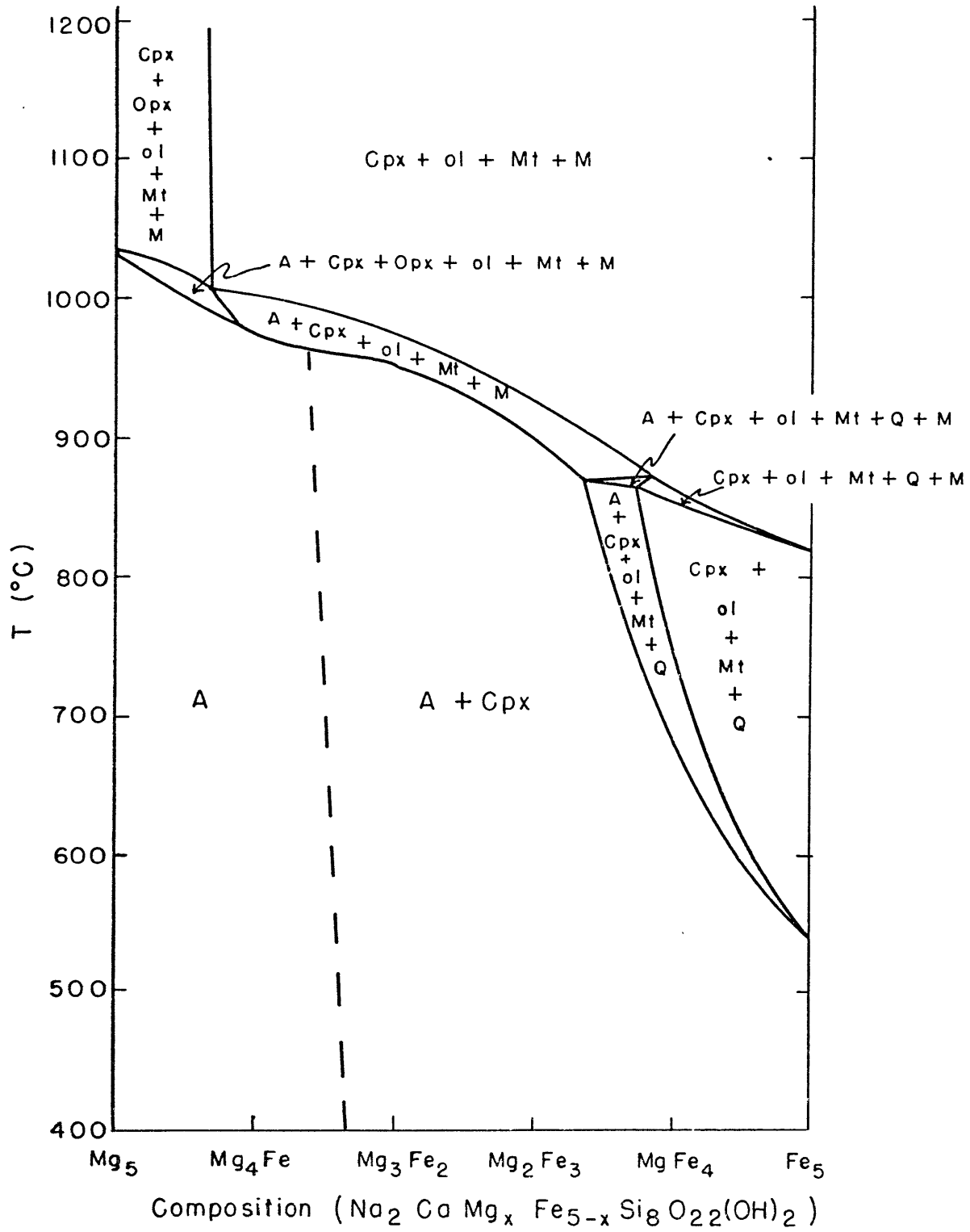


Figure II-11. Isobaric ( $P_{\text{Tot}} = 1 \text{ kb}$ ) T-X section for the pseudo-binary join richterite - ferrorichterite with oxygen fugacities defined by the C-CH<sub>4</sub> buffer.

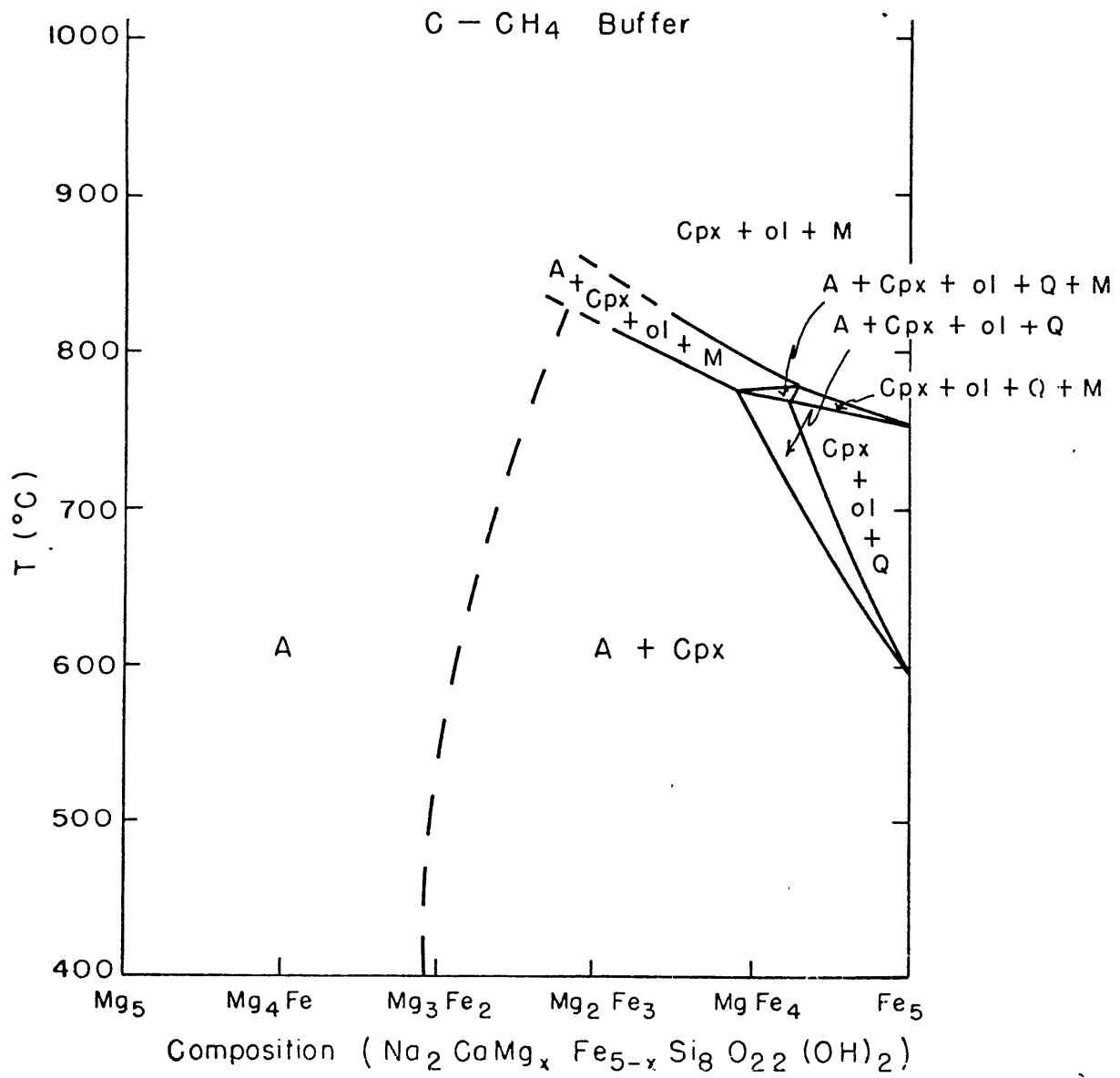


Figure II-12. Isobaric ( $P_{\text{Tot}} = 1 \text{ kb}$ ) T-X section for the pseudo-binary join richterite - ferrichterite with oxygen fugacities defined by the W-Mt buffer.

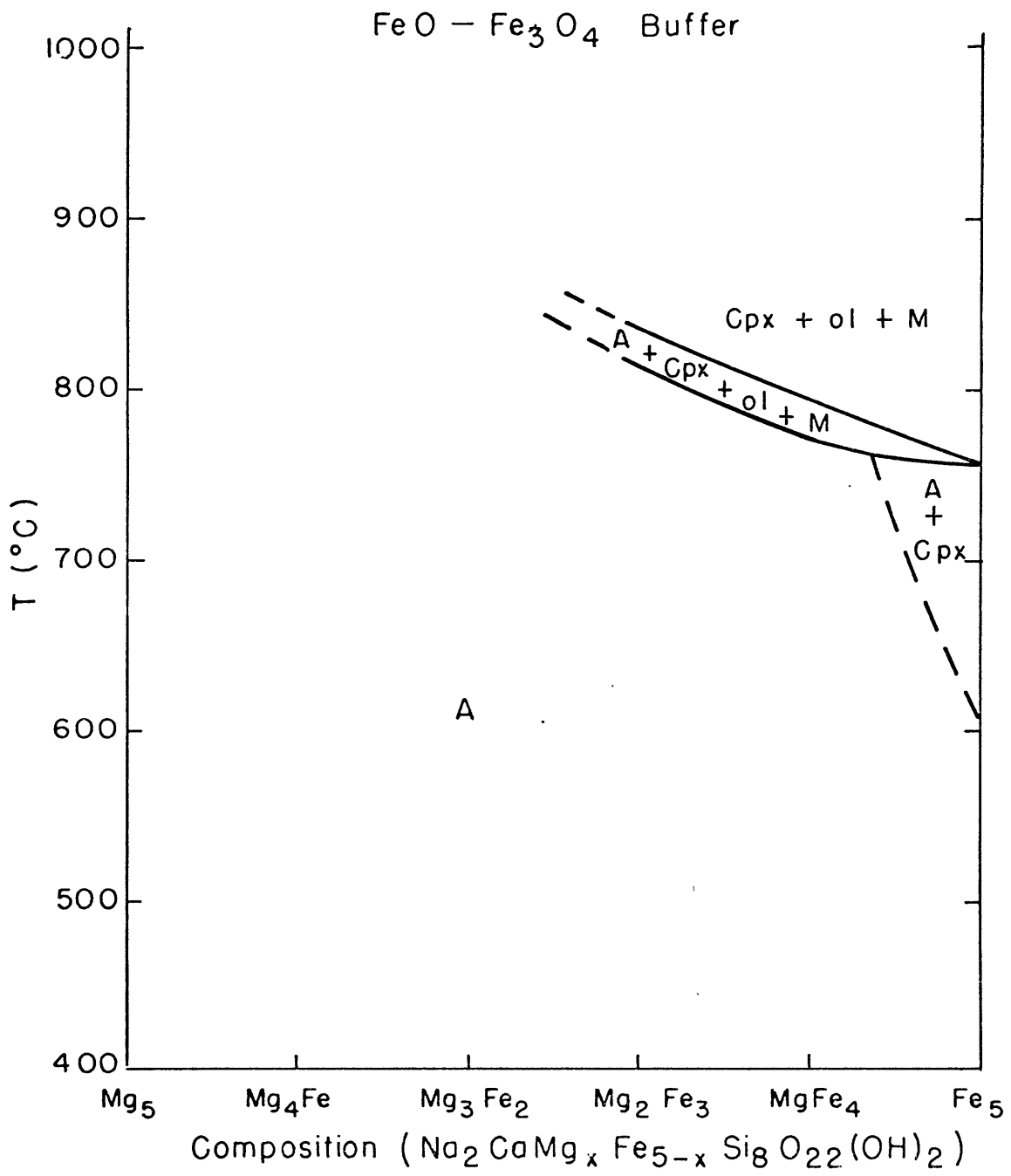
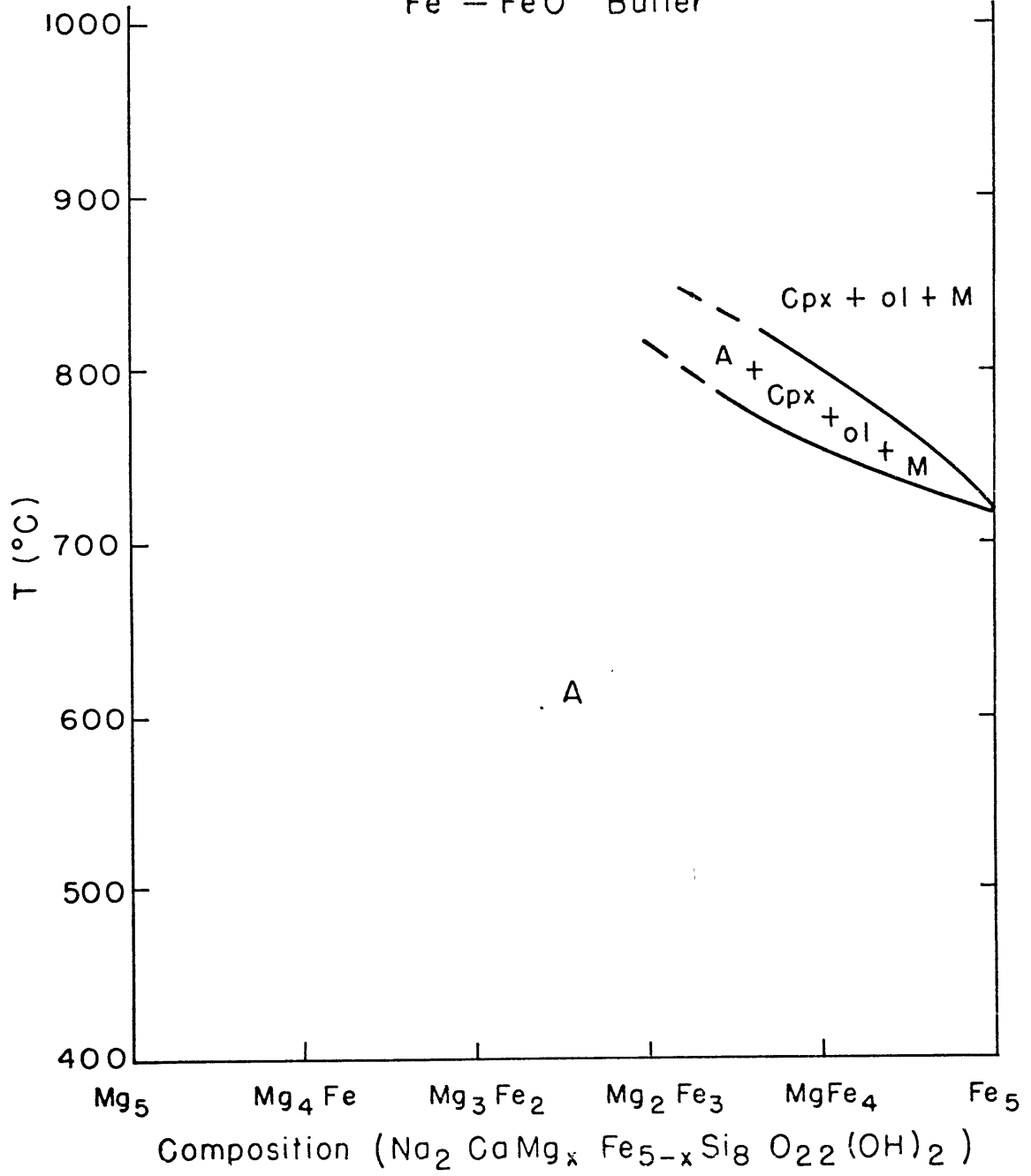


Figure II-13. Isobaric ( $P_{\text{Tot}} = 1 \text{ kb}$ ) T-X section for the pseudo-binary join richterite - ferrorichterite with oxygen fugacities defined by the I-W buffer.



Fe - FeO Buffer



point" places the transition for amphibole ( $Mg_5$  to above  $Mg_2Fe_3$ ) to melt subparallel to the x-axis. Conversely, the transition assemblage separating amphibole from its subsolidus assemblage intersects the x-axis at a high angle. Any fixed composition will encounter a much larger range of T in the latter transition loop. The partial melting region in the amphibole absent loop was not observed experimentally.

The thermal stability of amphibole is seen to increase with lower iron content. At lower  $f_{O_2}$  the subsolidus assemblage of clinopyroxene + quartz ( $\pm$  olivine  $\pm$  magnetite  $\pm$  hematite) decreases in area due to the decreasing stability of acmite with respect to ferrous amphibole. Free silica is only found at iron concentrations above  $Mg_2Fe_3$ . The fields ...  $\pm$  olivine  $\pm$  orthopyroxene + ... indicate the ambiguity in determining which phase disappears first with increasing Fe content. All other fields and their interrelationships are internally consistent with the experimental data. The dashed line separating amphibole and amphibole + clinopyroxene is a gradational change. Its shape for the C- $CH_4$  T-X section (figure II-11) is drawn based upon the relative maximum in the reaction  $C + 2H_2 \rightleftharpoons CH_4$  curve in  $\log f_{O_2}$  space.

The enthalpies of reaction for amphibole decomposition across the series were derived as follows:

For the composition ( $x_i$ ) and activity coefficients ( $\gamma_i$ ) and all species are expressed in mole fractions ( $v_i$ ) at equilibrium:

$$\sum v_i \mu_i = 0 = \sum v_i (\mu_i^0 + RT \ln \gamma_i x_i) \quad \text{or,}$$

$$\sum \nu_i \mu_i = -RT \ln \Pi (\gamma_i X_i)^{\nu_i}$$

but,  $K_{\text{reaction}} = \Pi (\gamma_i X_i)^{\nu_i}$ .

Therefore,

$$\sum \nu_i \mu_i = \Delta G_T^\circ = -RT \ln K.$$

$$R \ln K = - \sum \frac{\nu_i \mu_i}{T}.$$

Differentiating,

$$dR \ln K = - \sum \nu_i \left( \frac{\partial \mu_i^\circ / T}{\partial T} dT + \frac{\partial \mu_i^\circ / T}{\partial P} dP \right).$$

From this equation it can be shown that at constant P:

$$\left( \frac{\partial \ln K}{\partial T} \right)_P = \frac{\Delta H^\circ}{RT^2}$$

$$\left( \frac{\partial \ln K}{\partial (1/T)} \right)_P = - \frac{\Delta H^\circ}{R}.$$

For a reaction involving a single gas species with all other phases pure:

$$\left( \frac{\partial \ln f_{\text{cas}}}{\partial (1/T)} \right)_P = - \frac{\Delta H^\circ}{R}$$

The enthalpy of reaction can be calculated from these last two equations.

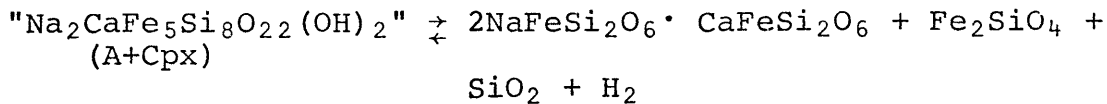
The enthalpies of reaction for  $\text{Mg}_5$  and  $\text{Fe}_5$  (I-W) are 148.5 Kcal and 150.9 Kcal, respectively. Since these two  $-\frac{\Delta H^\circ}{R}$  curves are almost parallel to each other, intermediate compositions may yield similar  $\Delta H$ 's. Since  $\text{H}_2\text{O}$  can dissolve in the melt, these are maximum values. For  $\text{Mg}_5$ :

$$K = \frac{a_{\text{fo}}^x a_{\text{en}}^y a_{\text{di}} a_{\text{M}}^z}{a_{\text{Mg}_5}} \sim a_{\text{M}}^z \text{H}_2\text{O}, \quad z < 1.$$

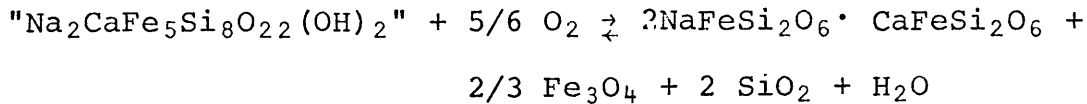
If  $a_M$  is much different from unity due to dissolved  $H_2O$ , as may be the case in Na-Si melts (Morey and Hesselgesser, 1951 and Morey, 1952), the calculated enthalpies are high.

$Fe_5$  decomposes in the subsolidus region according to:

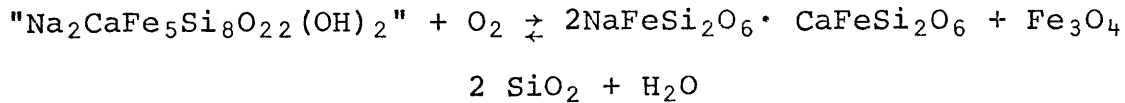
(1) between W-Mt and QFM,



(2) between QFM and H-Mt,



(3) above H-Mt,



Equilibrium constants for these reactions are:

$$K(1) = \frac{a_{\text{achd}} a_{\text{fa}} a_{\text{q}}^2 f_{\text{H}_2}}{a_{\text{"Fe}_5\text{"}}}$$

$$K(2) = \frac{a_{\text{achd}} a_{\text{mt}}^{2/3} a_{\text{q}}^2 f_{\text{H}_2\text{O}}}{a_{\text{"Fe}_5\text{"}} f_{\text{O}_2}^{5/6}}$$

$$K(3) = \frac{a_{\text{achd}} a_{\text{h}} a_{\text{q}}^2 f_{\text{H}_2\text{O}}}{a_{\text{"Fe}_5\text{"}} f_{\text{O}_2}}$$

Assuming no other gas species are present other than  $H_2$ ,  $H_2O$ , and  $O_2$ , the amphibole stability with respect to  $f_{H_2}$  and  $f_{H_2O}$  may be derived, in principle, producing diagrams similar to the isobaric  $\text{Log } f_{O_2} - T$  diagrams presented experimentally (Eugster and Wones, 1962). Since  $P_{O_2}$  is many orders of magnitude lower than  $P_{H_2O}$ ,

$$\text{H}_2\text{O} \rightleftharpoons \text{H}_2 + 1/2 \text{O}_2$$

$$(1) P_T = P_{\text{H}_2\text{O}} + P_{\text{H}_2} = \frac{f_{\text{H}_2\text{O}}}{\gamma_{\text{H}_2\text{O}}} + \frac{f_{\text{H}_2}}{\gamma_{\text{H}_2}}$$

$$(2) K_w = \frac{f_{\text{H}_2\text{O}}}{f_{\text{H}_2} f_{\text{O}_2}^{1/2}}$$

Solving these two equations for  $f_{\text{H}_2}$  and  $f_{\text{H}_2\text{O}}$ , the result is:

$$f_{\text{H}_2\text{O}} = \frac{P_T \gamma_{\text{H}_2} K_w f_{\text{O}_2}^{1/2} \gamma_{\text{H}_2\text{O}}}{\gamma_{\text{H}_2\text{O}} + \gamma_{\text{H}_2} K_w f_{\text{O}_2}^{1/2}}$$

$$f_{\text{H}_2} = \frac{P_T \gamma_{\text{H}_2} \gamma_{\text{H}_2\text{O}}}{f_{\text{O}_2}^{1/2} K_w \gamma_{\text{H}_2} + \gamma_{\text{H}_2\text{O}}}$$

In theory one can calculate the stability fields of amphibole with respect to  $\text{Log } f_{\text{H}_2\text{O}}$  and  $\text{Log } f_{\text{H}_2}$  as well as  $\text{Log } f_{\text{O}_2}$ . For most of the phase equilibria presented here partial melting results when the amphibole decomposes. Activities of the pyroxene solid solutions and melt are unknown and vary with changes in  $f_{\text{O}_2}$ . Consequently, the equilibrium constant cannot be a function simply of the gas species and plots in  $\text{Log } f_{\text{H}_2}$  and  $\text{Log } f_{\text{H}_2\text{O}}$  space are not straight lines.

In the subsolidus region  $\text{Fe}_5$  and  $\text{MgFe}_4$  do decompose without partial melting, however, the pyroxene grown in  $\text{MgFe}_4$  is of unknown composition. The pyroxene grown in  $\text{Fe}_5$  is known and remains uniform with changing  $f_{\text{O}_2}$  up to H-Mt in the subsolidus region. Unfortunately, reversals on H-Mt and Ni-NiO occur at too low T and were not experimentally determined. For the results

on QFM and C-CH<sub>4</sub>, the activity of the amphibole phase is unknown and variable. The equilibrium constants can be rewritten:

$$K(1) = \frac{f_{H_2}}{a_A a_{Cpx}} \quad \text{or} \quad \frac{f_{H_2O}}{a_A a_{Cpx} f_{O_2}^{1/2}}$$

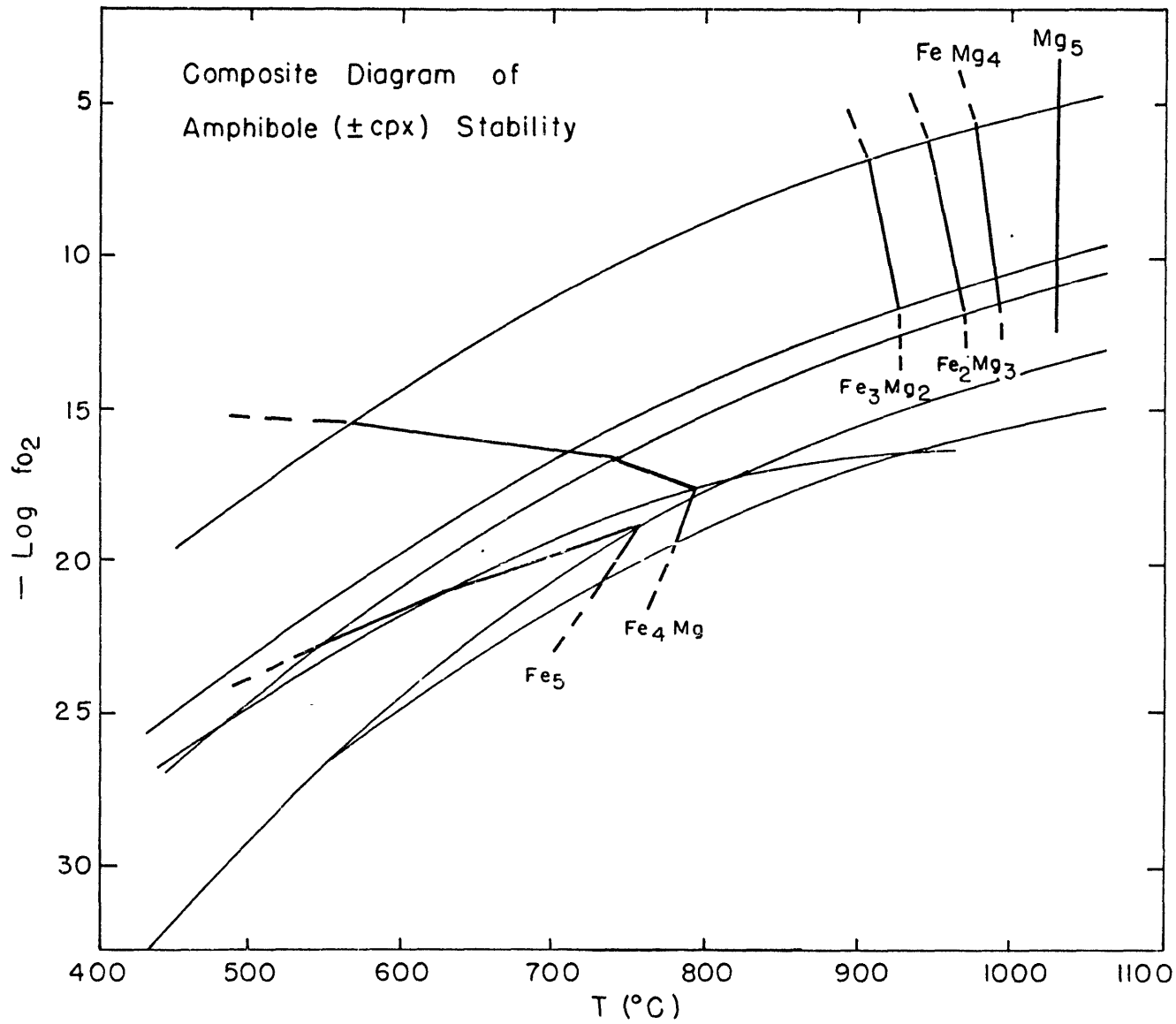
$$K(2) = \frac{f_{H_2O}}{a_A a_{Cpx} f_{O_2}^{5/6}}$$

$$K(3) = \frac{f_{H_2O}}{a_A a_{Cpx} f_{O_2}}$$

Until the variables  $a_A$  and  $a_{Cpx}$  are known,  $f_{H_2}$  and  $f_{H_2O}$  cannot be calculated directly. Work on solid solution series such as pargasite - ferropargasite and tremolite - ferrotremolite would not have this difficulty. Compositions in these ferrous amphibole series should yield only amphibole to their upper  $f_{O_2}$  stability limit.

Figure II-14 is a composite diagram showing the maximum amphibole stability for each bulk composition Mg<sub>5</sub> to Fe<sub>5</sub>. The maximum stability decreases with the addition of iron. Also, compositions Mg<sub>5</sub> through Mg<sub>2</sub>Fe<sub>3</sub> have much greater stability with respect to T and  $f_{O_2}$  than MgFe<sub>4</sub> and Fe<sub>5</sub>. This can be justified for two reasons. One, the 3 irons preferentially enter the larger 3 M(1) and M(3) sites discriminating against the smaller M(2) sites. A and M(4) are assumed to contain Na and Ca only. Addition of a fourth ferrous iron into the M(2) site greatly decreases the linking of the double chains of silicon tetrahedra. Addition of a fifth ferrous iron decreases the stability further for the same reason. Two, the amphiboles in the bulk compositions

Figure II-14. Composite isobaric  $\text{Log } f_{\text{O}_2}$  - T diagram showing the maximum amphibole stabilities for the labeled compositions.





Mg<sub>5</sub> through Mg<sub>2</sub>Fe<sub>3</sub> are stable to high  $f_{O_2}$  since they trend toward magnesioriebeckite (see table II-14) which is stable at high T and  $f_{O_2}$ . As in these noncalcic amphiboles, the ferric iron, caused by the local charge imbalance of Na in M(4) and made more favorable by high  $f_{O_2}$ , enters M(2) with loss of sodium from A to maintain overall charge balance. A similar alteration of an amphibole in MgFe<sub>4</sub> of Fe<sub>5</sub> bulk composition yields amphibole trending toward riebeckite which has a greatly lowered stability at high  $f_{O_2}$ .

Figure II-15 compares the thermal stability of Mg-richterite and ferrorichterite (I-W). At 1 kb the stability limits are:

Fe-richterite (I-W) : 715± 5°C

Mg-richterite : 1030±10°C

Substitution of 5 ferrous irons for 5 magnesiums causing a decreased linking of the silicon double chains lowers the stability limit 315°C at 1 kb. This compares with 245°C for similar conditions in pargasite - ferropargasite (Boyd, 1959 and Gilbert, 1966) and 365°C for tremolite - ferrotremolite (Boyd, 1959 and Ernst, 1966).

Using the phase equilibria presented here and the physical properties discussed in detail earlier, ferrorichterite can be compared with the other iron bearing amphiboles. The stabilities of ferropargasite ( $NaCa_2Fe_4^{+3}AlSi_6Al_2O_{22}(OH)_2$ ), ferrotremolite ( $Ca_2Fe_5Si_8O_{22}(OH)_2$ ), riebeckite-arfvedsonite ( $Na_{2.4}Fe_{4.9}^{+3}Fe_{0.7}^{+2}-Si_{7.7}Fe_{0.3}^{+3}(OH)_2$ ) (Ernst, 1962) and riebeckite ( $Na_2Fe_3^{+2}Fe_2^{+3}-Si_8O_{22}(OH)_2$ ) (Ernst, 1962) have been experimentally defined. Table II-15 and figure II-16 show pertinent data regarding their

Table II-14. Unit Cell Dimensions of Riebeckitic Amphibole

	a(Å)	b(Å)	c(Å)	$\beta$	V(Å <sup>3</sup> )	Ref.
riebeckite	9.73	18.03	5.33	103°18'	913	Ernst, 1962
riebeckite-arfvedsonite	9.85	18.15	5.32	103°12'	926	Ernst, 1962
magnesioriebeckite	9.73	17.95	5.30	103°18'	901	Ernst, 1960

Figure II-15. Comparison of the thermal stability limits of richterite and ferrorichterite (I-W).

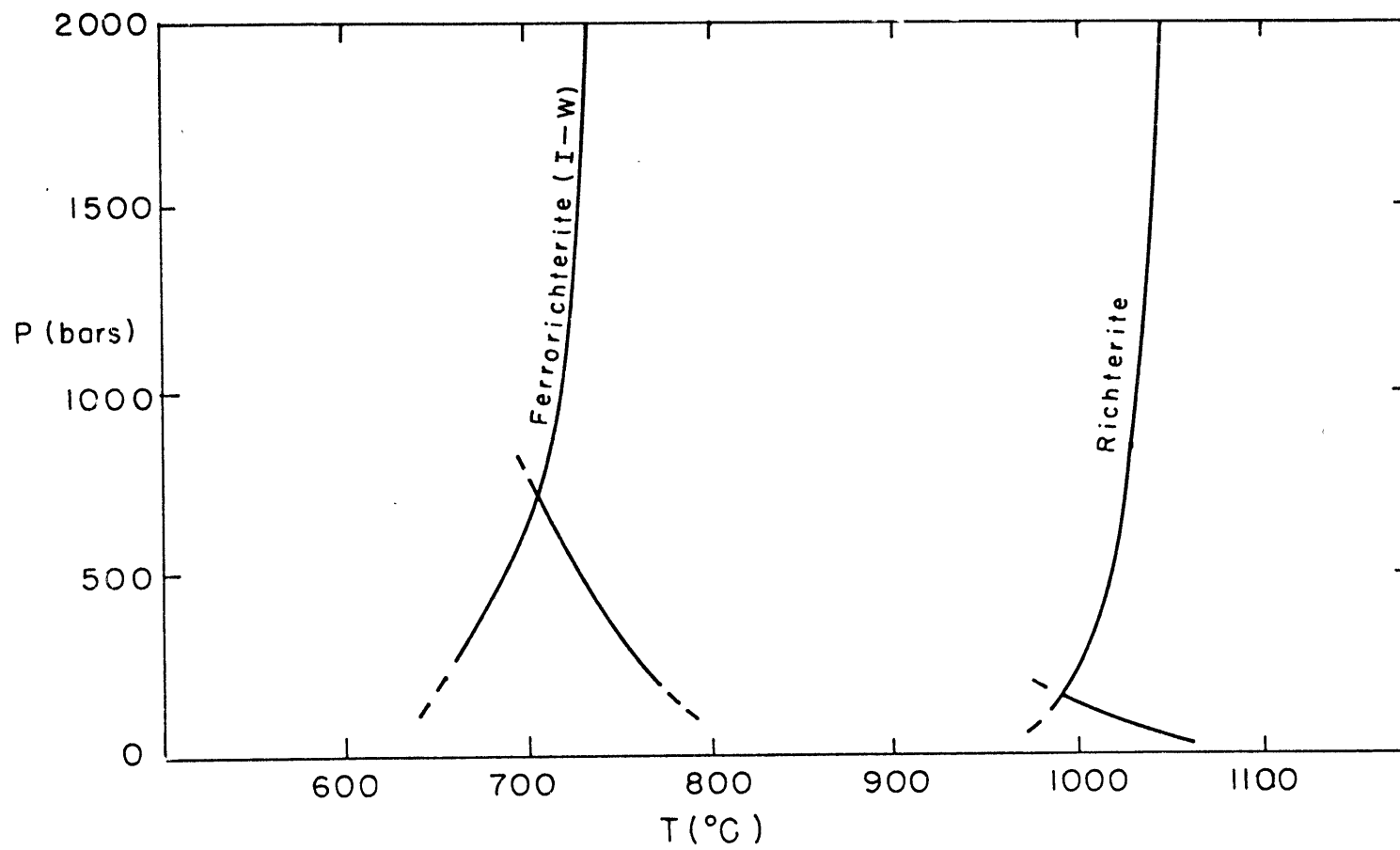


Figure II-16. Comparison of the thermal stability limits of ferrotremolite (Ernst, 1966), riebeckite (Ernst, 1962), riebeckite - arfvedsonite (Ernst, 1962), ferrorichterite, and ferropargasite (Gilbert, 1966). Oxygen fugacities are defined by the labeled buffer systems.

Iron amphiboles (buffers)

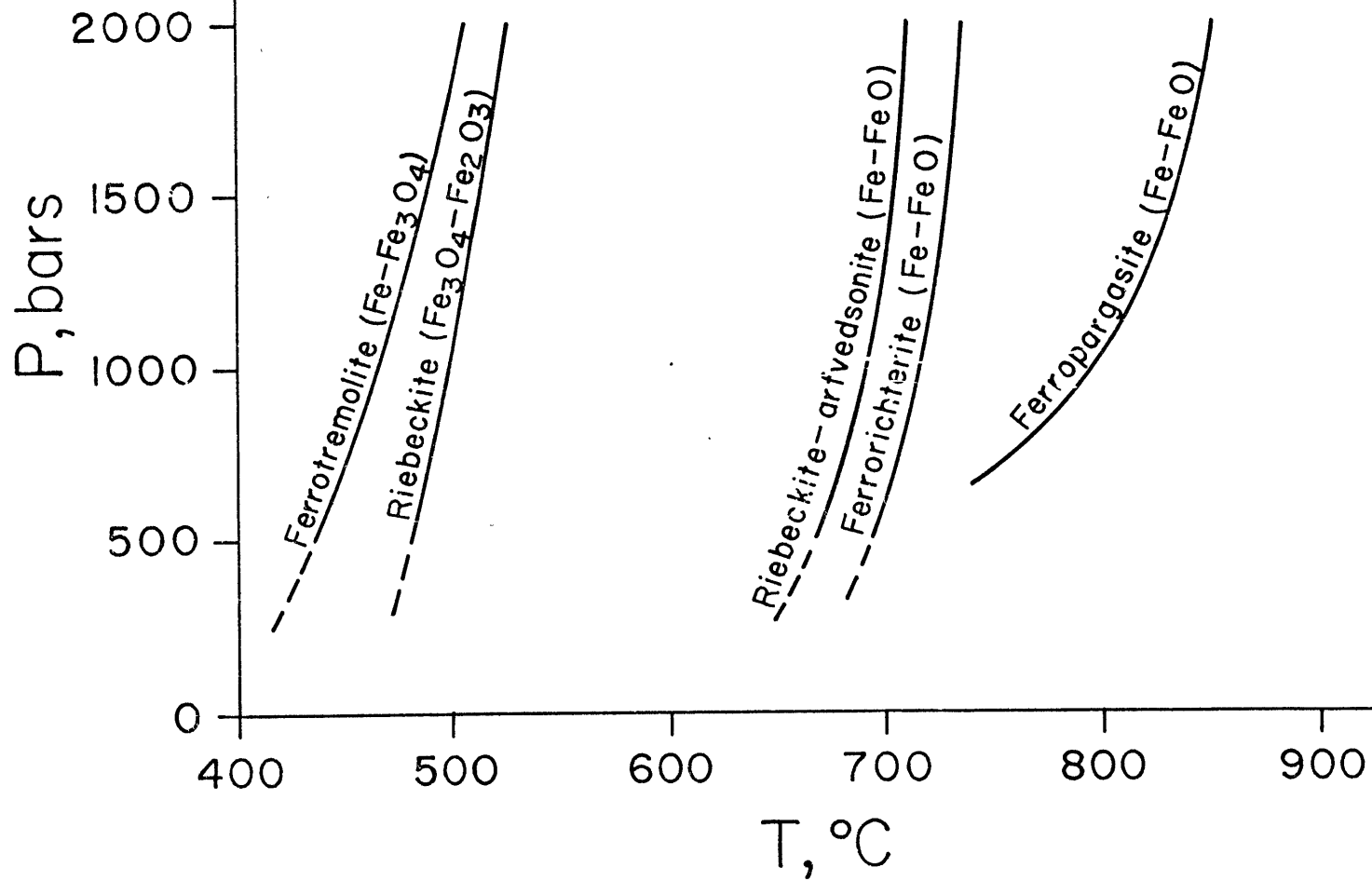


Table II-15. Iron Amphibole Stabilities

Phase and Composition	Buffer	Stability Limit		Reference
		P(bars)	T(°C)	
ferrotremolite	I-W	500	437	Ernst, 1966
$\text{Ca}_2\text{Fe}_5^{+2}\text{Si}_8\text{O}_{22}(\text{OH})_2$		1000	465	
		1500	485	
		2000	506	
riebeckite-arfvedsonite	"	500	670	Ernst, 1962
$\text{Na}_{2.4}\text{Fe}_{4.2}^{+2}\text{Fe}_{0.7}^{+3}\text{Si}_{7.7}\text{Fe}_{0.3}^{+3}\text{O}_{22}(\text{OH})_2$		1000	690	
		1500	700	
		2000	710	
ferrorichterite	"	500	690	This paper
$\text{Na}_2\text{CaFe}_5\text{Si}_8\text{O}_{22}(\text{OH})_2$		1000	715	
		1500	725	
		2000	735	
ferropargasite	"	500	682	Gilbert, 1966
$\text{NaCa}_2\text{Fe}_4^{+2}\text{AlSi}_6\text{Al}_2\text{O}_{22}(\text{OH})_2$		1000	800	
		1500	835	
		2000	850	
riebeckite	H-Mt	500	481	Ernst, 1962
$\text{Na}_2\text{Fe}_3^{+2}\text{Fe}_2^{+3}\text{Si}_8\text{O}_{22}(\text{OH})_2$		1000	496	
		1500	506	
		2000	515	

stability limits. The decomposition curve of ferrorichterite has been added. When comparing these results calcium vs. sodium should<sup>have</sup> little effect on the stability limit (Ernst, 1968).

Ferropargasite which shows the greatest stability has Al and  $\text{Fe}^{+2}$  in the M(2) site and Al in the double chains. Ferropargasite is stable to a much higher  $f_{\text{O}_2}$  owing principally to the lack of Na in M(4). At lower  $f_{\text{O}_2}$  (QFI) this amphibole becomes less stable with respect to temperature due to the great decrease in activity of  $\text{H}_2\text{O}$  under these conditions which is unrelated to the ferrous-ferric problem.

Ferrotremolite has complete local charge balance. Consequently, 5 ferrous irons are placed into the 5 available M sites. The predicted increase in  $b$  for the conversion of tremolite to ferrotremolite is  $0.32 \text{ \AA}$  (Colville *et al.*, 1966). Colville *et al.* observed  $0.29 \text{ \AA}$  which was considered within the error of the calculation. On this basis all iron is thought to be ferrous. Most of the decreased stability of ferrotremolite compared to other ferrous amphiboles is due to the vacant A site (Ernst, 1968). The decreased linking caused by the ferrous irons also adds to the amphibole instability. Riebeckite which also has a vacant A site is slightly more stable probably due to the 2 ferric irons in M(2).

The riebeckite-arfvedsonite synthesized by Ernst (1962) on the bulk composition riebeckite comes close to ferrorichterite in stability. Some vacancy in the A site as well as some local charge imbalance would account for its lowered stability.



It can be concluded from these studies that in order to investigate sodic ferrous amphiboles the interrelationship of sodium and ferric iron must be understood.

The next logical step is to investigate the series pargasite - ferropargasite which does not have local charge balance problems. Amphiboles on this join would yield a less complicated isobaric  $\text{Log } f_{\text{O}_2} - T$  diagram since amphibole should be stable as a single phase at higher  $f_{\text{O}_2}$ . Thermodynamic values such as the activities and free energies of intermediate compositions could be calculated without this complication. Chatterjee (personal communication) has prepared amphiboles along the join tremolite - ferrotremolite. Combining this with a study along pargasite - ferropargasite would yield data valuable in the interpretation of most natural hornblendes.

## APPENDIX I

Roedderites ( $\text{Na}_2(\text{Mg},\text{Fe})_5\text{Si}_{12}\text{O}_{30}$ )

Some preliminary work has been done on the join  $\text{Na}_2\text{Mg}_5\text{Si}_{12}\text{O}_{30}$ - $\text{Na}_2\text{Fe}_5\text{Si}_{12}\text{O}_{30}$  in order to more positively identify the low pressure assemblages encountered in the Mg-richterite - ferrichterite studies. The end member  $\text{K}_2\text{Mg}_5\text{Si}_{12}\text{O}_{30}$  has been studied hydrothermally by Siefert and Schreyer (1969) revealing that roedderites (Na of K) are low pressure - high temperature phases. Indeed, most occurrences of roedderite and the aluminum bearing variety, osumilite, are meteoritic (Olsen, 1967 and Dodd, *et al.*, 1965). The systems  $\text{K}_2\text{O} - \text{MgO} - \text{SiO}_2$  and  $\text{K}_2\text{O} - \text{FeO} - \text{SiO}_2$  have been examined by Roedder (1952). The systems  $\text{Na}_2\text{O} - \text{MgO} - \text{SiO}_2$  and  $\text{Na}_2\text{O} - \text{FeO} - \text{SiO}_2$  have been studied by Schairer and Yoder (1970). Both  $\text{Na}_2\text{Mg}_2\text{Si}_6\text{O}_{12}$  (1:2:6 Na-Mg silicate) and  $\text{Na}_2\text{Mg}_5\text{Si}_{12}\text{O}_{30}$  (roedderite) were found to exist on the liquidus. Analogous compositions containing iron were not encountered.

Six oxide mixes were prepared and the Fe reduced to the native state under hydrogen. These were studied at one atmosphere and at elevated pressure and temperature.  $f_{\text{O}_2}$  was buffered by standard buffering techniques. Tables A-1 and A-2 display the experimental results.

Mg-roedderite was grown at one atm. and hydrothermally yielding the same physical properties. Note that quartz is always leached from the mix in the hydrothermal experiments. This loss is not enough to shift the unit cell dimensions.

Table AI-1. Roedderites:  $\text{Na}_2(\text{Mg,Fe})_5\text{Si}_{12}\text{O}_{30}$

(Grown from reduced oxide mix)

<u>Bulk Composition</u>	<u>P</u> (bars)	<u>T</u> (°C)	<u>Duration</u> (hrs)	<u>Buffer</u>	<u>Products</u>
$\text{Na}_2\text{Mg}_5\text{Si}_{12}\text{O}_{30}$	1000	850	40	-	Roedderite + Q
"	1	960	72	-	Roedderite
"	1	960	96	-	"
"	1	950	72	-	"
$\text{Na}_2\text{Mg}_4\text{FeSi}_{12}\text{O}_{30}$	1000	764	158	QFM	Amphibole + Q
"	300	860	46	"	Roedderite + Q
$\text{Na}_2\text{Mg}_3\text{Fe}_2\text{Si}_{12}\text{O}_{30}$	"	812	44	"	"
$\text{Na}_2\text{Mg}_2\text{Fe}_3\text{Si}_{12}\text{O}_{30}$	"	900	48	"	"
"	"	850	18	I-W	"
"	"	764	45	QFM	Amphibole + Q
$\text{Na}_2\text{MgFe}_4\text{Si}_{12}\text{O}_{30}$	"	850	46	"	Hypersthene + Q + gl
"	"	800	66	"	1:2:6Na-(FeMg)Silicate+Fa+Q
$\text{Na}_2\text{Fe}_5\text{Si}_{12}\text{O}_{30}$	1000	800	40	I-W	Fa+Q+gl
"	"	750	48	"	"
"	"	700	76	"	1:2:6 Na-FeSilicate+Fa+Q
"	"	600	116	"	Amphibole + Q

Table AI-2. Roedderite Unit Cell Dimensions

Bulk Composition	P	T	Buffer	$a_0$ (Å)	$c_0$ (Å)	c/a	V (Å <sup>3</sup> )
$\text{Na}_2\text{Mg}_5\text{Si}_{12}\text{O}_{30}$	1000	850	-	10.148(1)	14.229(3)	1.402	1269.1(0.3)
"	1	960	-	10.155(2)	14.229(5)	1.401	1270.7(0.5)
"	1	"	-	10.147(1)	14.240(3)	1.403	1269.1(0.4)
"	1	950	-	10.147(2)	14.233(3)	1.403	1269.1(0.4)
$\text{Na}_2\text{Mg}_4\text{FeSi}_{12}\text{O}_{30}$	300	860	QFM	10.154(1)	14.270(2)	1.405	1274.1(0.2)
$\text{Na}_2\text{Mg}_3\text{Fe}_2\text{Si}_{12}\text{O}_{30}$	300	812	"	10.162(1)	14.304(3)	1.408	1279.1(0.3)
$\text{Na}_2\text{Mg}_2\text{Fe}_3\text{Si}_{12}\text{O}_{30}$	300	900	"	10.166(1)	14.303(3)	1.408	1280.0(0.3)

Only compositions up to  $Mg_2Fe_3$  were synthesized in the 1:5:12 structure.  $MgFe_4$  and  $Fe_5$  roedderites were not synthesized, but 1:2:6 Na-(Mg,Fe) silicate plus olivine was produced on I-W at 1 kb.  $Fe_5$  (Merrihueite) is found in nature, consequently, it must be a lower  $f_{O_2}$ , lower P phase if it is stable at all. The stability of 1:2:6 Na-Fe silicate at 1 kb (I-W) is from approximately 600°C to 750°C. At 600°C or below amphibole (riebeckite-arfvedsonite) + quartz appears and at 750°C or above fayalite + quartz + glass is the stable assemblage.

Variations in lattice parameters of  $Mg_5$  to  $Mg_3Fe_2$  show only a slight increase in a while c and V increase more markedly. The cell parameters level off above  $Mg_2Fe_3$  on QFM. The crystal structure of osumilite (Myashiro, 1956), P6/mcc, indicates only 2 sites in the 1:5:12 configuration will hold ferrous iron. This may explain the difficulty in growing more ferrous samples. The 1:2:6 phase in  $MgFe_4$  and  $Fe_5$  was identified from the powder patterns of Schairer and Yoder (1970) for the magnesium system.

## APPENDIX II

Herein are located the complete experimental tables for all compositions.

Table AII-1. Complete Experimental Table:  $\text{Na}_2\text{CaMg}_5\text{Si}_8\text{O}_{22}(\text{OH})_2$

P (±15 bars)	T (±5°C)	Duration (hrs.)	Reactants	Products
1000	1150	8	1:2:6+Fo+Ro+Di	Fo+Di+M+ (En) + (A)
"	"	"	Mix	"
"	1050	18	A	"
"	"	"	Fo+Di+M+ (En) + (A)	"
"	"	1 Min.	Ro+Fo+Di+M	Fo+Di+M+ (A) + (En?)
"	1035	23	A	Fo+Di+M+ (En) + (A)
"	"	"	1:2:6+Fo+Ro+Di	"
"	1025	"	A	A
"	"	7	Ro+Fo+Di+M	"
"	1000	18	"	"
"	850	464	Mix	"
"	"	48	"	"
483	905	24	"	"
230	1050	"	1:2:6+Fo+Ro+Di	Fo+Di+M+ (En)
"	"	"	A	"

Table AII-1. (Cont.)

P (±15°C)	T (±5°C)	Duration (hrs.)	Reactants	Products
200±25	1040	71	Ro+Fo+Di+M	Fo+Di+M+ (En)
"	"	"	Mix	"
"	"	"	"	"
"	"	"	"	"
"	1000	23	A	Fo+Di+M+ (En)
"	"	"	Fo+Di+M+ (En)	"
"	990	27	1:2:6+Fo+Ro+Di	A
"	"	"	A	"
"	975	24	1:2:6+Fo+Ro+Di	"
"	"	"	A	"
"	950	22	Fo+Di+M+ (En)	"
"	"	"	A	"
"	940	68	Mix	"
"	"	"	"	"
"	"	"	A	"
"	925	24	"	"
"	"	"	A	"
"	908	"	"	"



Table AII-1. (Cont.)

P (±15 bars)	T (±5°C)	Duration (hrs.)	Reactants	Products
150	1025	16	1:2:6+Fo+Ro+Di	Fo+Di+M+ (En)
"	"	"	A	"
100	930	24	Ro+Fo+Di+M	A
"	"	"	Mix	"
50	850	"	Ro+Fo+Di+M	"
1	1125	5	Mix	Fo+Di+M+ (En)
"	1090	5	Fo+Di+M+ (En)	"
"	1080	4	Mix	Ro+Fo+Di+M
"	1070	3	"	"
"	1025	19	"	"
"	1000	18	"	"
"	975	17	"	"
"	960	23	Ro+Fo+Di+M	1:2:6+Fo+Ro+Di
"	950	16	Mix	"
"	930	"	"	"
"	910	15	"	"
"	900	24	"	"

Table AII-2. Complete Experimental Table:  $\text{Na}_2\text{CaFe}_5\text{Si}_8\text{O}_{22}(\text{OH})_2$  (IW)

P	T	Duration	Reactants	Products
( $\pm 15$ bars)	( $\pm 5^\circ\text{C}$ )	(hrs.)		
5000	775	29	Cpx+Fa+M	Cpx+Fa+M+ (A)
"	750	48	"	"
"	725	83	"	A
"	700	78	"	"
"	"	72	A	"
"	600	120	Mix	A
"	525	721	"	"
2000	800	48	"	Cpx+Fa+M
"	750	47	Cpx+Fa+M	Cpx+Fa+M+ (A)
"	"	"	A	Cpx+Fa+M
"	735	54	Cpx+Fa+M	"
"	725	63	"	A
"	680	70	"	"
"	530	648	Mix	A
"	500	672	"	"
1000	800	36	"	Cpx+Fa+M

Table AII-2. (Cont.)

P (±15 bars)	T (±5°C)	Duration (hrs.)	Reactants	Products
1000	750	48	A	Cpx+Fa+M+ (A)
"	"	"	Cpx+Fa+M	Cpx+Fa+M
"	725	137	A	Cpx+Fa+M+ (A)
"	"	48	Cpx+Fa+M	"
"	710	52	A	A
"	700	46	Cpx+Fa+M	"
750	725	41	"	Cpx+Fa+M
"	700	72	"	A
500	750	51	"	Cpx+Fa+M
"	720	52	"	1:2:6+Cpx+Fa+M
"	710	78	"	"
"	700	69	"	"
"	685	51	A	A
"	675	67	Cpx+Fa+M	A+ (Cpx+Fa+M)
"	650	70	"	"
"	600	216	"	"

Table AII-3. Complete Experimental Table:  $\text{Na}_2\text{CaFe}_5\text{Si}_8\text{O}_{22}(\text{OH})_2$  (QFM)

P (±5 bars)	T (±5°C)	Duration (hrs.)	Reactants	Products
7000	850	28	Mix	Cpx+Fa+Mt+M
"	600	350	"	$\text{Ac}_{67}\text{Hd}_{33}$ +Fa+Q+Mt
"	550	336	$\text{Ac}_{67}\text{Hd}_{33}$ +Fa+Q+Mt	"
"	525	493	Mix	A+Cpx
"	500	545	"	"
5000	825	48	$\text{Ac}_{67}\text{Hd}_{33}$ +Fa+Q+Mt	Cpx+Fa+Mt+M
"	800	72	"	$\text{Ac}_{67}\text{Hd}_{33}$ +Fa+Q+Mt
"	775	66	"	"
"	680±10	280	Mix	"
"	575	240	$\text{Ac}_{67}\text{Hd}_{33}$ +Fa+Q+Mt	"
"	550	310	"	"
"	525	336	"	A+Cpx
4000	750	167	Mix	Cpx+Fa+Q+Mt+ (1:2:6)
"	700	162	$\text{Ac}_{67}\text{Hd}_{33}$ +Fa+Q+Mt	$\text{Ac}_{67}\text{Hd}_{33}$ +Fa+Q+Mt
"	525	356	"	A+Cpx
"	500	699	A+Cpx	"

Table AII-3. (Cont.)

P (±15 bars)	T (±5°C)	Duration (hrs.)	Reactants	Products
4000	500	495	Ac <sub>67</sub> Hd <sub>33</sub> +Fa+Q+Mt	A+Cpx
"	475	834	"	"
"	"	599	A+Cpx	"
1000	850	48	Mix	Cpx+Fa+Mt+M
"	835	52	Ac <sub>67</sub> Hd <sub>33</sub> +Fa+Q+Mt	"
"	820	72	Cpx+Fa+Mt+M	"
"	800	117	Ac <sub>67</sub> Hd <sub>33</sub> +Fa+Q+Mt	Ac <sub>67</sub> Hd <sub>33</sub> +Fa+Q+Mt
"	"	65	Mix	"
"	750	143	"	Cpx+Fa+Q+Mt+ (1:2:6)
"	"	116	A+Cpx	Ac <sub>67</sub> Hd <sub>33</sub> +Fa+Q+Mt
"	700	191	Ac <sub>67</sub> Hd <sub>33</sub> +Fa+Q+Mt	"
"	650	158	"	"
"	600	164	"	"
"	"	162	Mix	Cpx+Fa+Q+Mt+ (A)
"	550	504	Ac <sub>67</sub> Hd <sub>33</sub> +Fa+Q+Mt	Ac <sub>67</sub> Hd <sub>33</sub> +Fa+Q+Mt
"	525	504	"	A+Cpx
"	500	675	A+Cpx	"

Table AII-3. (Cont.)

P (±15 bars)	T (±5°C)	Duration (hrs.)	Reactants	Products
1000	500	495	Ac <sub>67</sub> Hd <sub>33</sub> +Fa+Q+Mt	A+Cpx
"	475	834	"	"
"	"	829	A+Cpx	"
"	450	2154	Ac <sub>67</sub> Hd <sub>33</sub> +Fa+Q+Mt	"

Table AII-4. Complete Experimental Table:  $\text{Na}_2\text{CaFe}_5\text{Si}_8\text{O}_{22}(\text{OH})_2$  ( $P_{\text{Tot}} = 1 \text{ kb}$ )

Buffer	T ( $\pm 5^\circ\text{C}$ )	Duration (hrs.)	Reactants	Products
HMt	850	48	Oxidized Mix	$\text{Ac}_{67}\text{Hd}_{33} + \text{Mt} + \text{H} + \text{Q}$
"	800	"	Mix	"
"	700	120	Oxidized Mix	"
"	"	"	Mix	"
"	"	"	$\text{Ac}_{67}\text{Hd}_{33} + \text{Mt} + \text{H} + \text{Q}$	"
NNO	850	96	Mix	$\text{Cpx} + \text{Mt} + \text{M}$
"	600	336	"	$\text{Ac}_{67}\text{Hd}_{33} + \text{Mt} + \text{Q}$
QFM	850	48	"	$\text{Cpx} + \text{Fa} + \text{Mt} + \text{M}$
"	835	52	$\text{Ac}_{67}\text{Hd}_{33} + \text{Fa} + \text{Mt} + \text{Q}$	"
"	820	72	$\text{Cpx} + \text{Fa} + \text{Mt} + \text{M}$	"
"	800	117	$\text{Ac}_{67}\text{Hd}_{33} + \text{Fa} + \text{Mt} + \text{Q}$	$\text{Ac}_{67}\text{Hd}_{33} + \text{Fa} + \text{Mt} + \text{Q}$
"	"	115	"	"
"	"	65	Mix	"
"	750	143	$\text{A} + \text{Cpx}$	"
"	"	116	Mix	$\text{Cpx} + \text{Fa} + \text{Mt} + \text{Q} + (1:2:6)$
"	700	191	$\text{Ac}_{67}\text{Hd}_{33} + \text{Fa} + \text{Mt} + \text{Q}$	$\text{Ac}_{67}\text{Hd}_{33} + \text{Fa} + \text{Mt} + \text{Q}$

Table AII-4. (Cont.)

Buffer	T (±5°C)	Duration (hrs.)	Reactants	Products
QFM	650	158	Ac <sub>67</sub> Hd <sub>33</sub> +Fa+Mt+Q	Ac <sub>67</sub> Hd <sub>33</sub> +Fa+Mt+Q
"	600	164	"	"
"	"	162	Mix	Cpx+Fa+Mt+Q+ (A)
"	550	504	Ac <sub>67</sub> Hd <sub>33</sub> +Fa+Mt+Q	Ac <sub>67</sub> Hd <sub>33</sub> +Fa+Mt+Q
"	525	"	"	A+Cpx
"	500	675	A+Cpx	"
"	"	495	Ac <sub>67</sub> Hd <sub>33</sub> +Fa+Mt+Q	"
"	475	834	"	"
"	"	829	A+Cpx	"
"	450	2154	Ac <sub>67</sub> Hd <sub>33</sub> +Fa+Mt+Q	"
C-CH <sub>4</sub>	820	48	Cpx+Fa+M	Cpx+Fa+M
"	"	"	Mix	"
"	800	"	"	"
"	775	92	Cpx+Fa+M	"
"	750	552	"	Ac <sub>67</sub> Hd <sub>33</sub> +Fa+Q
"	"	120	"	"
"	725	576	"	"



Table AII-4. (Cont.)

Buffer	T (±5°C)	Duration (hrs.)	Reactants	Products
C-CH <sub>4</sub>	725	48	Cpx+Fa+M	Ac <sub>67</sub> Hd <sub>33</sub> +Fa+Q
"	700	168	Mix	"
"	650	480	"	"
"	"	168	Cpx+Fa+M	"
"	625	192	"	"
"	600	240	A+Cpx	A+Cpx
"	550	336	Mix	"
"	500	1008	"	"
"	425	1344	"	"
Wmt	775	48	Cpx+Fa+M	Cpx+Fa+M+ (A)
"	750	"	"	A+ (Cpx+Fa+M)
"	725	"	"	"
IW	800	36	Mix	Cpx+Fa+M
"	750	48	A	Cpx+Fa+M+ (A)
"	"	"	Cpx+Fa+M	Cpx+Fa+M
"	725	"	"	"
"	"	137	A	"

Table AII-4. (Cont.)

Buffer	T (±5°C)	Duration (hrs.)	Reactants	Products
IW	710	52	A	A
"	700	46	Cpx+Fa+M	"

Table AII-5. Complete Experimental Table:  $\text{Na}_2\text{CaMg}_4\text{FeSi}_8\text{O}_{22}(\text{OH})_2$  ( $P_{\text{Tot}} = 1 \text{ kb}$ )

Buffer	T ( $\pm 5^\circ\text{C}$ )	Duration (hrs.)	Reactants	Products
HMt	1025	18	Mix	Cpx+Fo+Mt+H+M
"	1000	33	Oxidized Mix	"
"	"	29	A+Cpx	"
"	"	18	"	"
"	975	24	Cpx+Fo+Mt+H+M	A+Cpx
"	"	23	A+Cpx	"
"	950	24	Mix	"
"	800	96	"	"
"	"	72	"	"
"	650	360	"	"
"	"	240	"	"
NNO	800	96	"	A+ (Cpx)
"	"	72	"	"
"	650	240	"	"
"	"	137	"	"

Table AII-5. (Cont.)

Buffer	T (±5°C)	Duration (hrs.)	Reactants	Products
QFM	1025	24	A	Cpx+Ol+Mt+M
"	1000	28	"	"
"	975	23	"	A
"	950	24	Mix	"
"	800	96	"	"
"	"	72	"	"
"	650	240	"	"
"	"	144	"	"
C-CH <sub>4</sub>	800	100	"	"
"	700	168	"	"
"	650	360	"	"
"	"	240	"	"
"	"	144	"	"
IW	"	"	"	"
"	"	96	"	"
"	"	"	"	"

Table AII-6. Complete Experimental Table:  $\text{Na}_2\text{Ca Mg}_3\text{Fe}_2\text{Si}_8\text{O}_{22}(\text{OH})_2$  ( $P_{\text{Tot}} = 1 \text{ kb}$ )

Buffer	T ( $\pm 5^\circ\text{C}$ )	Duration (hrs.)	Reactants	Products
HMt	1000	33	Oxidized Mix	Cpx+Mt+H+M
"	"	26	A	"
"	"	18	Mix	"
"	975	19	Cpx+Mt+H+M	"
"	950	24	Mix	"
"	940	24	A+Cpx	A+Cpx+Mt+H+M
"	925	45	Cpx+Mt+H+M	A+Cpx
"	900	33	"	"
"	850	48	Mix	"
"	700	120	A+Cpx	"
NNO	800	48	Mix	"
"	700	119	A+Cpx	"
"	600	744	Mix	"
QFM	1000	35	Cpx+Ol+Mt+M	Cpx+Ol+Mt+M
"	"	28	A+Cpx	"

Table AII-6. (Cont.)

Buffer	T (±5°C)	Duration (hrs.)	Reactants	Products
QFM	975	26	A+Cpx	Cpx+Ol+Mt+M
"	950	24	Mix	A+Cpx
"	940	"	A+Cpx	"
"	925	45	Cpx+Ol+Mt+M	"
"	900	33	A+Cpx	"
"	850	96	Mix	"
"	700	131	Cpx+Ol+Mt+M	"
"	650	240	Mix	"
"	600	744	"	"
C-CH <sub>4</sub>	700	144	"	A
"	650	480	"	"
IW	950	10	A	Cpx+Ol+M+A
"	650	144	Mix	A
"	"	96	"	"

Table AII-7. Complete Experimental Table:  $\text{Na}_2\text{CaMg}_2\text{Fe}_3\text{Si}_8\text{O}_{22}(\text{OH})_2$  ( $P_{\text{Tot}} = 1 \text{ kb}$ )

Buffer	T ( $\pm 5^\circ\text{C}$ )	Duration (hrs.)	Reactants	Products
HMt	975	24	Cpx+Ol+Mt+M	Cpx+Mt+H+M
"	950	45	A+Cpx	"
"	925	26	Cpx+Ol+Mt+M	"
"	900	27	A+Cpx	A+Cpx
"	890	36	Cpx+Ol+Mt+M	"
"	850	43	Mix	"
"	800	162	"	"
"	"	71	Oxidized Mix	"
"	700	144	Mix	"
NNO	850	48	"	"
"	800	69	A+Cpx	"
"	700	120	"	"
"	650	168	Mix	"
QFM	975	24	Cpx+Ol+Mt+M	Cpx+Ol+Mt+M
"	950	34	A+Cpx	"

Table AII-7. (Cont.)

Buffer	T (±5°C)	Duration (hrs.)	Reactants	Products
QFM	925	26	Cpx+Ol+Mt+M	Cpx+Ol+Mt+M
"	900	27	A+Cpx	A+Cpx
"	875	48	Cpx+Ol+Mt+M	"
"	850	"	Mix	"
"	"	45	"	"
"	775	72	"	"
"	700	144	"	"
"	"	119	A+Cpx	"
C-CH <sub>4</sub>	820	48	Mix	"
"	700	144	"	"
"	650	480	"	"
"	600	240	A+Cpx	"
"	550	336	Mix	"
"	500	1008	"	"
IW	950	10	A	Cpx+Ol+M
"	500	960	Mix	A



Table AII-8. Complete Experimental Table:  $\text{Na}_2\text{CaMgFe}_4\text{Si}_8\text{O}_{22}(\text{OH})_2$  ( $P_{\text{Tot}} = 1 \text{ kb}$ )

Buffer	T ( $\pm 5^\circ\text{C}$ )	Duration (hrs.)	Reactants	Products
HMt	700	69	Cpx+Ol+Mt+Q	Cpx+Mt+H+Q
"	600	326	Mix	"
"	550	360	Cpx+Ol+M	A+Cpx
NNO	875	47	Cpx+Mt+ (Q) + (A)	Cpx+Mt+M
"	850	48	Mix	Cpx+Mt+M+ (A)
"	725	164	Cpx+Mt+ (Q)	Cpx+Mt+ (Q)
"	700	138	A+Cpx	A+Cpx+ (Q) + (Mt)
"	675	182	Cpx+Ol+M	A+Cpx
"	650	168	Mix	"
QFM	850	48	"	Cpx+Ol+Mt+M+ (1:2:6)
"	800	121	"	Cpx+Ol+Mt+ (1:2:6)
"	775	72	"	"
"	750	67	Cpx+Ol+Mt+ (Q) + (1:2:6)	Cpx+Ol+Mt+ (Q)
"	725	138	A+Cpx	A+Cpx
"	700	144	Mix	"

Table AII-8. (Cont.)

Buffer	T (±5°C)	Duration (hrs.)	Reactants	Products
C-CH <sub>4</sub>	820	49	Mix	Cpx+Ol+M
"	800	48	"	"
"	790	60	Cpx+Ol+M	A+Cpx+Ol+M
"	775	144	"	A+Cpx
"	"	"	A+Cpx	"
"	700	120	Mix	"
"	650	480	"	"
"	"	144	"	"
"	550	336	Mix	"
"	500	1008	"	"
"	600	240	A+Cpx	"
IW	850	17	A+(Cpx)	Cpx+Ol+M
"	800	36	Cpx+Ol+Mt+(1:2:6)	"
"	775	49	Cpx+Ol+M	Cpx+Ol+M+A
"	750	58	Mix	A+Cpx

## ACKNOWLEDGEMENTS

The author would like to thank Drs. David R. Wones, Hatten S. Yoder, Jr., David Virgo, Larry W. Finger, and Prof. John S. Dickey for their many comments and suggestions aiding in this study. A special thanks goes to Dr. Hatten S. Yoder, Jr., for arranging monetary support at the Carnegie Institute of Washington Geophysical Laboratory and the use of his laboratory equipment there. David Virgo aided greatly in the Mössbauer interpretations which are still in progress. Also, I wish to thank Mrs. Betsey McCrory and Miss Julie Golden for their careful help in preparation of the manuscript.

This investigation was supported by National Science Foundation grants GA1109 and GA13092 to Dr. David R. Wones and supported by the Geophysical Laboratory.

## Biographical Sketch

Robert Wilson Charles was born in Altoona, Penna. September 1, 1945. The only child of Robert Judson Charles and Phyllis Virginia Charles, he was raised in the village of Bald Eagle, Penna. He attended Oak Ridge Elementary School, Tyrone R.D., Penna., and Tyrone Area High School in Tyrone, Penna., receiving his high school diploma from the latter. While in high school he earned the Wilson Memorial Athletic Award and won a Pennsylvania State Scholarship.

He entered Bucknell University, Lewisburg, Penna., in September, 1963. During his senior year at Bucknell he served as captain of the track team and Commander of the ROTC Brigade. Professional honors included admission to Pi Mu Epsilon (Mathematics) and Sigma Pi Sigma (Physics) honor societies. He graduated from Bucknell Cum Laude in June, 1967, with a Bachelor of Science degree in physics.

In September, 1967, he entered the MIT Department of Earth and Planetary Sciences. He was awarded an NDEA Traineeship and entered a career in geology. In September, 1970, he became a research assistant. From September, 1971, to June, 1972, he was a Predoctoral Fellow at the Carnegie Institute of Washington Geophysical Laboratory and much of the thesis research was accomplished there.

Mr. Charles is a member of the American Association for the Advancement of Science, The American Mineralogical Society, The American Geophysical Union, and Sigma Xi.

## REFERENCES

- AOKI, K. (1964). Clinopyroxenes from alkaline rocks of Japan. *Amer. Mineral.* 49, 1199-1223.
- BAILEY, D. K. (1969). The stability of acmite in the presence of H<sub>2</sub>O. *Amer. J. Sci.* 267A, 1-16.
- BANCROFT, G. M. and R. G. BURNS (1969). Mossbauer and absorption spectral study of alkali amphiboles. *Mineral. Soc. Amer. Spec. Paper 2*, 137-148.
- BOYD, F. R. (1959). Hydrothermal investigations of the amphiboles, in *Researches in Geochemistry* (P. H. Abelson, ed.), John Wiley and Sons, Inc., N.Y., 377-396.
- BURNS, R. G. and C. GREAVES (1971). Correlations of infrared and Mossbauer site populations measurements of actinolites. *Amer. Mineral.* 56, 2010-2032.
- BURNS, R. G. and F. J. PRENTICE (1968). Distribution of iron cations in the crocidolite structure. *Amer. Mineral.* 53, 770-776.
- CAMERON, M. and G. V. GIBBS (1971). Refinement of the crystal structure of two synthetic fluor-rich richterites. *Carnegie Inst. Wash. Year Book 70*, 150-153.
- CHARLES, R. W., D. A. HEWITT and D. R. WONES (1971) H<sub>2</sub>O in Lunar processes: The stability of hydrous phases in lunar samples 10058 and 12013, in *Proc. Second Lunar Sci. Conf., Geochim. Cosmochim. Acta* supplement 2, Vol. 1, MIT Press, 645-664.
- COLVILLE, P. A., W. G. ERNST and M. C. GILBERT (1966). Relationships between cell parameters and chemical compositions of monoclinic amphiboles. *Amer. Mineral.* 51, 1727-1754.

- COMEFORO, J. E. and J. A. KOHN (1955). Synthetic asbestos investigations, II: X-ray and other data on synthetic fluor-rich-terite, -edenite, and -boron edenite. *Amer. Mineral.* 40, 410-421.
- DEER, W. A., R. A. HOWIE and J. ZUSSMAN (1963). *Rock Forming Minerals: Vol. 2, Chain Silicates*, John Wiley and Sons, Inc., N. Y., 352-358.
- DODD, R. T., JR., W. R. VAN SCHMUS, and U. B. MARVIN (1965). Merrihueite, a new alkali-ferromagnesian silicate from the Mezo-Madraras chondrite. *Science* 149, 972-974.
- DOUGLAS, J. A. V. and A. G. PLANT (1968). Amphibole: First occurrence in an enstatite chondrite (abst.). 31st Ann. Mtg. Meteorolog. Soc., Cambridge, Mass.
- EITEL, W. (1954). Synthesis of fluorosilicates in the mica and amphibole group. Proc. Int. Symp. Reactiv. Solids, Gothenberg, 1952, 335-347.
- ERNST, W. G. (1962). Synthesis, stability relations, and occurrence of riebeckite and riebeckite-arfvedsonite solid solutions. *J. Geol.* 70, 689-736.
- ERNST, W. G. (1960). Stability relations of Magnesioriebeckite. *Geochim. Cosmochim. Acta* 19, 10-40.
- ERNST, W. G. (1966). Synthesis and stability relations of ferro-tremolite. *Amer. J. Sci.* 264, 37-65.
- ERNST, W. G. (1968). *Amphiboles*, Springer Verlag, New York, 125 pp.
- EUGSTER, H. P. (1957). Heterogeneous reactions involving oxidation and reduction at high pressures and temperatures. *J. Chem. Phys.* 26, 1760-1761.

- EUGSTER, H. P. and G. B. SKIPPEN (1967). Igneous and metamorphic reactions involving gas equilibrium, in *Researches in Geochemistry* (P. H. Abelson, ed.), Vol. 2, John Wiley and Sons, Inc., N.Y., 377-396.
- EUGSTER, H. P. and D. R. WONES (1962). Stability relations of the ferruginous biotite annite. *J. Petrol.* 3, 82-125.
- EVANS, H. T., JR., D. E. APPLEMAN and D. S. HANDWERKER (1963). The least-squares refinement of crystal unit cells with powder diffraction data by an automatic computer indexing method (abst). Amer. Crystallog. Assoc. Ann. Mtg., Cambridge, Mass., Program, 42-43.
- FISHER, G. W. and L. G. MEDARIS (1969). Cell dimensions and X-ray determinative curve for synthetic Mg-Fe olivines. *Amer. Mineral.* 54, 741-753.
- FORBES, W. C. (1971). Synthesis and stability relations on richterite. *Amer. Mineral.* 56, 997-1004.
- GAY, P., G. M. BANCROFT and M. G. BOWN (1970a). Diffraction and Mossbauer studies of minerals from lunar rocks and soils, in *Proc. Apollo 11 Lunar Sci. Conf., Geochim. Cosmochim. Acta supplement 1*, Vol. 1, 481-497.
- GHOSE, S. (1966). A scheme of cation distribution in amphiboles. *Mineral. Mag.* 35, 46-54.
- GIBBS, G. V., J. L. MILLER and H. R. SHELL (1962). Synthetic fluor-magnesian richterite. *Amer. Mineral.* 47, 75-83.
- GILBERT, M. C. (1966). Synthesis and stability relations of the hornblende ferropargasite. *Amer. J. Sci.* 264, 698-742.

- HOUGEN, O. H. and K. M. WATSON (1959). *Chemical Process Principles. Vol. 2: Thermodynamics*, 2nd. ed., Wiley.
- HUEBNER, J. S. and J. J. PAPIKE (1970). Synthesis and crystal chemistry of sodium-potassium richterite,  $(\text{Na,K})\text{NaCaMg}_5\text{Si}_8\text{O}_{22}(\text{OH,F})_2$ : A model for amphiboles. *Amer. Mineral.* 55, 1973-1992.
- IIYAMA, J. T. (1963). Synthèse hydrothermale a 750°C, 1000 bars dans le système  $\text{Na}_2\text{O}-\text{MgO}-\text{Al}_2\text{O}_3-\text{SiO}_2-\text{H}_2\text{O}$  d'amphiboles orthorhombiques et monocliniques. *C.R. Acad. Sci. Paris* 256, 966-967.
- MITCHELL, J. T., D. BLOSS and G. V. GIBBS (1970). A refinement of the structure of actinolite. *Amer. Mineral.* 55, 302-303.
- MIYASHIRO, A. (1956). Osumilite, a new silicate mineral and its crystal structure. *Amer. Mineral.* 41, 104-115.
- MOREY, G. W. and J. M. HESSELGESSER (1951). The solubility of some minerals in superheated steam at high pressures. *Econ. Geol.* 46, 821-835.
- MOREY, G. W. and J. M. HESSELGESSER (1952). The system  $\text{H}_2\text{O}-\text{Na}_2\text{O}-\text{SiO}_2$  at 400°C. *Amer. J. Sci., Bowen Vol.*, 343-372.
- NICHOLLS, J. and J. S. E. CARMICHAEL (1969). Peralkaline acid liquids: A petrological study. *Contrib. Mineral. Petrol.* 20, 268-294.
- NOLAN, J. (1969). Physical properties of synthetic and natural pyroxenes in the system diopside-hedenbergite-acmite. *Mineral. Mag.* 37, 216-229.
- NOLAN, J. and A. D. EDGAR (1963). An X-ray investigation of synthetic pyroxene in the system acmite-diopside-water at 1000  $\text{Kg/cm}^2$  water-vapor pressure. *Mineral. Mag.* 33, 625-634.



- OLSEN, E. (1967). Amphibole: First occurrence in a meteorite. *Science* 156, 61-62.
- PAPIKE, J. J., M. ROSS and J. R. CLARK (1969). Crystal-chemical characterization of clinoamphiboles based on five new structure refinements. *Mineral Soc. Amer. Spec. Paper* 2, 117-136.
- PHILLIPS, R. and G. ROWBOTHAM (1968). Studies on synthetic alkali amphiboles. In, *Int. Mineral. Assoc. Papers & Proc. 5th Genl. Mtg., Cambridge, 1966, Mineral. Soc., London*, 249-254.
- ROBIE, R. A. and D. R. WALDBAUM (1968). Thermodynamic properties of minerals and related substances at 298.15°K (25.0°C) and one atmosphere (1.013 bars) pressure and at higher temperatures. *Geol. Surv. Bull.* 1259, 250 p.
- ROEDDER, E. W. (1952). The system  $K_2O-MgO-SiO_2$ : Part II. *Amer. J. Sci.* 249, 224-248.
- ROEDDER, E. W. (1952). A reconnaissance of liquidus relations in the system  $K_2O \cdot 2SiO_2-FeO-SiO_2$ . *Amer. J. Sci., Bowen Vol.*, 435-456.
- SCHAIRER, J. F. and N. L. BOWEN (1955). The system  $K_2O-Al_2O_3-SiO_2$ . *Amer. J. Sci.* 253, 681-746.
- SCHAIRER, J. F. and H. S. YODER, JR. (1970). The joins  $Na_2O \cdot 5MgO-12SiO_2$  - sodium disilicate and  $2Na_2O \cdot 3MgO \cdot 5SiO_2$  sodium disilicate in the system  $Na_2O-MgO-SiO_2$ . *Carnegie Inst. Wash. Year Book* 69, 157-159.
- SEIFERT, F. and W. SCHREYER (1969). Stability relations of  $K_2Mg_5Si_{12}O_{22}$ , an end member of the merrihueite-roedderite group of meteoritic minerals. *Contrib. Mineral. Petrol.* 22, 190-207.

- SHANNON, R. D. and C. T. PREWITT (1969). Effective ionic radii in oxides and fluorides. *Acta Crystallog.* B25, 925-927.
- SHAW, H. R. (1967). Hydrogen osmosis in hydrothermal experiments, in *Researches in Geochemistry* (P. H. Abelson, ed.), Vol. 2, John Wiley and Sons, Inc., N.Y., 521-541.
- TUTTLE, O. F. (1949). Two pressure vessels for silicate-water studies. *Bull. Geol. Soc. Amer.* 60, 1727-1729.
- WHITTAKER, E. J. W. (1949). The structure of Bolivia crocidolite. *Acta Crystallog.* 2, 312-317.
- WHITTAKER, E. J. W. (1960). The crystal chemistry of the amphiboles. *Acta Crystallog.* 13, 291-298.
- WILKINS, R. W. I. (1970). Iron-magnesium distribution in the tremolite-actinolite series. *Amer. Mineral.* 55, 1993-1998.